IN VIVO IMAGING OF THE ISLETS OF LANGERHANS

By

John Michael Virostko

Dissertation

Submitted to the Faculty of the

Graduate School of Vanderbilt University

in partial fulfillment of the requirements

for the degree of

DOCTOR OF PHILOSOPHY

in

Biomedical Engineering

December, 2006

Nashville, Tennessee

Approved:

E. Duco Jansen

Alvin C. Powers

John C. Gore

James M. Joers

Michael I. Miga

ACKNOWLEDGEMENTS

This dissertation reflects the efforts of many individuals whose presence and support have shaped my tenure in graduate school and beyond.

The members of my dissertation committee, in addition to being endless founts of knowledge, have allowed me the freedom to explore the various detours my research has taken. Some have proven fruitful, most have not, but the journey has provided me vital insight and experience.

My advisor, Duco Jansen, has guided me through this journey. A source of counsel and encouragement, even when half a world away, Duco has shown me how invaluable a mentor can be.

Working with Al Powers has exposed me to a whole realm of biomedical research outside of engineering. Most importantly, however, Al taught me volumes about professional development, from grant writing through conference presentations to the intricacies of running a lab. I would be remiss not to mention several members of the Powers lab who aided me with utmost patience: Mike Fowler, Radhika Aramandla, Greg Poffenberger, and Zhongyi Chen.

My graduate school career opportunely coincided with the arrival of John Gore, Jim Joers, and the rest of the Vanderbilt University Institute of Imaging Science. Their wealth of imaging expertise and resources afforded me the opportunity to learn and use many imaging techniques. My gratitude goes out to Charles Manning, Chad Quarles, Jennifer Begtrup, and Tuhin Sinha for help and fruitful discussion. Through it all, VUIIS has been a fantastic working environment; VUIIS members have been a constant source of friendship and support both at work and outside the office.

Several friends have been steadfast anchors when the trials of graduate school became overwhelming. When motivation waned, anecdotes from friends quickly

reassured me in my career path. My parents were my first educators and have been the strongest supporters of my formal education for 23 years now (although I think each will utter a sigh of relief when it finally ends). Other family members have provided impetus for my interest in diabetes. My fiancée Adrienne has given unending love and support throughout the course of this dissertation and is a lifelong source of inspiration.

TABLE OF CONTENTS

LIST OF TABLES

LIST OF FIGURES

CHAPTER I

INTRODUCTION

The islets of Langerhans play a central role in maintaining glucose homeostasis. Beta cells of the islet synthesize the polypeptide hormone insulin and regulate its secretion. The importance of insulin is readily apparent in its absence: islet apoptosis or defects in insulin secretion lead to diabetes mellitus, a metabolic disease characterized by persistent hyperglycemia. Diabetes is a chronic condition with a multitude of long-term complications, typically ameliorated with insulin injections. However, periodic insulin injections typically fail to achieve the rigorous glycemic control required to prevent diabetes-associated complications. An attractive treatment alternative is the newly emergent technique of islet transplantation, which seeks to restore insulin production by implanting functioning pancreatic islets into diabetic hosts.

The ability to non-invasively image or assess the pancreatic islet would yield valuable insight into the progression of diabetes. Techniques capable of detecting loss of islet mass prior to metabolic indicators could guide interventions intended to slow or halt diabetes progression. The ability to image and track islets after transplantation into the liver would help overcome the obstacles facing islet transplantation.

The islets of Langerhans pose a formidable challenge to imaging modalities. The functional importance of the islet is belied by its small size. A typical islet ranges in size from 50 microns to 300 microns, consisting of a cluster of several thousand cells, primarily the insulin-producing beta cells interspersed with other endocrine cells. The term ‘islet’ describes the appearance of these cell clusters under microscopic evaluation: the islets of Langerhans appear as small islands surrounded by a sea of pancreatic

acinar tissue. The islets are scattered sparsely throughout the pancreas, where they constitute only 1-2% of the total pancreatic mass, as well as after transplantation into the liver. Compounding this sparse distribution is the fact that islets lack any intrinsic contrast from the surrounding tissue.

1.1. Specific Aims

The primary objective of this research was to establish and validate a technique capable of non-invasively imaging the pancreatic islet. The bulk of this work focuses on the use of bioluminescence imaging in small animal models. The final aim focuses on modalities with the capacity for clinical translation and highlights the relative merits and obstacles facing each one.

Specific Aim 1: Label the islets of Langerhans with an optical reporter gene for bioluminescence imaging

Bioluminescent imaging (BLI) can be used for sensitive, high-throughput tracking of optically labeled cells. Pancreatic islets tagged with a bioluminescent reporter gene encoding firefly luciferase (luc) emit visible light. Using highly sensitive CCD cameras this light emission can be imaged non-invasively and repeatedly in small animal models. Our approach utilized two different techniques for integrating the luciferase reporter gene into pancreatic islets. Initial efforts employed viral transfection of isolated pancreatic islets, limiting experiments to studies of transplanted islets. We subsequently generated a transgenic mouse line expressing luciferase under control of the mouse insulin I promoter.

Specific Aim 2: Determine factors that influence bioluminescence signal quantification in order to correlate BLI with islet mass

This light emission from BLI is a quantifiable measure that can be imaged non-invasively and repeatedly in small animal models. However, several factors can influence the detected luminescence signal; these factors were accounted for using constant light-emitting probes to mimic bioluminescence. Detailed analysis of light transmission from the implantation source was used to correlate bioluminescence intensity to islet mass and determine islet survival rates post transplantation.

Specific Aim 3: Evaluate luminescent source reconstruction using single-view spectrally resolved bioluminescence imaging

Standard bioluminescence imaging yields low-resolution planar images of surface light projection. The application of three-dimensional techniques to BLI has the potential to vastly improve the image quality and information available. Light-emitting probes were used to provide constant, known light emission from a controllable and known location. Light source location and intensity were reconstructed in both an optically homogeneous phantom and optically heterogeneous mouse abdomen.

Specific Aim 4: Investigate clinically relevant modalities for imaging the islet of Langerhans

Bioluminescence imaging is limited by optical attenuation to small animal models, relegating its role to a pre-clinical tool. Several techniques were employed to image the islet using modalities that are translatable to human imaging. Islets were labeled with MRI contrast agents: both a paramagnetic gadolinium agent and superparamagnetic iron oxide particles. A targeted contrast agent was developed and evaluated using near infrared fluorescence imaging.

1.2. Dissertation Outline

This work has been organized in the following manner. This first chapter provides a brief introduction to the problem addressed in this research, establishing the significance of the work. The specific aims of the project are outlined and summarized.

The second chapter provides background information regarding islet transplantation. Studies attempting to image the pancreatic islet using various modalities are also described in Chapter II. Portions of this review were published in the August 2006 issue of *Current Diabetes Reports* [1].

Chapter III presents studies using islets virally transfected to express the luciferase optical reporter gene. In vivo BLI measurements are found to provide quantitative, serial measurements of pancreatic islet mass after transplantation. This work was published in the April 15, 2005 issue of the journal *Transplantation* [3].

Chapter IV reports on the generation and characterization of a transgenic animal expressing luciferase under control of the islet specific mouse insulin I promoter. Experiments employing this transgenic animal in disease models and transplantation studies are described. This work will be submitted for publication to *Endocrinology* in December 2006.

Chapter V details a set of experiments using luminescent standards to normalize and accurately quantify in vivo bioluminescence imaging (BLI). These experiments were essential for subsequent quantification of islet mass from bioluminescence intensity measurements. This manuscript was published in the October 2004 issue of *Molecular Imaging* [2].

Chapter VI presents a systemic evaluation of a three-dimensional luminescent source reconstruction algorithm. The benefits and limitations of the reconstruction algorithm are assessed. This manuscript was submitted to *Applied Optics* in August 2006.

Chapter VII outlines a series of attempts to image the islet using modalities translatable to human studies. A variety of approaches and modalities were pursued. The advantages and potential pitfalls of each technique are summarized.

Chapter VIII summarizes the results of Chapters III through VII and the overall objectives of this dissertation. The societal implications and potential for future studies are discussed.

1.3. Works Cited

1. J. Virostko, E. D. Jansen, and A. C. Powers. "Current status of imaging pancreatic islets." *Curr Diab Rep*. 6(4), 328-32 (2006).

2. J. Virostko, Z. Chen, M. Fowler, G. Poffenberger, A. C. Powers, and E. D. Jansen. "Factors influencing quantification of in vivo bioluminescence imaging: application to assessment of pancreatic islet transplants." *Mol Imaging*. 3(4), 333-42 (2004).

3. M. Fowler, J. Virostko, Z. Chen, G. Poffenberger, A. Radhika, M. Brissova, M. Shiota, W. E. Nicholson, Y. Shi, B. Hirshberg, D. M. Harlan, E. D. Jansen, and A. C. Powers. "Assessment of pancreatic islet mass after islet transplantation using in vivo bioluminescence imaging." *Transplantation*. 79(7), 768-76 (2005).

CHAPTER II

BACKGROUND AND SIGNIFICANCE

Portions of this chapter have been published in:

Virostko J, Jansen ED, Powers AC,

"Current status of imaging pancreatic islets,"

Curr Diab Rep. 6(4), 328-32 (2006).

2.1. Introduction

A technique capable of imaging the pancreatic islet would be of great utility to the diabetes research community. The inability to measure islet mass loss in pathological states precludes early diagnosis of Type 1 diabetes. Moreover, the inability to non-invasively track transplanted islets limits studies developing the technique. Despite the success of the Edmonton Protocol, a number of issues must be resolved before islet transplantation can be adopted as routine treatment [1-3]. Efforts to overcome these obstacles are hampered by lack of a non-invasive measure of transplanted islet mass. Hormone secretion testing measures islet function rather than islet mass; it is unclear if such techniques are sensitive enough and whether mass correlates with such functional measures. The primary difficulty in imaging the pancreatic islet stems from its small size (50 – 300 μm). Furthermore islets are sparsely distributed both natively, where they constitute only 2% of the pancreatic mass, and after transplantation to the liver. As islets possess no intrinsic contrast from surrounding tissue, imaging techniques have focused on labeling the pancreatic islet with exogenous contrast agents. The development of novel islet labeling techniques for islet imaging and quantification is an area of active research [4]. This article reviews the application of magnetic resonance imaging (MRI), positron emission tomography (PET), and optical imaging modalities to image the pancreatic islet.

2.2. Islet Transplantation

While the current success of islet transplantation has only recently established it as an effective clinical treatment for type 1 diabetes, the motivation behind islet transplantation is over a century old. The link between diabetes and the pancreas was first discovered in 1889 in studies of a pancreatectomized dog which developed acute

hyperglycemia and glucosuria [5]. Three years later Minkowski successfully transplanted autologous sections of the pancreas into a pancreatectomized dog [6]. The first human implementation of pancreas transplantation was performed in 1894 on a patient with diabetes ketoacidosis. Three pieces of a sheep pancreas were transplanted subcutaneously in a 13-year-old recipient. The patient showed temporary improvement in glucosuria before his death three days later from autoimmune rejection of the xenograft [7]. The first successful reversal of hyperglycemia was accomplished by Banting, et al, in 1922 by treatment with bovine pancreatic extract [8]. Purified insulin production commenced the following year. Insulin therapy became the definitive treatment for diabetics.

Despite the success of insulin injections in overcoming hyperglycemia, the treatment fails to prevent a number of the chronic ailments associated with diabetes. Renal failure, blindness, heart disease, neuropathy, and atherosclerosis continue to afflict diabetics despite insulin therapy [9]. The ability of the islets of Langerhans to exquisitely control carbohydrate metabolism cannot be fully accomplished by insulin injections alone, primarily due to lack of real-time feedback and consequent significant swings in blood glucose levels. These shortcomings of insulin renewed interest in pancreas transplantation. The first successful clinical pancreatic transplant was performed in 1967 [10]. The patient's hyperglycemia was reversed until complications later forced removal of the graft. Later attempts at pancreas transplantation proved more successful. Over 1000 pancreas transplants are now performed annually, with a success rate of 70% [11]. A successful pancreatic transplantation renders the recipient free from any exogenous insulin injections with normal blood glucose and HbA_{1c} levels [12]. The chronic effects of diabetes are lessened: diabetic retinopathy is partially reversed [13] and native renal structure is restored ten years post implant [14]. Transplant recipients report a higher quality of life [15].

Pancreatic transplants have demonstrated benefits over insulin injections for the alleviation of chronic ailments and improved quality of life. Patient survival rates one year after pancreatic transplantation surpass 90% [16]. However, pancreatic transplantation has disadvantages. Successful transplantation typically requires simultaneous transplantation of both the pancreas and kidneys. This surgery is plagued by complications resulting in prolonged hospital stays and repeat surgeries [3]. This in turn results in high medical cost. The diabetes community has thus begun focusing on transplanting solely the insulin-producing pancreatic islets. The majority of the pancreas is an exocrine digestive gland; only 1-2% of the pancreas is composed of the islets that contain insulin-producing β-cells. Transplanting solely the islets of the pancreas is a much less invasive procedure expected to be much safer and less costly to the patient [12]. Pancreatic islets removed from cadaver pancreata can be isolated using collagenase enzyme extracts to yield purified islets [3]. These purified islets can subsequently be transplanted into diabetic recipients. The first successful transplantation of islets into rats showed promise that it would soon become the definitive treatment for type 1 diabetes [17]. However, four years later the first clinical trial on seven diabetics using corticosteroid immunosuppression failed to render any of the seven patients insulin independent [18]. Success came with islet autotransplantation on patients undergoing a total pancreatectomy and infused with their own islets [19]. Without the need for any immunosuppressive drugs these patients with islet autografts delayed the onset of diabetes for over a decade [20]. Results with allografts – transplants from a different individual of the same species - have proven less promising. Of the 237 adult islet allotransplants reported to the International Islet Transplant Registry (IITR) by December 31, 2001 fewer than 12% remained free from insulin injections one year following transplantation [20,21].

The failure of allotransplants to succeed while autotransplants thrived focused attention on the high levels of immunosuppressive drugs given to patients with allografts. The potent immunosuppressive drugs tacrolimus (FK) and cyclosporine (CSA), regularly given to organ transplant recipients to prevent rejection, were found to be toxic to islets, causing distinct morphological damage to beta cells [22]. In 2000 researchers at the University of Alberta reported a modified protocol to treat seven patients with type 1 diabetes. The equivalencies of two donor pancreata were infused into patients via a percutaneous transhepatic portal embolization. Transplant recipients were given a glucocorticoid-free immunosuppressive regimen of sirolimus, tacrolimus, and daclizumab. All seven patients attained insulin independence following transplant and maintained freedom from insulin injections one year post op [2]. The modified protocol has subsequently been dubbed the Edmonton Protocol. A major multi-center study is now being conducted to test the feasibility of the Edmonton Protocol. Initial results are promising; a 90% success rate was recently reported by three participating centers with extensive experience in islet isolation [9].

However, despite these advances in islet transplantation, numerous obstacles remain before islet transplantation can be implemented as the de facto treatment for type 1 diabetes [23-25]. Typically the equivalent of two donor pancreata are necessary to successfully reverse diabetes [2]; using this quantity of islets per recipient means the donor islet supply is insufficient to treat even 0.1% of patients with type 1 diabetes [26]. Attempts to increase the supply of donor islets, whether by *in vitro* cultivation [27,28], use of islets from another species (typically porcine) [29-31], or beta cell differentiation from stem cells [32-34], show promise but are far from clinical implementation. Furthermore, the survival rate of transplanted islets is unknown. Evidence suggests that hypoxia, nutrient deprivation, and inflammation hamper islet engraftment and survival and result in significant islet loss in the early post-transplantation period [35,36]. Long-

term survival rates are also unknown. Native islets undergo apoptosis with an estimated turnover of <58 days [37], continuously replaced by islet replication and differentiation of islet precursors [4]. It is unclear if transplanted islets show similar apoptotic rates or retain potential for replication; however, the gradual loss of insulin independence seen in some studies indicates that transplanted islet mass or functionality declines over time.

Significant efforts are focused on increasing or sustaining islet mass post transplantation [38-40], however, these efforts are largely hampered by the inability to non-invasively measure pancreatic islet mass post transplantation. Islet mass is commonly estimated from insulin secretion following glucose tolerance testing [41] or additional biochemical assays [42]; however, these methods assess islet function, which does not necessarily correlate with islet mass. Morphometric analysis of histological sections of islet grafts can be used to measure islet mass [43], but requires removal of the organ containing the islets, preventing any sequential studies. Furthermore, while this analysis is useful for islets transplanted beneath the renal capsule in rodent models, it is difficult to perform when islets are scattered, as they are when embolized throughout the liver.

2.3. Magnetic Resonance Imaging of Islets

MRI is an attractive candidate for islet imaging due to its noninvasive nature and repeatable clinical application. MRI images have micron resolution and can be acquired using various sources of contrast. MRI remains expensive to implement, however, and imaging times are long compared to other modalities. Furthermore, MRI is relatively insensitive (millimolar concentrations required for detection), confounding its application to microscopic cellular imaging [44]. Attempts to circumvent this limitation have focused on labeling cells with exogenous contrast agents to enhance contrast.

Superparamagnetic iron oxide (SPIO) particles have long been used as a MRI contrast agent for imaging the vasculature. The disturbances these particles create in the local magnetic field lead to rapid proton dephasing detectable using MRI. More recently, SPIOs have been internalized into several cell types and subsequently imaged in studies of cell migration and trafficking [45]. The MR signal change due to iron oxide labeling has permitted imaging of a single cell [4]. Rat pancreatic islets co-cultured with SPIOs internalized the contrast agent and were visible on MRI in vitro. These iron-labeled islets were then transplanted into the liver of a rat and remained visible on MRI for 22 weeks post transplantation [46]. The SPIO islet labeling approach was used to compare the survival of transplanted syngenic and allogenic islets, showing a relative loss of MRI signal for the allogenic transplantation. The iron labeling technique used in the study was demonstrably benign, with no effect on islet survival or insulin secretion [47]. A similar method was used to label human islets with SPIOs and image them transplanted to both the kidney capsule and liver of a mouse [48]. A fluorescent dye was incorporated in the iron particle to determine its pattern of internalization and found SPIO uptake primarily in beta cells of the islet, in contrast with other results indicating SPIO internalization by islet macrophages and exclusion from beta cells [47]. The primary limitation of MRI of SPIO labeled islets is a difficulty in quantification. While the volume of contiguous islet grafts (such as those in the kidney capsule) can be correlated with the number of islets transplanted [48], islets transplanted into the liver prove more difficult to quantify. SPIOs result in ‘negative contrast’ on MR images: they appear as hypointense spots that can be difficult to distinguish from the heterogeneous hepatic MRI background. Furthermore, as the area of contrast exceeds the size of the islets themselves a single hypointense spot can represent either a single labeled islet or a cluster of many islets closely spaced [47]. Further work is also needed to confirm that

SPIOs remain sequestered in the islet and are not metabolized in the liver, leading to false positive results [49].

A second class of MRI contrast agents uses paramagnetic ions (typically Gd^{3+}) to generate positive contrast enhancement. The resulting hyperintense spots are easier to identify and quantify than SPIO labeled cells, as the volume of enhancement is equal to the cell size. Zheng *et al*. synthesized a novel lipophillic Gd^{3+} complex which binds to the cell membrane and labeled islets by co-culture in the complex [50]. They then performed MRI imaging on labeled islets in vitro and on a labeled beta cell line housed in an implanted fiber tube. The labeled cell line remained visible on MRI for 15 days post implantation. Despite these successes, the contrast enhancement currently achieved with Gd^{3+} agents is currently lower than that possible with SPIOs. The development of novel paramagnetic MR contrast agents with high relaxivities (and thus high contrast) is an area of active investigation [51].

Two novel methods show great promise for labeling cells for MRI, and while they are currently still in their infancy, show potential for future islet labeling experiments. The first technique avoids the issue of background by utilizing ^{19}F rather than hydrogen for an MR contrast agent [52]. As the body contains negligible endogenous ^{19}F there is effectively no background and quantification is straightforward. The second new approach derives from other imaging modalities that previously benefited from transgenic technology. A MRI reporter vector has been developed for monitoring transgene expression using viral transfection to introduce a ferretin metalloprotein into cells [53]. This protein then sequesters endogenous iron from the organism within the cell, becoming superparamagnetic similarly to SPIO labeling, but without requiring internalization of the bulky SPIO.

With the low inherent sensitivity of MRI for imaging transplanted islets, several studies have attempted to image surrogate markers of islet engraftment and

inflammation. MR imaging of patients who previously received islet transplantation revealed fat deposition in the liver of two individuals [54]. Interestingly, the presence of steatosis correlated with graft function (steatosis was present for successful grafts and absent in patients with degraded graft function), raising the prospect of steatosis as a surrogate marker of transplanted islet functionality. However, subsequent larger scale studies found steatosis in only a small minority of islet transplant recipients and found that the incidence of steatosis was highest for partially functioning grafts rather than fully functional grafts [4,55]. Histological studies of liver morphology post transplantation revealed focal, drop-shaped fatty degenerations matching the expected islet distribution [56]. It is hypothesized that the observed steatosis is due to a paracrine action of insulin promoting sequestration of free fatty acids within hepatocytes [4]. This conclusion is supported by previous studies of insulinoma metastases in the liver revealing similar patterns of focal steatosis [57]. The pathological significance of steatosis is unknown, but its irregular occurrence in fully functional grafts and prevalence in partially dysfunctional grafts indicates that it does not correlate with transplanted islet mass or function.

Another surrogate imaging candidate is islet infiltration by cells mediating the autoimmune attack of Type 1 diabetes. Much as islets can be labeled with SPIO particles for MRI detection, diabetogenic lymphocytes can be labeled for MRI visualization [58]. These autoimmune cells were then tracked non-invasively and temporally to investigate their recruitment to the pancreas in a mouse model of diabetes. MRI can be used to image the vasculature by infusing SPIO particles into the systemic circulation. The alterations in islet microvasculature caused by leukocyte infiltration can then be imaged [59]. Denis *et al*. applied this technique to a mouse model of Type 1 diabetes to monitor the progression of insulitis in real time [60]. They found positive correlation between the degree of insulitis and SPIO uptake and tracked SPIO

accumulation temporally. It is unclear, however, whether SPIO retention was caused by microvascular changes such as vascular permeability, blood flow, or vessel size; or due to SPIO uptake by phagocytic cells in the islet infiltrate.

2.4. Positron Emission Tomography of Islets

PET has been used extensively in molecular imaging to non-invasively image cellular events. The sensitivity of PET is much higher than MRI, on the order of picomoles [44]. Nuclear imaging instrumentation is typically less expensive than MRI with shorter imaging times, but scanners must be located near a cyclotron for access to radioisotopes. While the spatial resolution of PET has improved in recent years to several millimeters, it is still inferior to MRI. Nuclear imaging also requires administration of radioactive substances, raising questions of safety for repeated exposures.

Targeted PET contrast agents bind specific cell types in vivo, eliminating the need for ex vivo labeling methods and permitting imaging of native pancreatic islets. An extensive library of contrast agents has been developed to image various cellular surface receptors using PET reporters. While these radiopharmaceutical agents were developed primarily for neurological application, the application of existing agents and development of novel compounds has potential to target pancreatic islets. Potential beta cell labeling strategies include targeting the sulfonylurea receptor, compounds that are sequestered in secretory granules, and molecules that exploit the unique glucose metabolism of the beta cell. A systematic approach for screening potential imaging compounds in vitro was applied to these PET reporters and determined that none achieved the necessary signal to background ratio [61]. Human studies targeting the sulfonylurea receptor verified these predictions. High levels of the radiotracer in the liver and plasma led to high background unsuitable for imaging, although chemical modifications may be able to increase signal to background ratio [62]. Similarly,

application of dopaminergic PET compounds found enhanced uptake by islets in focal hyperinsulinism of infancy, but did not show sufficient sensitivity to image normal islets [63]. An alternate strategy targets the autonomic innervation of the pancreas through the presynaptic vesicular acetylcholine transporter [64]. The high acetylcholine-related enzyme content of islets suggests that such an approach may bind islets specifically, although binding by the exocrine pancreas again raises the issue of signal to background ratio.

Researchers are actively pursuing novel islet and beta cell specific peptides and antibodies that can be tagged with PET reporters. Phage display of combinatorial peptide libraries has revealed a candidate under investigation for islet specific targeting [65]. Immunohistochemistry has demonstrated islet specificity of the peptide although the peptide has not been attached to a PET reporter for imaging validation. Moore *et al*. fused a radionuclide to the beta cell specific monoclonal antibody IC2 for PET imaging [66]. Following systemic administration of the PET reporter the radioactivity of the excised pancreas correlated with beta cell mass (as assessed by post-mortem morphometry). Another group used a similar approach, using a different monoclonal antibody that specifically binds to the beta cell membrane [67]. Despite demonstrated beta cell specificity the technique was unable to measure a difference in PET signals between control rats and those treated with the beta cell toxin STZ. This finding demonstrates the primarily limitation of targeted PET imaging of islets: probe binding to the exocrine pancreas, blood plasma, and liver leads to low signal to background ratio. Taking into account the relatively small islet contribution to the pancreatic mass, analysis of PET capabilities indicates that beta cells must retain a PET probe 1000 times more strongly than the exocrine pancreas to be an adequate imaging candidate [61]. The anatomical location of the pancreas further complicates matters, as radiolabel

accumulation in the neighboring liver can be difficult to distinguish from the pancreatic signal.

An alternate PET strategy for islet imaging is ex vivo cell labeling. These methods are similar to MRI studies involving islet impregnation with SPIO, although radiolabels have demonstrably higher sensitivity and easier signal quantification [68]. Islets co-cultured with the radiotracer Fluorodeoxyglucose (FDG) uptake the compound through glucose channels and can then be imaged with PET following hepatic transplantation [69]. However, washout of the label from islets and the relatively short half-life of the radioactive isotope limit imaging to six hours post transplantation. Use of isotopes with longer half-lives such as ^{64}Cu permit imaging 24-36 hours post labeling, although these compounds use passive methods for cellular internalization and have yet to be applied to islets [70]. Transgenic cell labeling with a thymidine kinase reporter gene avoids the time-limiting issues of radio decay [71]. After cells are labeled with the reporter gene, a PET radiolabel that specifically binds to the reporter gene can be infused repeatedly, allowing for serial imaging.

2.5. Optical Imaging of Islets

Optical imaging has the highest sensitivity of any modality, with a detection threshold exceeding femtomoles [72]. Optical imaging equipment tends to be the lowest priced and easiest to implement. Imaging times are short and several subjects can be imaged at once, leading to very high throughput. However, as light (measured in photons) traverses through tissue it is subject to fundamental optical phenomena. Photons are absorbed by chromophores – primarily water, hemoglobin, and melanin – limiting optical penetration to several centimeters of tissue depth. Thus while optical imaging has proven useful for research studies imaging small animal models, the

techniques are not translatable to human studies. Photons are also scattered from their initial path by mismatches in the refractive index of tissue. The practical implication of this scattering is a blurring of deep light sources. The nanometer resolution of superficial optical techniques such as fluorescence microscopy degrades to the order of centimeters for deeper light sources.

Bioluminescence imaging (BLI) is a promising optical technique for imaging islets. To perform BLI, a luciferase reporter gene (typically from the firefly) is first transfected into the cell of interest. This reporter gene catalyzes a chemiluminescent reaction that emits visible light and can be visualized from outside the body of small animal models [73]. Bioluminescence holds the advantage of extremely high sensitivity with relatively no background and relatively easy quantification [74]. The luciferase optical reporter gene was virally transfected into rodent and human islets with no effect on islet morphology or function [4,75]. The amount of light emission from labeled islets correlated with the number of islets in vitro. These bioluminescent islets were subsequently transplanted to either the renal capsule or liver of mice. The amount of light emission post transplantation correlated with the number of islets transplanted with a stable optical signal up to 140 days post transplantation [4]. The method proved sensitive enough to detect as few as 50 islets transplanted to a mouse liver [75]. Quantification of islet bioluminescence before and after transplantation revealed information regarding the survival rate of transplanted islets [76]. One caveat of viral islet transfection is that all islet cell types express the optical reporter gene. Park *et al*. generated a transgenic mouse line expressing luciferase under control of the mouse insulin promoter [44]. As light is produced by the native pancreatic beta cells (requiring no ex vivo labeling), this animal model provides a sensitive, quantitative measure of beta cell mass or function.

Fluorescence has also proven useful for studies imaging the pancreatic islet. Fluorescence differs from bioluminescence in that excitation light is required to generate the light signal, rather than a chemical substrate. Researchers have generated a transgenic mouse line expressing green fluorescent protein (GFP) under control of the mouse insulin promoter [77]. These fluorescent islets can be imaged after hepatic transplantation to visualize microscopic processes of islet engraftment. However, as this wavelength of light is highly attenuated by tissue, the tissue overlying the fluorescent islets must be removed. A transgenic mouse expressing red fluorescent protein (RFP) under control of the same mouse insulin promoter has also been developed [78]. These islets were imaged in an excised pancreas in studies of islet development and distribution. Fluorescence imaging can also be used to track other markers of islet pathology. After systemic administration of a fluorescent marker of apoptosis, fluorescence signal was detected ex vivo in the pancreas of a mouse model of diabetes corresponding to regions of islet apoptosis [79]. The incorporation of fluorescent reporter proteins in both islets and islet markers will allow for high-resolution cell trafficking studies, although limited penetration depth typically requires removal of the islet-bearing organ.

2.6. Conclusions

Techniques under development for imaging the pancreatic islet illustrate the capabilities and limitations of each imaging modality. The choice of optimal imaging technique is dependent on the information sought by each study. MRI provides high-resolution images but requires ex vivo islet labeling that is not beta cell specific. MRI techniques must also overcome issues of difficult signal quantification. PET has higher sensitivity than MRI and more straightforward quantification. As with MRI, islets can be labeled with PET radiotracers ex vivo. However, the radioactivity of these labels

diminishes over time, limiting the time course over which these labels can be imaged. Systemically administered PET compounds are an alternate labeling strategy that can label both native and transplanted islets. However, despite demonstrated beta cell specificity of several compounds, none have achieved the high signal to background ratio needed to distinguish islets from exocrine pancreas, blood plasma, and liver. Optical methods have proven useful in studies of small animal models, providing highly sensitive, easily quantifiable signals. However, the shallow optical penetration of biological tissue currently limits bioluminescence studies to small animal models. Imaging of fluorescent probes provides highly spatially resolved images of islet microstructure but optical attenuation limits application to ex vivo studies. Further advances in each imaging modality are needed to address these limitations and optimize techniques for imaging the pancreatic islet.

2.7. Works Cited

1. D. E. Sutherland. "Current status of beta-cell replacement therapy (pancreas and islet transplantation) for treatment of diabetes mellitus." *Transplant Proc*. 35(5), 1625-7 (2003).

2. A. M. Shapiro, J. R. Lakey, E. A. Ryan, G. S. Korbutt, E. Toth, G. L. Warnock, N. M. Kneteman, and R. V. Rajotte. "Islet transplantation in seven patients with type 1 diabetes mellitus using a glucocorticoid-free immunosuppressive regimen." *N Engl J Med*. 343(4), 230-8 (2000).

3. B. Hirshberg, K. I. Rother, I. B. Digon, J. Venstrom, and D. M. Harlan. "State of the art: islet transplantation for the cure of type 1 diabetes mellitus." *Rev Endocr Metab Disord*. 4(4), 381-9 (2003).

4. R. Bhargava, P. A. Senior, T. E. Ackerman, E. A. Ryan, B. W. Paty, J. R. Lakey, and A. M. Shapiro. "Prevalence of hepatic steatosis after islet transplantation and its relation to graft function." *Diabetes*. 53(5), 1311-7 (2004).

5. J. von Mering, and O. Minkowski. "Diabetes mellitus after pancreas extirpation." *Archiv fur Exper Path und Pharmakol*. 26(111 (1889).

6. O. Minkowski. "Weitere Mitteilungen uber den diabetes mellitus nach extirpation des pancreas." *Berl Klin Wochenschr*. 2(1303 (1892).

7. P. Williams. "Notes on diabetes treated with extract and by grafts of sheep's pancreas." *Br Med J*. 2(1303 (1894).

8. F. Banting, C. Best, J. Collip, W. Campbell, and A. Fletcher. "Pancreatic extracts in the treatment of diabetes mellitus: preliminary report." *Can Med Assoc J*. 12(141 (1922).

9. J. R. Lakey, P. W. Burridge, and A. M. Shapiro. "Technical aspects of islet preparation and transplantation." *Transpl Int*. 16(9), 613-32 (2003).

10. W. D. Kelly, R. C. Lillehei, F. K. Merkel, Y. Idezuki, and F. C. Goetz. "Allotransplantation of the pancreas and duodenum along with the kidney in diabetic nephropathy." *Surgery*. 61(6), 827-37 (1967).

11. R. P. Robertson, and D. E. Sutherland. "Pancreas transplantation as therapy for diabetes mellitus." *Annu Rev Med*. 43(395-415 (1992).

12. R. P. Robertson, C. Davis, J. Larsen, R. Stratta, and D. E. Sutherland. "Pancreas and islet transplantation for patients with diabetes." *Diabetes Care*. 23(1), 112-6 (2000).

13. X. Navarro, D. E. Sutherland, and W. R. Kennedy. "Long-term effects of pancreatic transplantation on diabetic neuropathy." *Ann Neurol*. 42(5), 727-36 (1997).

14. P. Fioretto, M. W. Steffes, D. E. Sutherland, F. C. Goetz, and M. Mauer. "Reversal of lesions of diabetic nephropathy after pancreas transplantation." *N Engl J Med*. 339(2), 69-75 (1998).

15. C. R. Gross, C. Limwattananon, B. Matthees, J. L. Zehrer, and K. Savik. "Impact of transplantation on quality of life in patients with diabetes and renal dysfunction." *Transplantation*. 70(12), 1736-46 (2000).

16. R. P. Robertson. "Pancreas transplantation in humans with diabetes mellitus." *Diabetes*. 40(9), 1085-9 (1991).

17. W. F. Ballinger, and P. E. Lacy. "Transplantation of intact pancreatic islets in rats." *Surgery*. 72(2), 175-86 (1972).

18. J. S. Najarian, D. E. Sutherland, A. J. Matas, M. W. Steffes, R. L. Simmons, and F. C. Goetz. "Human islet transplantation: a preliminary report." *Transplant Proc*. 9(1), 233-6 (1977).

19. J. S. Najarian, D. E. Sutherland, D. Baumgartner, B. Burke, J. J. Rynasiewicz, A. J. Matas, and F. C. Goetz. "Total or near total pancreatectomy and islet autotransplantation for treatment of chronic pancreatitis." *Ann Surg*. 192(4), 526-42 (1980).

20. R. P. Robertson, K. J. Lanz, D. E. Sutherland, and D. M. Kendall. "Prevention of diabetes for up to 13 years by autoislet transplantation after pancreatectomy for chronic pancreatitis." *Diabetes*. 50(1), 47-50 (2001).

21. M. Brendel. "International Islet Transplant Registry Newsletter #9." 8, (2001).

22. C. B. Drachenberg, D. K. Klassen, M. R. Weir, A. Wiland, J. C. Fink, S. T. Bartlett, C. B. Cangro, S. Blahut, and J. C. Papadimitriou. "Islet cell damage associated with tacrolimus and cyclosporine: morphological features in pancreas allograft biopsies and clinical correlation." *Transplantation*. 68(3), 396-402 (1999).

23. G. C. Weir, and S. Bonner-Weir. "Scientific and political impediments to successful islet transplantation." *Diabetes*. 46(8), 1247-56 (1997).

24. T. Zwillich. "Diabetes research - Islet transplants not yet ready for prime time." *Science*. 289(5479), 531-+ (2000).

25. N. Cretin, L. Buhler, B. Fournier, A. Caulfield, J. Oberholzer, G. Mentha, and P. Morel. "Human islet allotransplantation: world experience and current status." *Dig Surg*. 15(6), 656-62 (1998).

26. K. I. Rother, and D. M. Harlan. "Challenges facing islet transplantation for the treatment of type 1 diabetes mellitus." *J Clin Invest*. 114(7), 877-83 (2004).

27. G. M. Beattie, A. Hayek, and F. Levine. "Growth and genetic modification of human beta-cells and beta-cell precursors." *Genet Eng (N Y)*. 22(99-120 (2000).

28. G. M. Beattie, A. M. Montgomery, A. D. Lopez, E. Hao, B. Perez, M. L. Just, J. R. Lakey, M. E. Hart, and A. Hayek. "A novel approach to increase human islet cell mass while preserving beta-cell function." *Diabetes*. 51(12), 3435-9 (2002).

29. S. Magre, Y. Takeuchi, and B. Bartosch. "Xenotransplantation and pig endogenous retroviruses." *Rev Med Virol*. 13(5), 311-29 (2003).

30. D. Kolber-Simonds, L. Lai, S. R. Watt, M. Denaro, S. Arn, M. L. Augenstein, J. Betthauser, D. B. Carter, J. L. Greenstein, Y. Hao, G. S. Im, Z. Liu, G. D. Mell, C. N. Murphy, K. W. Park, A. Rieke, D. J. Ryan, D. H. Sachs, E. J. Forsberg, R. S. Prather, and R. J. Hawley. "Production of alpha-1,3-galactosyltransferase null pigs by means of nuclear transfer with fibroblasts bearing loss of heterozygosity mutations." *Proc Natl Acad Sci U S A*. 101(19), 7335-40 (2004).

31. A. Tucker, C. Belcher, B. Moloo, J. Bell, T. Mazzulli, A. Humar, A. Hughes, P. McArdle, and A. Talbot. "The production of transgenic pigs for potential use in clinical xenotransplantation: microbiological evaluation." *Xenotransplantation*. 9(3), 191-202 (2002).

32. A. Ianus, G. G. Holz, N. D. Theise, and M. A. Hussain. "In vivo derivation of glucose-competent pancreatic endocrine cells from bone marrow without evidence of cell fusion." *J Clin Invest*. 111(6), 843-50 (2003).

33. N. Lumelsky, O. Blondel, P. Laeng, I. Velasco, R. Ravin, and R. McKay. "Differentiation of embryonic stem cells to insulin-secreting structures similar to pancreatic islets." *Science*. 292(5520), 1389-94 (2001).

34. Y. Dor, J. Brown, O. I. Martinez, and D. A. Melton. "Adult pancreatic beta-cells are formed by self-duplication rather than stem-cell differentiation." *Nature*. 429(6987), 41-6 (2004).

35. S. T. Grey, C. Longo, T. Shukri, V. I. Patel, E. Csizmadia, S. Daniel, M. B. Arvelo, V. Tchipashvili, and C. Ferran. "Genetic engineering of a suboptimal islet graft with A20 preserves beta cell mass and function." *J Immunol*. 170(12), 6250-6 (2003).

36. A. M. Davalli, L. Scaglia, D. H. Zangen, J. Hollister, S. Bonner-Weir, and G. C. Weir. "Vulnerability of islets in the immediate posttransplantation period. Dynamic changes in structure and function." *Diabetes*. 45(9), 1161-7 (1996).

37. S. Bonner-Weir. "Life and death of the pancreatic beta cells." *Trends Endocrinol Metab*. 11(9), 375-8 (2000).

38. J. C. Ferrer-Garcia, J. F. Merino-Torres, G. Perez Bermejo, C. Herrera-Vela, J. L. Ponce-Marco, and F. Pinon-Selles. "Insulin-induced normoglycemia reduces islet number needed to achieve normoglycemia after allogeneic islet transplantation in diabetic mice." *Cell Transplant*. 12(8), 849-57 (2003).

39. N. S. Kenyon, L. A. Fernandez, R. Lehmann, M. Masetti, A. Ranuncoli, M. Chatzipetrou, G. Iaria, D. Han, J. L. Wagner, P. Ruiz, M. Berho, L. Inverardi, R. Alejandro, D. H. Mintz, A. D. Kirk, D. M. Harlan, L. C. Burkly, and C. Ricordi. "Long-term survival and function of intrahepatic islet allografts in baboons treated with humanized anti-CD154." *Diabetes*. 48(7), 1473-81 (1999).

40. L. Visser, S. Poppema, B. De Haan, P. Klok, J. Van Der Leij, A. Van Den Berg, and P. De Vos. "Prolonged survival of rat islet xenografts in mice after CD45RB monotherapy." *Transplantation*. 77(3), 386-91 (2004).

41. D. K. McCulloch, D. J. Koerker, S. E. Kahn, S. Bonner-Weir, and J. P. Palmer. "Correlations of in vivo beta-cell function tests with beta-cell mass and pancreatic insulin content in streptozocin-administered baboons." *Diabetes*. 40(6), 673-9 (1991).

42. E. A. Ryan, B. W. Paty, P. A. Senior, J. R. Lakey, D. Bigam, and A. M. Shapiro. "Beta-score: an assessment of beta-cell function after islet transplantation." *Diabetes Care*. 28(2), 343-7 (2005).

43. H. Yamauchi, J. Chiba, K. Kakizaki, M. Maeda, K. Miyagawa, and R. Nakamura. "Effect of islet transplantation on diabetes mellitus after subtotal pancreatectomy in rat: a quantitative analysis of islet tissue." *Tohoku J Exp Med*. 147(4), 365-77 (1985).

44. P. J. Cassidy, and G. K. Radda. "Molecular imaging perspectives." *Journal of the Royal Society Interface*. 2(3), 133-144 (2005).

45. J. W. Bulte, and D. L. Kraitchman. "Iron oxide MR contrast agents for molecular and cellular imaging." *NMR Biomed*. 17(7), 484-99 (2004).

46. D. Jirak, J. Kriz, V. Herynek, B. Andersson, P. Girman, M. Burian, F. Saudek, and M. Hajek. "MRI of transplanted pancreatic islets." *Magn Reson Med*. 52(6), 1228-33 (2004).

47. T. Koblas, P. Girman, Z. Berkova, D. Jirak, J. Kriz, E. Dovolilova, K. Zacharovova, M. Hajek, and F. Saudek. "Magnetic resonance imaging of intrahepatically transplanted islets using paramagnetic beads." *Transplant Proc*. 37(8), 3493-5 (2005).

48. N. V. Evgenov, Z. Medarova, G. Dai, S. Bonner-Weir, and A. Moore. "In vivo imaging of islet transplantation." *Nat Med*. 12(1), 144-8 (2006).

49. E. Okon, D. Pouliquen, P. Okon, Z. V. Kovaleva, T. P. Stepanova, S. G. Lavit, B. N. Kudryavtsev, and P. Jallet. "Biodegradation of magnetite dextran nanoparticles in the rat. A histologic and biophysical study." *Lab Invest*. 71(6), 895-903 (1994).

50. Q. Zheng, H. Dai, M. E. Merritt, C. Malloy, C. Y. Pan, and W. H. Li. "A new class of macrocyclic lanthanide complexes for cell labeling and magnetic resonance imaging applications." *J Am Chem Soc*. 127(46), 16178-88 (2005).

51. A. M. Morawski, P. M. Winter, K. C. Crowder, S. D. Caruthers, R. W. Fuhrhop, M. J. Scott, J. D. Robertson, D. R. Abendschein, G. M. Lanza, and S. A. Wickline. "Targeted nanoparticles for quantitative imaging of sparse molecular epitopes with MRI." *Magn Reson Med*. 51(3), 480-6 (2004).

52. E. T. Ahrens, R. Flores, H. Xu, and P. A. Morel. "In vivo imaging platform for tracking immunotherapeutic cells." *Nat Biotechnol*. 23(8), 983-7 (2005).

53. G. Genove, U. DeMarco, H. Xu, W. F. Goins, and E. T. Ahrens. "A new transgene reporter for in vivo magnetic resonance imaging." *Nat Med*. 11(4), 450-4 (2005).

54. J. F. Markmann, M. Rosen, E. S. Siegelman, M. C. Soulen, S. Deng, C. F. Barker, and A. Naji. "Magnetic resonance-defined periportal steatosis following intraportal islet transplantation: a functional footprint of islet graft survival?" *Diabetes*. 52(7), 1591-4 (2003).

55. P. Maffi, E. Angeli, F. Bertuzzi, C. Paties, C. Socci, C. Fedeli, F. De Taddeo, R. Nano, V. Di Carlo, A. Del Maschio, and A. Secchi. "Minimal focal steatosis of liver after islet transplantation in humans: a long-term study." *Cell Transplant*. 14(10), 727-33 (2005).

56. M. Eckhard, D. Lommel, N. Hackstein, D. Winter, A. Ziegler, W. Rau, M. Choschzick, R. G. Bretzel, and M. D. Brendel. "Disseminated periportal fatty degeneration after allogeneic intraportal islet transplantation in a patient with type 1 diabetes mellitus: a case report." *Transplant Proc*. 36(4), 1111-6 (2004).

57. J. Sohn, E. Siegelman, and A. Osiason. "Unusual patterns of hepatic steatosis caused by the local effect of insulin revealed on chemical shift MR imaging." *AJR Am J Roentgenol*. 176(2), 471-4 (2001).

58. A. Moore, J. Grimm, B. Han, and P. Santamaria. "Tracking the recruitment of diabetogenic CD8+ T-cells to the pancreas in real time." *Diabetes*. 53(6), 1459-66 (2004).

59. J. S. Pober, and R. S. Cotran. "The role of endothelial cells in inflammation." *Transplantation*. 50(4), 537-44 (1990).

60. M. C. Denis, U. Mahmood, C. Benoist, D. Mathis, and R. Weissleder. "Imaging inflammation of the pancreatic islets in type 1 diabetes." *Proc Natl Acad Sci U S A*. 101(34), 12634-9 (2004).

61. I. R. Sweet, D. L. Cook, A. Lernmark, C. J. Greenbaum, and K. A. Krohn. "Non-invasive imaging of beta cell mass: a quantitative analysis." *Diabetes Technol Ther*. 6(5), 652-9 (2004).

62. S. Schneider, P. J. Feilen, M. Schreckenberger, M. Schwanstecher, C. Schwanstecher, H. G. Buchholz, O. Thews, K. Oberholzer, A. Korobeynikov, A. Bauman, S. Comagic, M. Piel, E. Schirrmacher, C. Y. Shiue, A. A. Alavi, P. Bartenstein, F. Rosch, M. M. Weber, H. H. Klein, and R. Schirrmacher. "In vitro and in vivo evaluation of novel glibenclamide derivatives as imaging agents for the non-invasive assessment of the pancreatic islet cell mass in animals and humans." *Exp Clin Endocrinol Diabetes*. 113(7), 388-95 (2005).

63. T. Otonkoski, K. Nanto-Salonen, M. Seppanen, R. Veijola, H. Huopio, K. Hussain, P. Tapanainen, O. Eskola, R. Parkkola, K. Ekstrom, Y. Guiot, J. Rahier, M. Laakso, R. Rintala, P. Nuutila, and H. Minn. "Noninvasive Diagnosis of Focal Hyperinsulinism of Infancy With [18F]-DOPA Positron Emission Tomography." *Diabetes*. 55(1), 13-8 (2006).

64. P. B. Clark, H. D. Gage, C. Brown-Proctor, N. Buchheimer, J. Calles-Escandon, R. H. Mach, and K. A. Morton. "Neurofunctional imaging of the pancreas utilizing the cholinergic PET radioligand [18F]4-fluorobenzyltrozamicol." *Eur J Nucl Med Mol Imaging*. 31(2), 258-60 (2004).

65. K. N. Samli, M. J. McGuire, C. B. Newgard, S. A. Johnston, and K. C. Brown. "Peptide-mediated targeting of the islets of Langerhans." *Diabetes*. 54(7), 2103-8 (2005).

66. A. Moore, S. Bonner-Weir, and R. Weissleder. "Noninvasive in vivo measurement of beta-cell mass in mouse model of diabetes." *Diabetes*. 50(10), 2231-6 (2001).

67. L. Ladriere, F. Malaisse-Lagae, R. Alejandro, and W. J. Malaisse. "Pancreatic fate of a (125)I-labelled mouse monoclonal antibody directed against pancreatic B-cell surface ganglioside(s) in control and diabetic rats." *Cell Biochem Funct*. 19(2), 107-15 (2001).

68. D. L. Kraitchman, M. Tatsumi, W. D. Gilson, T. Ishimori, D. Kedziorek, P. Walczak, W. P. Segars, H. H. Chen, D. Fritzges, I. Izbudak, R. G. Young, M. Marcelino, M. F. Pittenger, M. Solaiyappan, R. C. Boston, B. M. Tsui, R. L. Wahl,

and J. W. Bulte. "Dynamic imaging of allogeneic mesenchymal stem cells trafficking to myocardial infarction." *Circulation*. 112(10), 1451-61 (2005).

69. C. Toso, H. Zaidi, P. Morel, M. Armanet, A. Andres, N. Pernin, R. Baertschiger, D. Slosman, L. H. Buhler, D. Bosco, and T. Berney. "Positron-emission tomography imaging of early events after transplantation of islets of Langerhans." *Transplantation*. 79(3), 353-5 (2005).

70. N. Adonai, K. N. Nguyen, J. Walsh, M. Iyer, T. Toyokuni, M. E. Phelps, T. McCarthy, D. W. McCarthy, and S. S. Gambhir. "Ex vivo cell labeling with 64Cu-pyruvaldehyde-bis(N4-methylthiosemicarbazone) for imaging cell trafficking in mice with positron-emission tomography." *Proc Natl Acad Sci U S A*. 99(5), 3030-5 (2002).

71. S. S. Gambhir, J. R. Barrio, M. E. Phelps, M. Iyer, M. Namavari, N. Satyamurthy, L. Wu, L. A. Green, E. Bauer, D. C. MacLaren, K. Nguyen, A. J. Berk, S. R. Cherry, and H. R. Herschman. "Imaging adenoviral-directed reporter gene expression in living animals with positron emission tomography." *Proc Natl Acad Sci U S A*. 96(5), 2333-8 (1999).

72. T. F. Massoud, and S. S. Gambhir. "Molecular imaging in living subjects: seeing fundamental biological processes in a new light." *Genes Dev*. 17(5), 545-80 (2003).

73. C. H. Contag, S. D. Spilman, P. R. Contag, M. Oshiro, B. Eames, P. Dennery, D. K. Stevenson, and D. A. Benaron. "Visualizing gene expression in living mammals using a bioluminescent reporter." *Photochem Photobiol*. 66(4), 523-31 (1997).

74. J. M. Ignowski, and D. V. Schaffer. "Kinetic analysis and modeling of firefly luciferase as a quantitative reporter gene in live mammalian cells." *Biotechnol Bioeng*. 86(7), 827-34 (2004).

75. M. Fowler, J. Virostko, Z. Chen, G. Poffenberger, A. Radhika, M. Brissova, M. Shiota, W. E. Nicholson, Y. Shi, B. Hirshberg, D. M. Harlan, E. D. Jansen, and A. C. Powers. "Assessment of pancreatic islet mass after islet transplantation using in vivo bioluminescence imaging." *Transplantation*. 79(7), 768-76 (2005).

76. J. Virostko, Z. Chen, M. Fowler, G. Poffenberger, A. C. Powers, and E. D. Jansen. "Factors influencing quantification of in vivo bioluminescence imaging: application to assessment of pancreatic islet transplants." *Mol Imaging*. 3(4), 333-42 (2004).

77. M. Hara, D. Yin, R. F. Dizon, J. Shen, A. S. Chong, and V. P. Bindokas. "A mouse model for studying intrahepatic islet transplantation." *Transplantation*. 78(4), 615-8 (2004).

78. M. Hara, R. F. Dizon, B. S. Glick, C. S. Lee, K. H. Kaestner, D. W. Piston, and V. P. Bindokas. "Imaging Pancreatic B-cells in the Pancreas." *Am J Physiol Endocrinol Metab*. (2005).

79. Z. Medarova, S. Bonner-Weir, M. Lipes, and A. Moore. "Imaging beta-cell death with a near-infrared probe." *Diabetes*. 54(6), 1780-8 (2005).

CHAPTER III

ASSESMENT OF PANCREATIC ISLET MASS AFTER ISLET TRANSPLANTATION USING IN VIVO BIOLUMINESCENCE IMAGING

Michael Fowler[1]*, John Virostko[2]*, Zhongyi Chen[1]*, Greg Poffenberger[1], Aramandla Radhika[1], Marcela Brissova[1], Masakazu Shiota[3], Wendell E. Nicholson[1], Yubin Shi[4], Boaz Hirshberg[5], David M. Harlan[5], E. Duco Jansen[2], and Alvin C. Powers[1,6]

*M. Fowler, J. Virostko, and Z. Chen contributed equally to this work.

[1]Department of Medicine, Division of Diabetes, Endocrinology, and Metabolism, Vanderbilt University School of Medicine, Nashville, TN.

[2]Department of Biomedical Engineering, Vanderbilt University School of Medicine, Nashville, TN.

[4]Department of Pathology, Vanderbilt University School of Medicine, Nashville, TN.

[5]Islet and Autoimmunity Branch of the National Institute of Diabetes and Digestive and Kidney Diseases of the National Institutes of Health, Bethesda, MD.

[6]VA Tennessee Valley Healthcare System, Nashville, TN.

Portions of this manuscript have been published in:

"Assessment of pancreatic islet mass after islet transplantation using in vivo bioluminescence imaging,"

Transplantation. 79(7), 768-76 (2005).

3.1. Abstract

Background: Pancreatic islet transplantation is an emerging therapy for type 1 diabetes, but it is difficult to assess islets after transplantation and thus to design interventions to improve islet survival. Methods: To image and quantify islets, the authors transplanted luciferase-expressing murine or human islets (by adenovirus-mediated gene transfer) into the liver or beneath the renal capsule of immunodeficient mice and quantified the in vivo bioluminescence imaging (BLI) of mice using a cooled charge-coupled device camera and digital photon counting image analysis. To account for variables that are independent of islet mass such as transplant site, animal positioning, and wound healing, the BLI of transplanted islets was calibrated against measurement of luminescence of an implanted bead emitting a constant light intensity. Results: BLI of mice bearing islet transplants was seen in the expected anatomic location, was stable for more than 8 weeks after transplantation, and correlated with the number of islets transplanted into the liver or kidney. BLI of the luminescent bead and of transplanted islets in the kidney was approximately four times greater than when transplanted in the liver, indicating that photon emission is dependent on optical absorption of generated light and thus light source location. Conclusion: In vivo BLI allows for quantitative, serial measurements of pancreatic islet mass after transplantation and should be useful in assessing interventions to sustain or increase islet survival of transplanted islets.

3.2. Introduction

For transplantation of pancreatic islets—an emerging therapy for type 1 diabetes—to achieve its full potential, a number of scientific obstacles must be overcome [1-4]. One obstacle is the large number of pancreatic islets required to reverse diabetes, which is further compounded by the presumed death of a substantial number of islets

posttransplant. Furthermore, neither the long-term survival of transplanted islets nor the stability of islet mass is known with certainty, but recent data suggest that it may decline as some patients, once independent after islet transplantation, now require insulin supplementation to maintain near-normoglycemia. However, assessment of islet mass after transplantation is imprecise and thus interventions to increase or sustain islet mass are not available and cannot be rigorously evaluated. In humans, pancreatic islets are transplanted into the liver by infusion into the portal vein, but the assessment of intrahepatic islets in humans or in animal models of islet transplantation is extremely difficult. The scattered location of intrahepatic islets limits studies examining basic processes such as changes in islet mass, cell proliferation, and vascularization. A technique capable of noninvasively measuring pancreatic islet mass would facilitate efforts to increase or sustain islet survival after transplantation and to understand the natural history of islet mass in the native pancreas during islet development or when diabetes develops. As pancreatic islets range in diameter from 50 to 300 μm and account for only 1% to 2% of pancreatic mass, the challenge for imaging or assessing native or transplanted islets is great. Currently available imaging techniques using magnetic resonance, positron emission tomography, or computed tomography have not been useful to image or assess islets in the pancreas because of a lack of sensitivity, contrast, and spatial resolution. The most widely used approach to assess islet mass estimates islet mass from the amount of insulin secreted after a glucose or meal challenge [5]. Although it provides a measurement of islet function, insulin secretion does not necessarily correlate with islet mass or islet survival. In a second approach, pancreatic islet mass can be accurately quantified by morphometric analysis of histologic sections in the native pancreas or in islet grafts beneath the renal capsule (as developed by Bonner-Weir and colleagues [6-8]). Obviously, this requires removal of the organ bearing the islets. Although useful for islets transplanted beneath the renal capsule in

rodents, this approach is not easily adapted to the study of intrahepatic islets and cannot be performed sequentially. To address the challenge of assessing islet mass, we describe the development of a system to quantitatively assess the survival of transplanted human and murine islets. The components of this system, similar to the recent report by Lu and colleagues [9], are the expression of luciferase in pancreatic islets and the use of in vivo bioluminescence imaging (BLI) [10]. BLI refers to the emission of visible light from a living organism; that light is generated by an enzyme-catalyzed reaction of molecular oxygen with a substrate (in our case, the enzyme is firefly luciferase and the substrate is luciferin). Bioluminescent imaging techniques have recently been used successfully to study tumor growth, to investigate spatiotemporal patterns of gene expression in a variety of transgenic mice, and to monitor inflammatory processes [11-25].

3.3. Materials and Methods

3.3.1. Mouse and Human Islets

Murine islets were isolated from B6D2 mice by ductal infusion of collagenase P digestion (Roche Molecular Biochemicals, Mannheim, Germany) and dissection of the splenic portion of the pancreas as described [26]. All animal studies adhered to the animal care guidelines of the Vanderbilt University Institutional Animal Care and Use Committee. Murine islets were handpicked under microscopic guidance, washed three times with 10 mM phosphate-buffered saline (PBS) containing 1% mouse serum, and suspended in 30 μL of the same solution before transplantation. Human islets, obtained from the Islet and Autoimmunity Branch of the National Institute of Diabetes and Digestive and Kidney Diseases of the National Institutes of Health and through the

Juvenile Diabetes Foundation Human Islet Distribution Program, were shipped in CMRL media by overnight courier to Vanderbilt, assessed for viability in a cell-perifusion system, and then cultured for an additional 24 hr in CMRL media and 95% carbon dioxide/5% oxygen at 37°C. Before transplantation, human islet function was verified by ensuring insulin secretion by human islets increased more than fourfold in response to an increase in glucose from 2.8 to 16.8 mM or 16.8 mM glucose plus 0.045 mM isobutylmethyl xanthine in a cell perifusion system (data not shown). Mouse islets were evaluated in the cell perifusion apparatus by changing the perfusate from 5.6 mM glucose to 16.8 mM glucose or 16.8 mM glucose plus 0.045 mM isobutylmethyl xanthine.

3.3.2. Luciferase Adenovirus

An adenovirus (Adv-luciferase) that bicistronically encodes firefly luciferase and green fluorescent protein (GFP) under the control of the cytomegalovirus (CMV) promoter was created to express luciferase in pancreatic islets. An XbaI/SmaI DNA fragment containing an internal ribosome entry site (IRES) and GFP was isolated from pIRES-EGFP (Clontech,Palo Alto, CA). To construct the adenovirus, a XbaI/XhoI luciferase DNA fragment was cut from pGL-Basic (Promega, Madison, WI) and separately subcloned into the pShuttle-CMV vector (Quantum Biotechnologies, Montreal, Canada). The resulting plasmid was co-transformed into BJ5381 cells with an Ad-Easy-1 adenoviral backbone DNA that is E1 and E3 deleted and is replication-deficient. The recombinant adenoviral construct was transfected into 293A cells to produce viral particles. Murine and human islets were infected in culture with Adv-luciferase at a multiplicity of infection of 500 to 1,000 (assuming 500 cells per islet) for approximately 16 hr beginning on the day of arrival at Vanderbilt (human) or isolation (murine). Adenovirus infection at these multiplicities of infection did not alter the glucose-

stimulated insulin secretion profile in the cell perifusion system (data not shown); by confocal microscopy, only a minority of islet cells (<10%) were infected with the adenovirus. Luciferase activity in islet extracts was measured with the Pharmingen Monolight 3010 Luminometer (BD Biosciences Pharmingen, San Diego, CA).

3.3.3. Islet Transplantation

Nonobese diabetic (NOD)-severe combined immunodeficient (SCID) mice (8–12 weeks of age) from Jackson Laboratories (Bar Harbor, ME) were used as transplant recipients as described [26]. Murine or human islets were transplanted into the liver of NOD-SCID mice by injection into the portal venous system or beneath the renal capsule of NOD-SCID mice approximately 24 hr (murine) or 48 hr (human) after islet isolation as described [26]. After transplantation of human islets into nondiabetic NOD-SCID mice, insulin secretion in vivo was measured in response to intraperitoneal glucose administration (2 g/kg) by radioimmunoassay of mouse plasma using species-specific antisera from Linco Research, Inc. (St. Charles, MO) (human C-peptide, catalogue No. 1020; human insulin, catalogue No. 1014) [27]. To determine the effectiveness of transplanted islets to reverse diabetes, we developed a model system where islets are transplanted and engraft under normoglycemic conditions. NOD-SCID mice were rendered diabetic by the intraperitoneal injection of streptozotocin (175 mg/kg in 0.1 M citrate buffer, pH 4.5). After hyperglycemia was documented by a blood glucose greater than 350 mg/dL (saphenous vein blood measured with an Accu-chek glucose meter; Roche Diagnostics, Indianapolis, IN), an Alzet minipump (model 1002 with a pump volume of 100 μL; Durect Corporation, Cupertino, CA) containing regular human insulin (diluted to 3 U/100 μL; Eli Lilly Corporation, Indianapolis, IN) was implanted in the subcutaneous area near the scapula. Implantation of the pump normalized the blood

glucose within 2 to 3 days. At that time, murine islets expressing luciferase or control islets were transplanted beneath the renal capsule. After 7 to 10 days, the pump was removed and the blood glucose was monitored on a weekly basis. To document that the diabetes reversal was indeed attributable to the islet transplant, a nephrectomy of the islet-bearing kidney was performed.

3.3.4. Implantation of Luminescent Beads

Luminescent beads were obtained from Mb-Microtec (Bern, Switzerland). These beads consist of glass capillaries (0.9 mm wide and 2 mm long) filled with tritium (a β-emitter with a half-life > 10 years) that excites a phosphor and emits constant-intensity light, with peak emission at 600 nm and an emission spectrum similar to that of firefly luciferase [28,29]. As described [29], a single luminescent bead was surgically placed to anatomically simulate where transplanted islets are placed; the bead was fixed in position with a surgical adhesive (Vetbond; 3M Animal Care Products, St. Paul, MN). For the kidney site, the location was on the lateral aspect of the left kidney. For the liver site, the location was within the midhepatic lobes. At the conclusion of the experiment (6 weeks after implantation), the anatomic location of the bead was confirmed at autopsy.

3.3.5. Imaging Luminescence

Bioluminescence imaging was performed using a backthinned, back-illuminated, liquid nitrogen-cooled, charge coupled device (CCD) camera with a 1,300x1,340-pixel chip (Roper Scientific, Trenton, NJ) or on an IVIS 200 imaging system (Xenogen Corp., Alameda, CA). Mice or islets in a culture dish were placed on the imaging stage of a light-tight imaging chamber. For all images, a 1-msec background image was taken to enable subtraction of chip bias and readout noise. An overlay image (black-and-white picture) was taken with a light inside the imaging chamber turned on to illuminate the

subject. Luminescence was quantified using Metamorph software (Version 4.6r6; Universal Imaging Corporation, Downingtown, PA). Using Metamorph, regions of equal area were drawn around the region of interest (ROI). Luminescence was quantified by summing pixel intensities within the ROI as described [10,29].

3.3.6. In Vitro Bioluminescence

Islets were suspended in 10 mM PBS with 1% fetal bovine serum (Invitrogen, Carlsbad, CA) and kept on ice before imaging. Islets were then placed in six-well plates in PBS. The bioluminescence substrate D-luciferin (Promega) was added in excess (10 μL of 15-mg/mL solution) to each well. The six-well plate was placed in the light-tight box of the camera system. Bioluminescence was imaged with a 4-min CCD camera exposure using the Roper imaging system. Peak luminescence was found to occur in the initial 4-min post luciferin administration for in vitro samples. On-chip binning of 2 was used for imaging to increase the signal-to-noise ratio (i.e., four adjacent pixels [a 2x2 square] were combined to generate one pixel). Background subtraction was performed on the image.

3.3.7. In Vivo Imaging of Luminescence

After bead implantation, each mouse was imaged weekly for 6 weeks as described [29]. For imaging of mice with islet transplants, the hair overlying the implanted bead was shaved before imaging to reduce light scattering. Mice were anesthetized using an intraperitoneal injection of 50 mg/kg of sodium pentobarbital and then gently secured to a black felt pad using Velcro to minimize motion during imaging (using the Roper imaging system) or anesthetized with isoflurane (using the Xenogen system). Mice were placed in the lateral decubitus position for renal transplant imaging and the supine position for hepatic transplant imaging. A 1-sec exposure was taken for

all bead images. A saturating concentration of the substrate D-luciferin was injected intraperitoneally (150 mg/kg; data not shown). Serial 4-min exposures (using the Roper imaging system) or serial 1-min exposures (using the Xenogen imaging system) were used to generate a bioluminescence image. Peak light emission was determined to occur by 10 to 15 min after luciferin injection and images for BLI were collected during this time frame. On-chip binning of 5 was used for imaging to increase the signal-to-noise ratio (i.e., 25 adjacent pixels [a 5x5 square] were combined to generate 1 pixel). Background subtraction was performed on all images. Bioluminescence was quantified by summing pixel intensities within equal area ROI.

3.3.8. Tissue Collection and Histologic Assessment of Islet Graft

Insulin, glucagon, or GFP expression in kidneys or livers bearing islet transplants (4–8 weeks after transplantation) was assessed by immunocytochemistry of whole-mount images as described [26].

3.4. Results

3.4.1. In Vitro and In Vivo Bioluminescence

Bioluminescence of murine and human islets infected with an adenovirus encoding luciferase (Adv-luc) was easily detectable by the CCD camera on addition of luciferin to the culture media; bioluminescence from individual islets was clearly visible (Fig. 3.1A) [29]. No bioluminescence was observed from islets not expressing luciferase. Quantification of photon emission from luciferase-expressing islets in vitro correlated with the number of islets per well and with the amount of luciferase activity detected in islet extracts (Fig. 3.1B and C). By histology and immunocytochemistry for insulin and glucagon, luciferase-expressing human or murine islets transplanted beneath the renal

capsule or infused into the portal vein of NOD-SCID mice were similar to islets not infected with the adenovirus (Fig. 3.2A–D) (and data not shown). BLI of islets was seen in the expected anatomic location (liver or kidney) with an extremely low background over other regions (Fig. 3.2E and F). After luciferin injection, transplanted islet in vivo bioluminescence peaked at 5 to 20 min, was detectable for 6 to 8 hr, and could be reassessed repeatedly for more than 4 months in the same animal (see below).

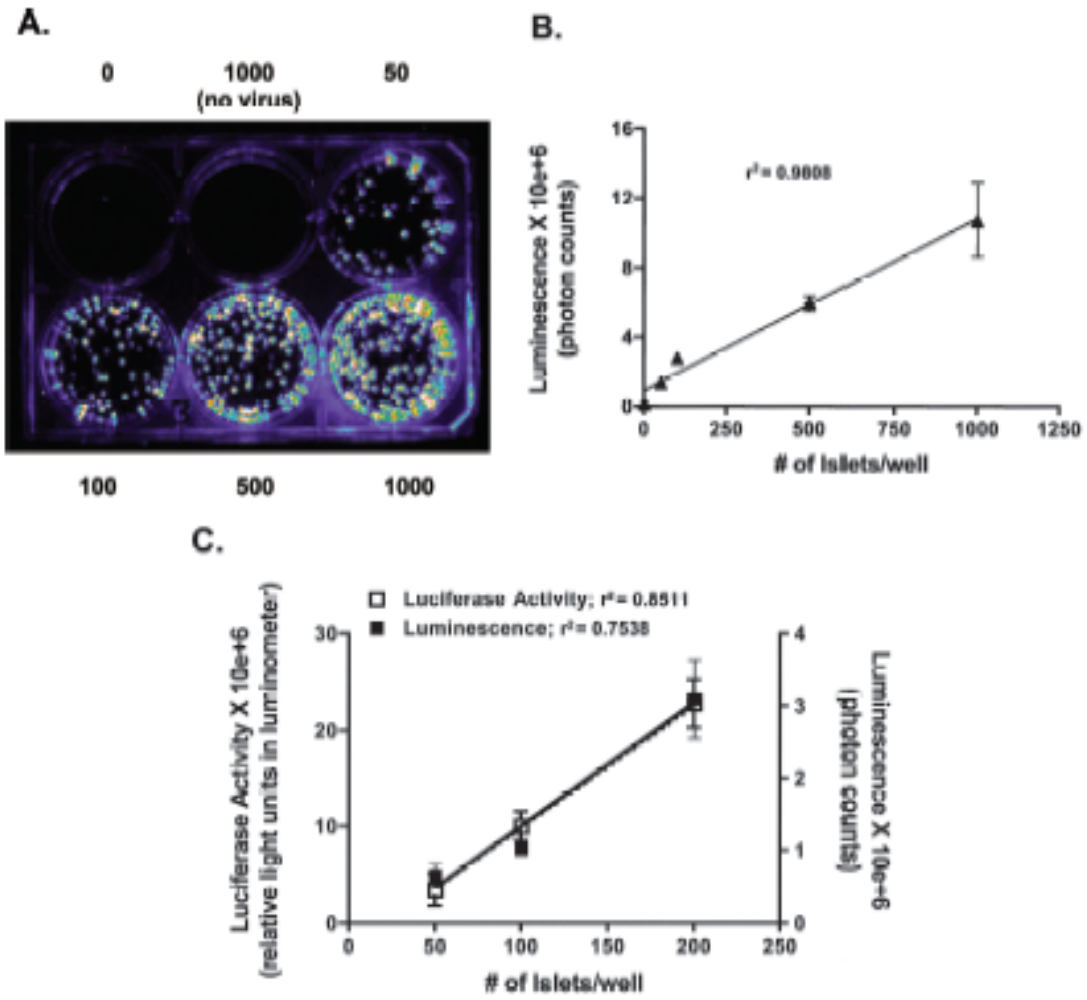

Figure 3.1. In vitro bioluminescence of murine and human pancreatic islets. (A) Human islets, infected with Ad-luciferase, were quantified for size and number, and 0, 50, 100, 500, or 1,000 islets were placed into different wells of a six-well plate. Five minutes after addition of luciferin to the culture medium, the plate was imaged for bioluminescence. The middle well of the upper row contains 1,000 islets not infected with the adenovirus. (B) Luminescence (photon counts) from wells with different numbers of human islets (triplicate wells) expressing luciferase were quantified and graphed as a function of the number of islets per well. (C) Luminescence (photon counts; open squares) as assessed with a CCD camera or luciferase activity (relative light units as assessed in a Luminometer; filled squares) in extracts from 50, 100, and 200 murine islets (triplicates) infected with Adv-luciferase were quantified and graphed as a function of the number of islets in the extract or well.

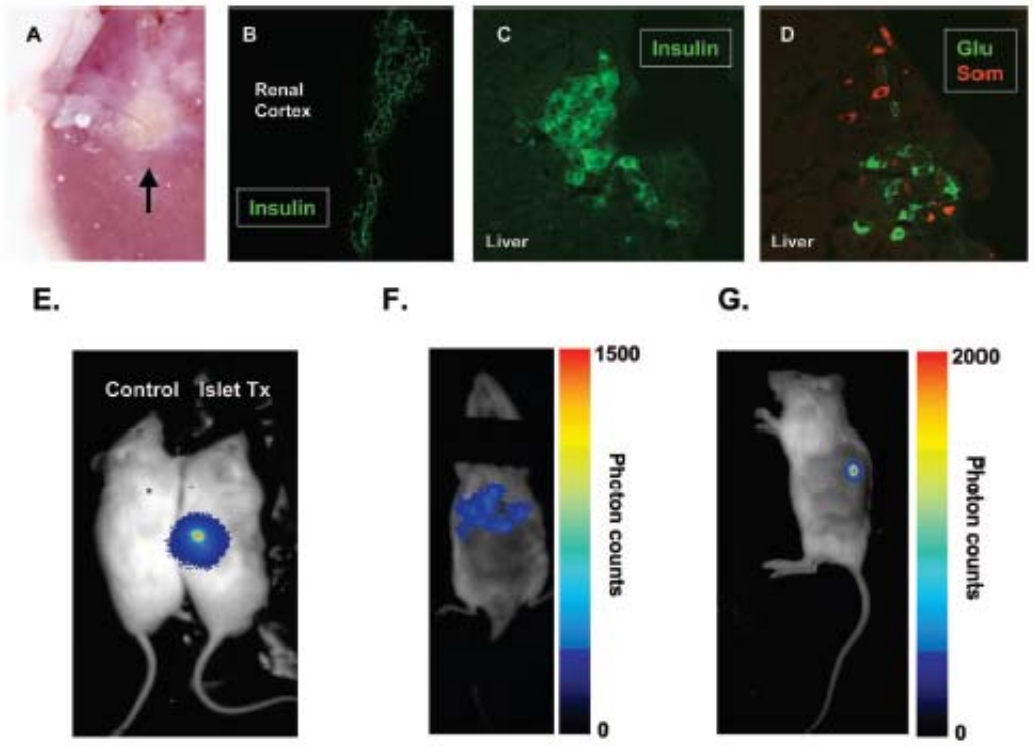

Figure 3.2. Transplantation of luciferase-expressing murine and human pancreatic islets into NOD-SCID mice. Murine or human islets were transplanted beneath the renal capsule or infused into the portal vein of NOD-SCID mice and the kidney or liver was removed 4 to 8 weeks later. (A) Human islet graft (arrow) in the kidney; (B) immunocytochemistry for insulin (green) in a renal graft of human islets (magnification x10); (C) immunocytochemistry for insulin (green) of an intrahepatic human islet (magnification x20); (D) immunocytochemistry for glucagon (green) or somatostatin (red) of an intrahepatic human islet; (E) an anesthetized mouse bearing a renal graft of human islets (1,000 islet equivalents) infected with Adv-luciferase was imaged after the intraperitoneal injection of luciferin (Islet Tx). A control mouse is shown on the left. (F) An anesthetized mouse bearing a hepatic graft of murine islets (50 islet equivalents) infected with Adv-luciferase was imaged after the intraperitoneal injection of luciferin. A color scale on the right shows the relative color intensity (photon counts). A black cloth band, placed loosely over the anesthetized mouse to prevent movement during imaging, is seen over the neck area. (G) Imaging of an anesthetized mouse bearing a luminescent bead implanted onto the renal capsule. A color scale on the right shows the luminescence (photon counts) or relative color intensity.

3.4.2. Quantification of In Vivo Bioluminescence

To determine the effect of the transplant site on BLI and to standardize imaging parameters, we implanted a luminescent bead emitting a constant light intensity at the sites used for islet transplantation (Fig. 3.2G) [29]. Using integrated photon measurements before implantation, light emission from a bead was constant and stable

for a period of several months (< 5% variation in photon measurements). Furthermore, light emission from luminescent beads before transplantation closely matched the emission spectrum of light from the luciferase reaction [29]. Implantation of the luminescent bead allowed a systematic and detailed examination of the effects of animal position, light scattering, and the effect of posttransplant recovery on light emission [29]. For example, in vivo luminescence of beads beneath the renal capsule increased slightly for the first 2 weeks after surgical implantation and then became constant, presumably because of a subsiding of factors (sutures, inflammatory response, tissue edema) influencing light transport from the surgical site to the surface of the animal [29]. On the basis of the information for imaging and photon emission quantification of mice bearing a luminescent bead regarding animal position and time after implantation [29], we imaged mice that underwent transplantation with different numbers of luciferase-expressing murine or human islets and quantified photon emission. Murine islets expressing luciferase had greater in vitro and in vivo bioluminescence per islet than human islets. Presumably, this reflects species differences in parameters such as efficiency of adenovirus infection, activity of the CMV promoter, islet purity, and islet health. In vivo bioluminescence from transplanted luciferase-expressing islets was detectable from as few as 25 murine islets or 200 human islets. The number of human islets transplanted beneath the renal capsule of NOD-SCID mice correlated with in vivo bioluminescence and with human islet function as reflected by insulin secretion from the transplanted islets after a glucose challenge (Fig. 3.3A and B). The BLI of luciferase-expressing murine islets transplanted beneath the renal capsule correlated with the number of islets

transplanted and was stable for at least 18 weeks after transplantation (Figs. 3.3C and D and 3.4A). The BLI of luciferase-expressing murine islets transplanted into the liver was relatively stable for at least 8 weeks after transplantation but appeared to decline slightly at the longer time points (Fig. 3.4B). Luciferase-expressing islets transplanted beneath the renal capsules were similar to uninfected islets in their ability to reverse streptozotocin-induced diabetes (Fig. 3.4C) (data not shown). Using the imaging information from the implanted luminescent beads, we estimated that differences in light

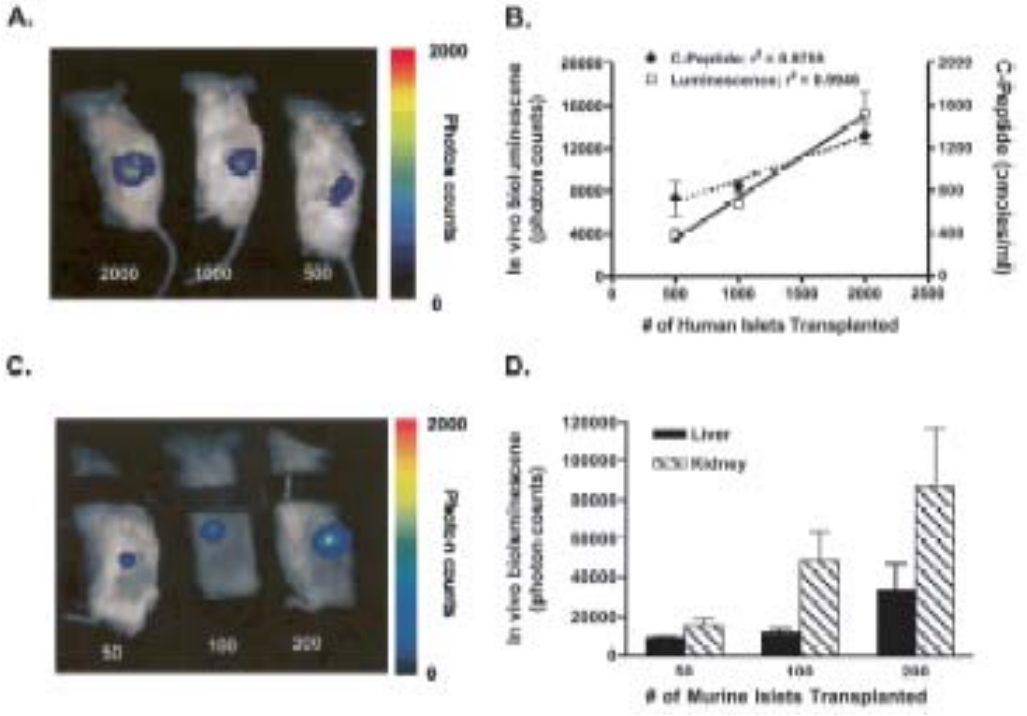

Figure 3.3. Quantification of in vivo bioluminescence of transplanted murine and human pancreatic islets. (A) Different numbers of human islets (500, 1,000, and 2,000) infected with Adv-luciferase were transplanted beneath the renal capsule of NOD-SCID mice; approximately 1 month later, the mice were imaged after the intraperitoneal injection of luciferin. (B) Luminescence over the renal area of mice bearing human islet transplants was quantified (photon counts; open squares) and plotted as a function of the number of islets transplanted; the amount of human C-peptide (filled diamonds) in the plasma after an intraperitoneal glucose injection is expressed as a function of the number of transplanted islets. Each point represents the mean ± SEM of three or four mice. (C) Murine islets infected with Adv-luciferase (50, 100, and 200 islets) were transplanted beneath the renal capsule of NOD-SCID mice or infused into the portal vein and the mice were imaged 4 weeks later. The images of mice with hepatic transplants are not shown. (D) Luminescence over the renal or hepatic area of mice bearing murine islet transplants was quantified (photon counts) and plotted (y-axis); the number of islets transplanted is shown on the x-axis.

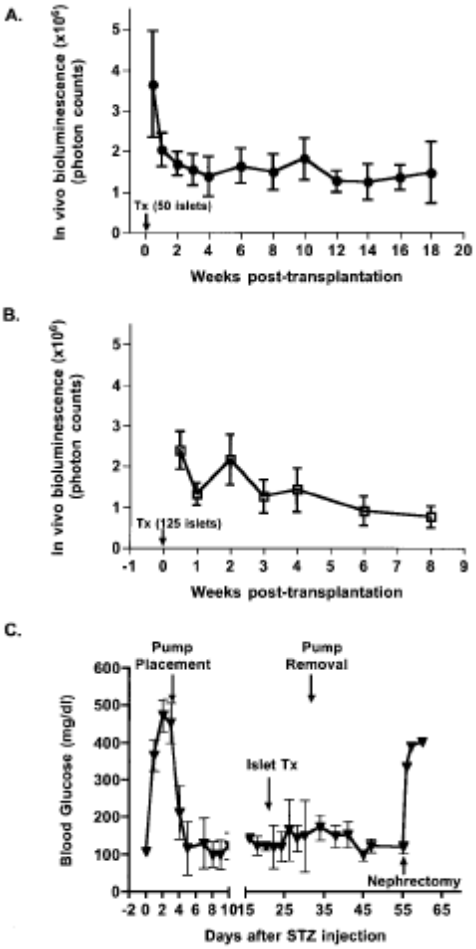

Figure 3.4. Long-term survival of luciferase-expressing transplanted islets. (A) Mice bearing 50 Adv-luciferase–infected murine islets transplanted beneath the renal capsule were imaged each week and the in vivo bioluminescence was quantified. (B) Mice bearing 125 Adv-luciferase–infected murine islets transplanted intrahepatically were imaged each week and the in vivo bioluminescence was quantified. Each point represents the mean ± SEM of three or four mice. (C) Mice rendered diabetic with streptozotocin (n=3) were implanted with an Alzet pump that infused human insulin. After normoglycemia was established, 125 islets (approximately 250 islet equivalents) of luciferase-expressing murine islets were transplanted beneath the renal capsule. The pump was removed 7 to 10 days later and the blood glucose of the mice was monitored on a weekly basis. At the conclusion of the experiment, a nephrectomy was performed to document that the islet transplant was responsible for the diabetes reversal.

attenuation at the hepatic and renal sites resulted in three- to fourfold less in vivo bioluminescence for intrahepatic murine islets compared with murine islets transplanted beneath the renal capsule (Fig. 3.3D) [29]. By combining the data about the implanted beads [29], the in vitro bioluminescence of murine islets before transplantation, and the in vivo bioluminescence of mice bearing islet transplants, we calculated the expected in vivo bioluminescence at each site if all islets survived the transplant procedure [29]. For both the renal and hepatic sites, the ratio of in vivo to in vitro luminescence for the luminescent bead was approximately sixfold greater than for luciferase-expressing murine islets transplanted at the corresponding site [29]. This suggests that only a minority of transplanted islets survive posttransplant in the renal or hepatic site or that the surviving islets no longer express luciferase.

3.5. Discussion

New methods to assess the survival and function of transplanted islets are needed to improve the outcome of pancreatic islet transplantation, as current methods for assessing islet survival are limited and imprecise. This report describes the use of BLI as a new method for assessing transplanted pancreatic islets. BLI of luciferase-expressing murine and human islets transplanted into NOD-SCID mice is a sensitive and noninvasive technique with a high signal-to-noise ratio. In addition, bioluminescence of transplanted islets persisted for an extended period of time (months), is a quantitative surrogate marker for the number of islets transplanted, and allowed for serial measurements of islets transplanted beneath the renal capsule or into the liver. When combined with a similar recent report by Lu and colleagues [9], these results indicate that BLI of transplanted islets provides a powerful approach for addressing a number of important questions about islet transplantation, such as islet survival and the stability of islet mass after transplantation and studies to monitor human islets after transplantation in immunodeficient xenograft models. Furthermore, BLI should be useful in testing interventions that may increase or sustain islets after transplantation. For example, quantitative analysis of BLI of in vitro and in vivo islets relative to similar data from our luminescent bead study [29] suggest that only a minority of transplanted islets survive when transplanted into the liver or kidney site. However, for BLI to be a reliable and quantitative surrogate for a biologic phenomena (in this case, islet mass), the specific animal model must be carefully characterized to account for variables that may affect photon measurements (e.g., transplant site, animal positioning, wound healing) [29]. Other new approaches that exploit unique islet properties to noninvasively measure or assess islet mass are under development. One approach is using a labeled β-cell– or islet specific antibody as reported by Moore and colleagues using the monoclonal antibody IC2 (rat immunoglobulin M antibody that binds a 103-kDa cell surface protein

by immunoblotting or immunocytochemistry) [30] and by Ladriere and colleagues using a monoclonal antibody directed at an islet ganglioside [31]. The latter group concluded that such an approach was not promising in terms of quantifying islet mass by positron emission tomographic scanning because of the inability to distinguish islet mass in diabetic and normal animals [31]. In contrast, Moore et al. found that ^{111}InCl2- labeled IC2 monoclonal antibody preferentially bound murine pancreatic islets and distinguished the β-cell mass of normal and diabetic mice (streptozotocin-induced) by nuclear imaging [30]. These investigators hope to adapt this antibody for use with magnetic resonance imaging or nuclear medicine imaging. However, there are theoretical and practical concerns about using antibodies to quantify β-cell mass. Although the IC2 antibody is β-cell specific, the binding of this monoclonal antibody varies with the functional state of the β cell (reduced binding with abnormal β cells or increased binding after glucose stimulation) [32,33]. Furthermore, because many antibodies fix complement, cell surface antibodies may be toxic to β cells. Another approach to noninvasively assess islet mass attempted to use the β cell's distinctive metabolism as influenced by GLUT2 and glucokinase. Malaisse and colleagues found that D-[3H]mannoheptulose and [2-(14)C]alloxan are preferentially concentrated in islets after the pancreas is perfused with these compounds [34-36]. Although promising, the metabolic state of the β cell will influence the amount of activity and thus such an approach may not correlate with actual β-cell number under fluctuating metabolic conditions (such as after islet transplantation or during the development of type 1 or type 2 diabetes). Bertera and colleagues recently reported that transgenic expression of a mutated form of the red fluorescent protein in the murine insulin gene allowed one to monitor insulin secretion in islets transplanted beneath the renal capsule [37]. We envision that BLI will complement such new approaches while overcoming some of the limitations such as sensitivity and will be

applicable to murine and human islets at renal and hepatic sites of transplantation. Several features of our BLI model system merit further discussion. First, the lack of an immune reaction to the luciferase enzyme or to the adenovirus-infected islet cells in the NOD-SCID model system and the slow proliferation rate of islet cells allow for persistent expression of the episomally located adenoviral transgene (Fig. 3.4A and B). In contrast to immunocompetent transplant recipients, our system with NOD-SCID mice allowed for luciferase expression for up to 18 weeks. Second, transplantation of human islets into this xenograft model system allows one to examine insulin secretion using species-specific insulin or C-peptide assays. Third, because currently the assessment of surviving intrahepatic islets is extremely difficult, BLI of transplanted islets should allow new studies to monitor the mass of murine and human islets that are transplanted at the same site used for human islet transplantation. Finally, using the luminescent beads in the murine model should allow comparison of other sites of islet transplantation in addition to the liver and kidney.

As currently applied, there are several limitations or questions that have yet to be addressed about BLI as a method for assessing transplanted islets. In vivo bioluminescence simply reflects photons generated by luciferase-mediated oxidation of luciferin and is dependent on Mg^{2+}, adenosine triphosphate, and oxygen as co-factors. Therefore, although in vivo bioluminescence appears to be a surrogate for islet cell survival, additional studies are needed to address this in greater detail. Whether islet health or function influences photon generation must also be examined. Although adenovirus-mediated gene transfer is efficient in introducing transgenes into normal islets, the transgene is not integrated into the islet genome. Thus, interventions that stimulate islet proliferation will not stimulate propagation of the luciferase transgene and in vivo bioluminescence will not accurately reflect the increased islet cell number. Adaptation of BLI to immunocompetent mice will likely require use of vectors that do not

incite an immunologic reaction. Both limitations can be overcome by adopting alternative methods for gene transfer into the islet genome (adenoassociated virus or lentivirus) as reported by Flotte and colleagues [38] or lentivirus as shown by Lu et al. [9]. Lu and colleagues studied BLI-transplanted islets using a lentivirus or an adenovirus to express luciferase [9]. They concluded that lentivirus-mediated BLI was superior because of the rapid decline in BLI using the adenovirus approach. However, lentivirus-mediated BLI was not assessed as early as adenovirus-mediated BLI in their report, presumably because expression after lentivirus-mediated gene transfer is slower. Similar to our results (Fig. 3.4D), Lu and colleagues noted adenovirus-mediated BLI was stable after the first week in their system [9]. An alternative explanation for the decline in adenovirus-mediated BLI in the first week is that a large number of islets die in the immediate posttransplant period; our results using the luminescent bead (Fig. 3.4E and F) suggest that this may be an important component of the decline in BLI in the first week. With any viral approach to introduce luciferase, it is likely that expression is greater in the periphery of the islet, and thus BLI may not completely reflect cell survival in the core of the islet. Another limitation of our gene transfer approach is that it uses the CMV promoter to express luciferase and thus luciferase will be expressed in all cells within the islet preparation. In our handpicked murine islets, luciferase is likely to be expressed in β as well as non-β cells. In the less pure human islet preparations, luciferase could also be expressed in non–insulin producing islet cells and pancreatic exocrine cells. Shapiro et al. and other investigators have shown that a significant number of cells within isolated human islets are not β cells (produce glucagon or amylase) [2]. A refinement of the BLI model would be to restrict expression of the luciferase transgene to β cells using a β-cell–specific promoter like the insulin promoter. Finally, current technical limitations of bioluminescent imaging prevent this imaging

modality from being adapted to large-animal model systems used to study islet transplantation (canine or nonhuman primate). Although the spatial resolution of BLI is less than that of other imaging modalities, if BLI can be combined with other reporter genes (i.e., GFP) or with improved image reconstruction, improvements in spatial resolution will be possible.

3.6. Conclusion

BLI in appropriate animal models of diabetes should provide a unique approach that may elucidate strategies directly relevant to human diabetes or islet transplantation. For example, measurement of islet mass by a technique independent of insulin secretory capacity may provide insight into the problem of islet graft nonfunction and determine whether the inability to reverse diabetes or recurrence of diabetes after initially successful islet transplantation is the result of cell death or islet cell nonfunction. Furthermore, the ability to measure islet mass noninvasively should allow future studies to assess interventions to increase islet mass and reduce the number of transplanted islets required to achieve insulin independence.

3.7. Works Cited

1. B. Hirshberg, K. I. Rother, I. B. Digon, J. Venstrom, and D. M. Harlan. "State of the art: islet transplantation for the cure of type 1 diabetes mellitus." *Rev Endocr Metab Disord*. 4(4), 381-9 (2003).

2. A. M. J. Shapiro, J. R. T. Lakey, E. A. Ryan, G. S. Korbutt, E. Toth, G. L. Warnock, N. M. Kneteman, and R. V. Rajotte. "Islet transplantation in seven patients with type 1 diabetes mellitus using a glucocorticoid-free immunosuppressive regimen." *New England Journal of Medicine*. 343(4), 230-238 (2000).

3. R. P. Robertson. "Islet transplantation as a treatment for diabetes - a work in progress." *N Engl J Med*. 350(7), 694-705 (2004).

4. C. Ricordi. "Islet transplantation: a brave new world." *Diabetes*. 52(7), 1595-603 (2003).

5. D. K. McCulloch, D. J. Koerker, S. E. Kahn, S. Bonner-Weir, and J. P. Palmer. "Correlations of in vivo beta-cell function tests with beta-cell mass and pancreatic insulin content in streptozocin-administered baboons." *Diabetes*. 40(6), 673-9 (1991).

6. S. Bonner-Weir. "Perspective: Postnatal pancreatic beta cell growth." *Endocrinology*. 141(6), 1926-9 (2000).

7. A. M. Davalli, Y. Ogawa, L. Scaglia, Y. J. Wu, J. Hollister, S. Bonner-Weir, and G. C. Weir. "Function, mass, and replication of porcine and rat islets transplanted into diabetic nude mice." *Diabetes*. 44(1), 104-11 (1995).

8. A. M. Davalli, Y. Ogawa, C. Ricordi, D. W. Scharp, S. Bonner-Weir, and G. C. Weir. "A selective decrease in the beta cell mass of human islets transplanted into diabetic nude mice." *Transplantation*. 59(6), 817-20 (1995).

9. Y. Lu, H. Dang, B. Middleton, Z. Zhang, L. Washburn, M. Campbell-Thompson, M. A. Atkinson, S. S. Gambhir, J. Tian, and D. L. Kaufman. "Bioluminescent monitoring of islet graft survival after transplantation." *Mol Ther*. 9(3), 428-35 (2004).

10. A. C. Powers, and E. D. Jansen. "In vivo bioluminescence to assess pancreatic islets." *Curr Med Chem*. 4(339 (2004).

11. J. Y. Adams, M. Johnson, M. Sato, F. Berger, S. S. Gambhir, M. Carey, M. L. Iruela-Arispe, and L. Wu. "Visualization of advanced human prostate cancer lesions in living mice by a targeted gene transfer vector and optical imaging." *Nature Medicine*. 8(8), 891-896 (2002).

12. T. J. Sweeney, V. Mailander, A. A. Tucker, A. B. Olomu, W. Zhang, Y. Cao, R. S. Negrin, and C. H. Contag. "Visualizing the kinetics of tumor-cell clearance in living animals." *Proc Natl Acad Sci U S A*. 96(21), 12044-9 (1999).

13. H. L. Rocchetta, C. J. Boylan, J. W. Foley, P. W. Iversen, D. L. LeTourneau, C. L. McMillian, P. R. Contag, D. E. Jenkins, and T. R. Parr, Jr. "Validation of a noninvasive, real-time imaging technology using bioluminescent Escherichia coli in the neutropenic mouse thigh model of infection." *Antimicrob Agents Chemother*. 45(1), 129-37 (2001).

14. A. Nakajima, C. M. Seroogy, M. R. Sandora, I. H. Tarner, G. L. Costa, C. Taylor-Edwards, M. H. Bachmann, C. H. Contag, and C. G. Fathman. "Antigen-specific T cell-mediated gene therapy in collagen-induced arthritis." *J Clin Invest*. 107(10), 1293-301 (2001).

15. G. S. Lipshutz, C. A. Gruber, Y. Cao, J. Hardy, C. H. Contag, and K. M. Gaensler. "In utero delivery of adeno-associated viral vectors: intraperitoneal gene transfer produces long-term expression." *Mol Ther*. 3(3), 284-92 (2001).

16. M. L. Koransky, T. K. Ip, S. Wu, Y. Cao, G. Berry, C. Contag, H. Blau, and R. Robbins. "In vivo monitoring of myoblast transplantation into rat myocardium." *J Heart Lung Transplant*. 20(2), 188-189 (2001).

17. J. Hardy, M. Edinger, M. H. Bachmann, R. S. Negrin, C. G. Fathman, and C. H. Contag. "Bioluminescence imaging of lymphocyte trafficking in vivo." *Exp Hematol*. 29(12), 1353-60 (2001).

18. M. Edinger, T. J. Sweeney, A. A. Tucker, A. B. Olomu, R. S. Negrin, and C. H. Contag. "Noninvasive assessment of tumor cell proliferation in animal models." *Neoplasia*. 1(4), 303-10 (1999).

19. C. H. Contag, D. Jenkins, P. R. Contag, and R. S. Negrin. "Use of reporter genes for optical measurements of neoplastic disease in vivo." *Neoplasia*. 2(1-2), 41-52 (2000).

20. C. H. Contag, S. D. Spilman, P. R. Contag, M. Oshiro, B. Eames, P. Dennery, D. K. Stevenson, and D. A. Benaron. "Visualizing gene expression in living mammals using a bioluminescent reporter." *Photochem Photobiol*. 66(4), 523-31 (1997).

21. D. J. Bornhop, C. H. Contag, K. Licha, and C. J. Murphy. "Advance in contrast agents, reporters, and detection." *J Biomed Opt*. 6(2), 106-10 (2001).

22. W. Zhang, P. R. Contag, A. Madan, D. K. Stevenson, and C. H. Contag. "Bioluminescence for biological sensing in living mammals." *Advances in Experimental Medicine and Biology*. 471(775-84 (1999).

23. D. A. Benaron, P. R. Contag, and C. H. Contag. "Imaging brain structure and function, infection and gene expression in the body using light." *Philos Trans R Soc Lond B Biol Sci*. 352(1354), 755-61 (1997).

24. R. T. Sadikot, W. Han, M. B. Everhart, O. Zoia, R. S. Peebles, E. D. Jansen, F. E. Yull, J. W. Christman, and T. S. Blackwell. "Selective I kappa B kinase expression in airway epithelium generates neutrophilic lung inflammation." *J Immunol*. 170(2), 1091-8 (2003).

25. A. D. Izzo, M. A. Mackanos, J. T. Beckham, and E. D. Jansen. "In vivo optical imaging of expression of vascular endothelial growth factor following laser incision in skin." *Lasers Surg Med*. 29(4), 343-50 (2001).

26. M. Brissova, M. Fowler, P. Wiebe, A. Shostak, M. Shiota, A. Radhika, P. C. Lin, M. Gannon, and A. C. Powers. "Intraislet endothelial cells contribute to revascularization of transplanted pancreatic islets." *Diabetes*. 53(5), 1318-25 (2004).

27. M. Brissova, W. E. Nicholson, M. Shiota, and A. C. Powers. "Assessment of insulin secretion in the mouse." *Methods Mol Med*. 83(23-45 (2003).

28. B. W. Rice, M. D. Cable, and M. B. Nelson. "In vivo imaging of light-emitting probes." *J Biomed Opt*. 6(4), 432-40 (2001).

29. J. Virostko, Z. Chen, M. Fowler, G. Poffenberger, A. C. Powers, and E. D. Jansen. "Factors influencing quantification of in vivo bioluminescence imaging:

application to assessment of pancreatic islet transplants." *Mol Imaging*. 3(4), 333-42 (2004).

30. A. Moore, S. Bonner-Weir, and R. Weissleder. "Noninvasive in vivo measurement of beta-cell mass in mouse model of diabetes." *Diabetes*. 50(10), 2231-6 (2001).

31. L. Ladriere, F. Malaisse-Lagae, R. Alejandro, and W. J. Malaisse. "Pancreatic fate of a (125)I-labelled mouse monoclonal antibody directed against pancreatic B-cell surface ganglioside(s) in control and diabetic rats." *Cell Biochem Funct*. 19(2), 107-15 (2001).

32. K. Buschard, C. H. Brogren, C. Ropke, and J. Rygaard. "Antigen expression of the pancreatic beta-cells is dependent on their functional state, as shown by a specific, BB rat monoclonal autoantibody IC2." *Apmis*. 96(4), 342-6 (1988).

33. K. Aaen, J. Rygaard, K. Josefsen, H. Petersen, C. H. Brogren, T. Horn, and K. Buschard. "Dependence of antigen expression on functional state of beta-cells." *Diabetes*. 39(6), 697-701 (1990).

34. W. J. Malaisse, and L. Ladriere. "Assessment of B-cell mass in isolated islets exposed to D-[3H]mannoheptulose." *Int J Mol Med*. 7(4), 405-6 (2001).

35. L. Ladriere, V. Leclercq-Meyer, and W. J. Malaisse. "Assessment of islet beta-cell mass in isolated rat pancreases perfused with D-[(3)H]mannoheptulose." *Am J Physiol Endocrinol Metab*. 281(2), E298-303 (2001).

36. W. J. Malaisse, M. Doherty, L. Ladriere, and F. Malaisse-Lagae. "Pancreatic uptake of [2-(14)C]alloxan." *Int J Mol Med*. 7(3), 311-5 (2001).

37. S. Bertera, X. Geng, Z. Tawadrous, R. Bottino, A. N. Balamurugan, W. A. Rudert, P. Drain, S. C. Watkins, and M. Trucco. "Body window-enabled in vivo multicolor imaging of transplanted mouse islets expressing an insulin-Timer fusion protein." *Biotechniques*. 35(4), 718-22 (2003).

38. T. Flotte, A. Agarwal, J. Wang, S. Song, E. S. Fenjves, L. Inverardi, K. Chesnut, S. Afione, S. Loiler, C. Wasserfall, M. Kapturczak, T. Ellis, H. Nick, and M. Atkinson. "Efficient ex vivo transduction of pancreatic islet cells with recombinant adeno-associated virus vectors." *Diabetes*. 50(3), 515-20 (2001).

CHAPTER IV

BIOLUMINESCENCE IMAGING OF THE PANCREATIC BETA CELL IN DISEASE AND TRANSPLANTATION

John Virostko[1], Aramandla Radhika[2], Greg Poffenberger[2], Zhongyi Chen[2], Marcela Brissova[2], E. Duco Jansen[1], and Alvin C. Powers[2,3]

[1]Department of Biomedical Engineering, Vanderbilt University, Nashville, TN.

[2]Department of Medicine, Division of Diabetes, Endocrinology, and Metabolism, Vanderbilt University School of Medicine, Nashville, TN.

[3]VA Tennessee Valley Healthcare System, Nashville, TN.

Portions of this manuscript will be submitted for publication in *Endocrinology* in December 2006.

4.1. Introduction

The integral role of the pancreatic beta cell in the etiology of diabetes has resulted in a large body of research dedicated to this unique cell type. Both type 1 and type 2 diabetes are characterized by death of the insulin-producing beta cells [1-3]. However, studies of the complex dynamics of beta cell loss in the diabetic state are complicated by current limitations in non-invasively monitoring the pancreatic beta cell. Non-invasive imaging capabilities would aid the development of therapeutic interventions intended to slow or halt diabetes-induced beta cell loss. The novel technique of islet transplantation for diabetes reversal would similarly benefit from the capacity for tracking islet engraftment and survival post transplantation [4-7]. Islet mass is commonly estimated from measurements of beta cell insulin secretion [8]. However, such metabolic assays monitor aspects of beta cell function rather than mass; the two metrics do not necessarily correlate, especially in pathological diabetic states. For instance, fasting hyperglycemia typically presents only after beta cell mass has been reduced by over 50% [9-14], supporting a paradigm of compensatory insulin secretion. Islet mass can be accurately measured by morphometric analysis of histological sections [15,16]. Unfortunately this technique requires sacrificing the animal, preventing sequential studies in the same animal.

From the perspective of imaging physics, the pancreatic beta cell is a problematic candidate for imaging. The pancreatic islet is small, ranging in diameter from 50 to 300 μm. The islets are distributed sparsely throughout the pancreas and constitute only 2% of the total pancreatic mass [17]. These scattered islets possess no intrinsic contrast from the surrounding exocrine pancreas. Studies seeking to specifically image the beta cell rather than the entire islet are further complicated by the fact that the beta cell comprises only one of the four major islet cell types, interspersed

with the glucagon secreting alpha cell, the somatostatin producing delta cell, and a fourth cell type which secretes pancreatic polypeptide.

Several international workshops have focused on overcoming the difficulties in imaging the beta cell and spurring development of novel islet imaging techniques [18]. A variety of modalities have now been applied in attempts to image the beta cell. Efforts using MRI have largely focused on labeling islets *in vitro* with MRI contrast agents [19-23]. Studies using positron emission tomography (PET) have also used *in vitro* islet labeling techniques [24,25] as well as radioligands targeted *in vivo* to the beta cell [26-30]. While such techniques have shown promise, obstacles remain before they can be adopted for clinical application. MRI relies on labeling of isolated islets, limiting its use to studies of transplanted islets; quantification of islet mass using MRI is also difficult [21,22]. Targeted PET agents suffer low beta cell binding ratios leading to low signal to noise ratio [31,32], although the radioligand recently proposed by Souza, et al. shows promise for sufficient beta cell specificity [30].

Bioluminescence imaging (BLI) was recently developed as a means of imaging gene expression non-invasively using an optical reporter gene [33]. While optical attenuation precludes bioluminescence imaging from clinical administration, the extremely high throughput and sensitivity of BLI have cemented its position as an invaluable pre-clinical tool [34,35]. Early attempts to harness BLI for islet imaging by our group and others [36-38] labeled isolated islets with a viral vector encoding the optical reporter gene. As with studies using MRI, this strategy was limited to studies of transplanted islets. More recently, transgenic mice expressing the luciferase optical reporter under control of the insulin promoter have been created [39-41]. These mice have been used to track pancreatic islet bioluminescence in animal models of diabetes and post transplantation. However, *in vitro* experiments have indicated that luciferase expression may reflect up-regulation of the insulin promoter in the hyperglycemic state

[39,40]. This study compares the bioluminescence signal with conventional measures of beta cell mass and insulin content in a diabetic mouse model.

4.2. Materials and Methods

4.2.1. Generation of Transgenic Mouse Line

We generated transgenic mice expressing the luciferase optical reporter gene under control of the insulin regulatory region. The transgene consisted of the 9.2 kb mouse insulin I promoter and a 1.7 kb sequence encoding firefly luciferase. A β globin region and 3' non-transgenic region flanked the firefly fragment on each side to stabilize the transgene. The fragment was released from the blue script vector (Stratagene) by digestion with Kpm I and Not I and purified by agarose gel electrophoresis. The purified DNA was submitted to the Vanderbilt University transgenic mouse core. The transgene was integrated in FVB mice by pronuclear microinjection into mouse embryos. Five founder lines were generated and genotyped by Southern blot. In vivo bioluminescence imaging was used to phenotype the founder lines, as previously described by Contag and co-workers [42]. From this screening the founder line with the highest and most consistent luciferase expression was selected for further studies. The copy number of this transgene was found to be 3 using Southern blot standardized to a known amount of DNA. Mice used in these studies were heterozygous for the transgene. The Vanderbilt University Institutional Animal Care and Use Committee approved all experiments involving animal subjects.

4.2.2. Islet Isolation

Islets were isolated from transgenic insulin/luciferase mice by ductal infusion of collagenase P digestion (Roche Molecular Biochemicals, Mannheim, Germany) and dissection of the splenic portion of the pancreas as previously described [43]. Islets were handpicked under microscopic guidance and washed three times with 10 mM phosphate-buffered saline (PBS) containing 1% mouse serum, and suspended in 30 μL of the same solution before transplantation. A cell perifusion system was used to test the response of transgenic islet preparations to stimuli of 16.8 mM glucose, 16.8 mM glucose + 250 μM isobutylmethyl xanthine, and 2.8 mM glucose + 300 μM tolbutamide as described [44].

4.2.3. Diabetes Induction

Transgenic mice (males 8 weeks of age) were rendered diabetic by the intraperitoneal injection of streptozotocin (STZ, 175 mg/kg in 0.1 M citrate buffer, pH 4.5). A separate cohort of mice was injected with streptozotocin at a concentration of 100 mg/kg, a concentration insufficient to induce hyperglycemia. Blood glucose measurements were obtained using tail vein blood measured with an Accu-chek glucose meter (Roche Diagnostics, Indianapolis, IN).

4.2.4. Islet Transplantation

Immunodeficient (NOD-SCID) mice (8–12 weeks of age) from Jackson Laboratories (Bar Harbor, ME) were used as transplant recipients as described [43]. Transgenic insulin-luciferase islets were transplanted after overnight culture in RPMI with 11 mM glucose and 10% FBS. Islets were transplanted into the liver of NOD-SCID

mice by injection into the portal venous system or beneath the renal capsule of NOD-SCID mice [43].

4.2.5. Insulin Content

Pancreata of transgenic mice or renal islet grafts were excised from anesthetized animals. Pancreata or grafts were cleaned of other tissues, blotted dry, and weighed. Tissue was homogenized in 1 mL HCl in 100 mL of 95% ethanol and incubated for 48 hours at 4°C under mild agitation. The homogenate was centrifuged at 2500 rpm for 30 minutes at 4°C. The supernatant was collected for radioimmunoassay and stored at -20°C. Insulin content was measured with a heterospecies specific radioimmunoassay using antibody-coated tubes (ICN Diagnostics, Costa Mesa, CA), I^{125}-human insulin (Diagnostic Products, Los Angeles, California) and a rat insulin standard (Linco Research, St. Charles, Missouri) at a 1:1000 dilution, as previously described [45].

4.2.6. Immunocytochemistry

Dissected mouse pancreata were rinsed in ice-cold 10 mM PBS and fixed in freshly prepared 4% paraformaldehyde (Electron Microscopy Sciences; Washington, PA)/100 mM PBS for 1.5 hr on ice using methods previous described [46]. Following fixation, tissues were washed with 100 mM PBS and equilibrated in 30% sucrose/10 mM PBS overnight at 4°C. The tissues were embedded in optimum cutting temperature compound (VWR Scientific Products; Willard, OH) at –80°C. Seven µm sections were cut and mounted on charged slides. Cryosections were permeabilized with 0.2% Triton X-100 for 10 min at room temperature, blocked with 5% normal donkey serum (Jackson ImmunoResearch Laboratories, Inc.) for 1.5 hr, and then incubated with primary antibodies overnight at 4°C. Guinea pig anti-insulin IgG (1:1000) and rabbit anti-

glucagon IgG (1:5000) were from Linco Research, Inc. (St. Charles, MO). Rabbit anti-luciferase (1:250) was obtained from Cortex Biochem, Inc (San Leandro, CA). Secondary antibodies conjugated with Cy2, Cy3, and Cy5 fluorophores (1:1000, Jackson ImmunoResearch Laboratories, Inc., West Grove, PA) were applied to the tissue sections for 1 hr at room temperature. Both primary and secondary antibodies were diluted in 10 mM PBS containing 1% BSA and 0.1% Triton X-100. Digital images of the 7-μm cryosections mounted with AquaPoly/Mount (Polysciences; Warrington, PA) were acquired with a MagnaFire digital camera (Optronics; Goleta, CA) connected to an Olympus BX-41 fluorescence microscope (Olympus; Tokyo, Japan).

To systematically examine β cell mass and luciferase expression in the pancreas of transgenic mice treated with streptozotocin, pancreatic sections spaced by 250 μm from three different levels of the pancreatic tissue block were imaged. To determine populations of β cells and luciferase expressing cells, islets were imaged under x4 objectives. Using MetaMorph v6.1 software (Universal Imaging, Downington, PA), integrated morphometry of 10–15 islets per section (3 sections/mouse) was used to calculate the relative area of islet β cells and luciferase expressing cells [45,47].

4.2.7. Bioluminescence Imaging

All bioluminescence imaging was performed using an IVIS 200 CCD camera (Xenogen, Alameda, CA). For studies using BLI in vitro, islets were cultured overnight in RPMI with 10% FBS and 2.5, 5.6, 11.0, or 25.0 mM glucose. Islets were placed in a black well plate (10 islets per well) and placed on the imaging platform of the IVIS system. Thirty-five μL of the substrate D-luciferin (Promega, Madison, WI) at a concentration of 15 mg/ml was added to 500 μL of solution prior to imaging. Bioluminescence images were integrated for a period of 1 minute. Images were taken

from immediately post substrate addition to 5 minutes post administration, in order to capture the peak in bioluminescence intensity. The luciferase activity of islet homogenates was measured with a Pharmingen Monolight 3010 Luminometer (BD Biosciences Pharmingen, San Diego, CA).

For in vivo BLI, anesthesia was induced and maintained with isoflurane and animals were placed on the imaging platform. D-luciferin was injected via the intraperitoneal cavity at a concentration of 150 mg/kg. Bioluminescence images were again integrated for 1 minute. However, as in vivo bioluminescence tended to peak later after substrate administration, animals were imaged up to 12 minutes post injection to ensure peak bioluminescence was captured. Bioluminescence was quantified using Living Image analysis software (Xenogen, Alameda, CA). Equal area regions of interest (ROI) were centered over the bioluminescent region. Photon counting measurements summed bioluminescent intensity for all pixels within the ROI over the integration time. Measurements were normalized for exposure time, ROI area, and solid angle.

4.2.8. Three-Dimensional BLI Image Reconstruction

Three-dimensional reconstruction of in vivo bioluminescence was performed using the Living Image® Software 3D Analysis Package (Xenogen, Alameda, CA) as described [Virostko et al, manuscript submitted]. Briefly, the diffusion model of light propagation was applied to spectrally filtered bioluminescent image information to reconstruct the bioluminescent source location and intensity. Spectral imaging was obtained by imaging bioluminescence through six 20 nm bandpass filters at wavelengths from 560 to 660 nm. Additionally, a structured light image was taken to reconstruct the surface topography of the mouse. Images were reconstructed using the optical properties of muscle tissue.

4.3. Results

4.3.1. In Vivo Bioluminescence Imaging

After injection of the substrate luciferin into transgenic mice expressing luciferase under control of the insulin promoter, bioluminescence was visible in an area consistent with the anatomical location of the pancreas (Figure 4.1A). A lateral abdominal incision was performed and the viscera were shifted to expose the pancreas of the transgenic animal. A bioluminescence image of the exposed pancreas confirmed that all light was emanating from the pancreas (Figure 4.1B). No light was emitted from any other organs of the mouse. A three-dimensional bioluminescence reconstruction was performed on an intact transgenic mouse. This three-dimensional bioluminescence image of the animal reconstructed the location of bioluminescent islets (Figure 4.1C).

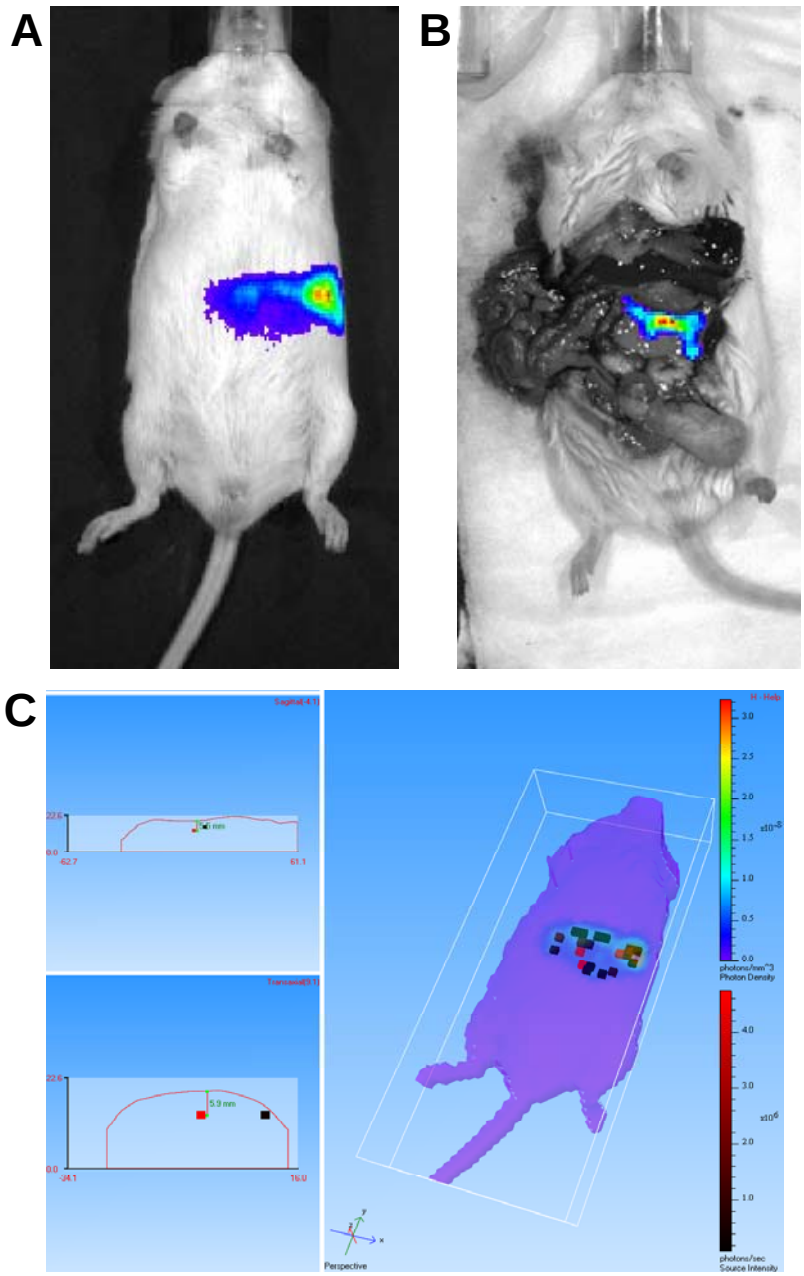

Figure 4.1. In vivo bioluminescence imaging of transgenic insulin luciferase mice. (A) Mice expressing luciferase under control of the mouse insulin I promoter emitted light after administration of the luciferin substrate in an anatomical region consistent with the pancreas. This bioluminescence was visible through the skin of the animal. (B) However, an incision was made in the animal to expose the pancreas to verify that all light emission was emanating from the pancreas; no other organs emitted light. (C) Three dimensional reconstruction of light emission from a transgenic MIP-Luc mouse revealed the spatial location of bioluminescent islets. In the image red voxels indicate bioluminescent sources, the cutaway views on the left reveal depth of these cells.

4.3.2. Transgenic Islet Function

Rigorous functional testing of transgenic animals was performed to ensure that the transgene driving luciferase expression did not affect islet function. Intraperitoneal glucose tolerance testing of transgenic animals confirmed normal response to a glucose challenge (Figure 4.2A). Islets isolated from transgenic animals were tested in a cell perifusion system. Transgenic islets displayed a similar response to islet secretagogues as wild type islets (Figure 4.2B). Immunocytochemistry of transgenic pancreata revealed the typical murine islet architecture: a core of β cells surrounded by a mantle of α and δ cells (Figure 4.2C).

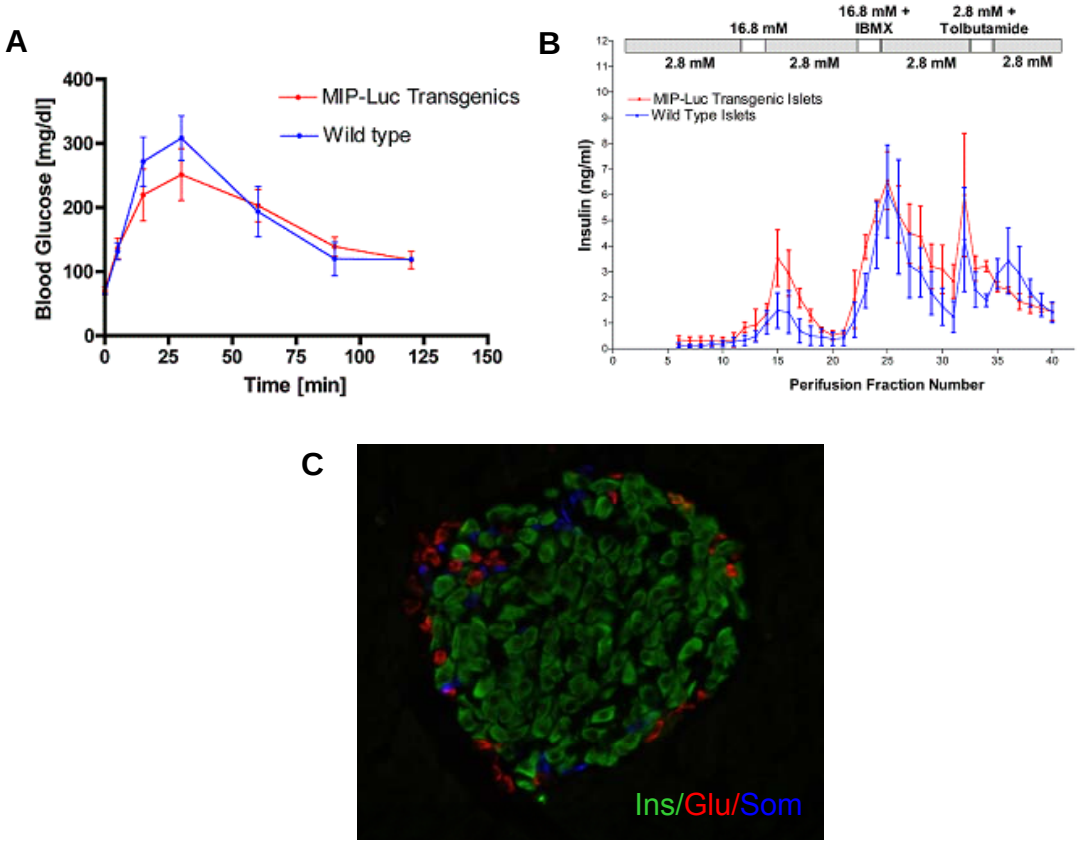

Figure 4.2. Functional characterization of transgenic insulin luciferase mice. (A) Intraperitoneal glucose tolerance testing of transgenic animals revealed similar response to a glucose bolus as wild type control animals (n = 5 each group) . (B) Isolated transgenic islets were tested in a cell perifusion apparatus. Transgenic islets displayed similar insulin release in response to several islet secretagogues as control islets isolated from wild type animals (n = 4 each group). (C) Immunocytochemistry of transgenic islets verified normal murine islet architecture with a core of beta cells (shown in green) and mantel of alpha and delta cells (shown in red and blue, respectively).

4.3.3. In Vitro Bioluminescence Imaging

After addition of luciferin to the culture media isolated islets emitted bioluminescence. Individual islets and islet clusters could be detected by CCD camera (Figure 4.3A). The amount of bioluminescence detected was proportional to the number of islets in each well (Figure 4.3B). The luciferase activity of islet lysates similarly correlated with the number of islets (Figure 4.3B).

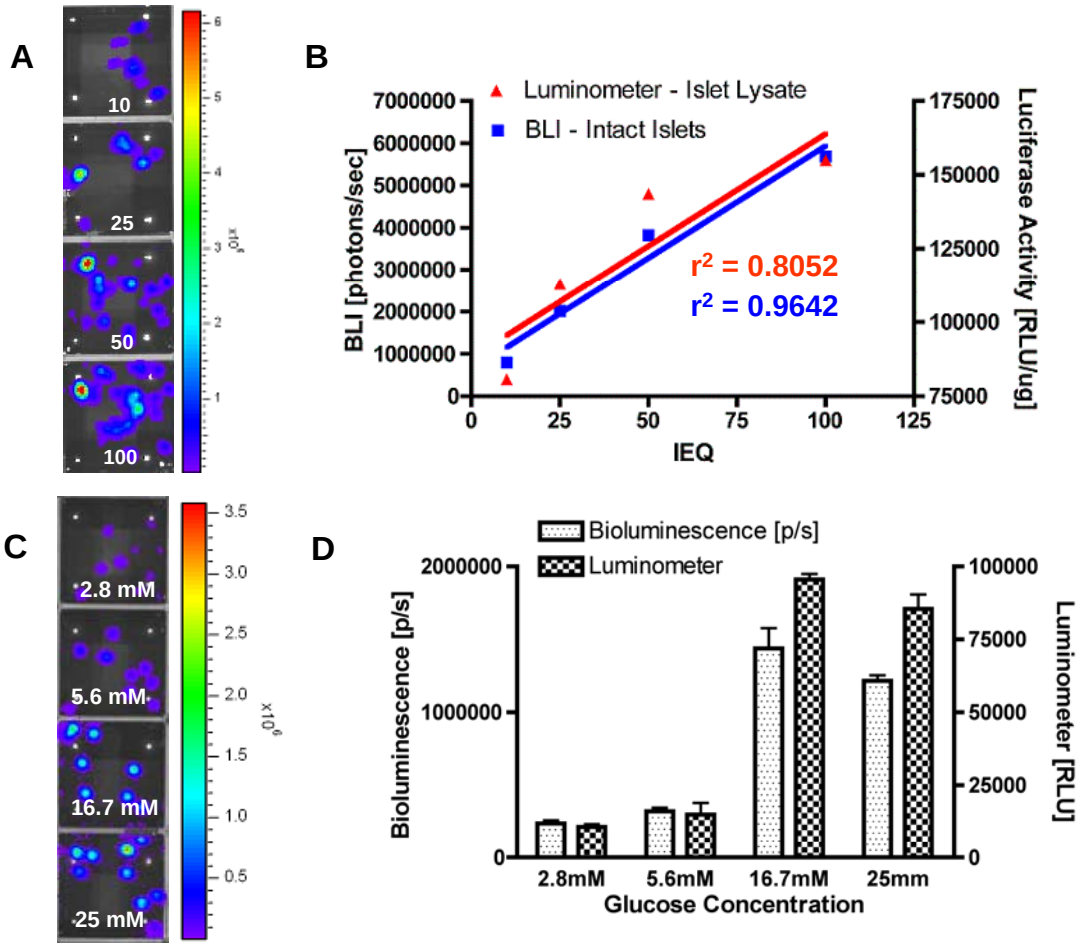

Figure 4.3. Factors affecting bioluminescence quantification. (A) *In vitro* bioluminescence image of islets in a 24 well plate after addition of luciferin. Islets are in quantities of 10, 25, 50, and 100 islets, top to bottom. (B) Quantification of *in vitro* bioluminescence reveals correlation between bioluminescence intensity and the number of islets. Luciferase activity, as measured by luminometer, also correlates with the number of islets. (C) *In vitro* bioluminescence image of islets cultured overnight in increasing glucose concentrations. Top to bottom: 2.8 mM, 5.6, 16.7, and 25 mM glucose. (D) Quantification of bioluminescence shows that the glucose level islets are exposed to affects the amount of light emitted. Islets exposed to 16.7 mM glucose emit the most of light as determined by BLI and produce the most luciferase, as determined by luminometer.

The glucose levels at which isolated islets were incubated also affected the emitted bioluminescence. Ten islets incubated overnight in different glucose concentrations emitted differing amounts of light (Figure 4.3C). Increasing glucose concentrations from 5.6 mM (levels corresponding to a non-diabetic animal) to 11 mM (a level consistent with a diabetic animal) led to increasing bioluminescence (Figure 4.3D). A further increase in glucose level to 25 mM led to a decline in bioluminescence, likely owing to glucose toxicity. The luciferase activity of islet lysates again correlated with the quantification of bioluminescence from intact islets (Figure 4.3D).

4.3.4. In Vivo Imaging of Diabetes

The injection of the beta cell toxin streptozotocin was employed as a model of diabetes. Following the injection of STZ into transgenic insulin-luciferase mice there was a gradual decline in bioluminescence intensity (Figure 4.4A). The blood glucose levels of these mice rose from normal values before STZ administration to levels exceeding 500 mg/dl 8 days after STZ injection, reflected marked hyperglycemia (Figure 4.4B). During this same period BLI measurements fell approximately 6 fold (Figure 4.4B). However, the insulin content of pancreata from mice receiving STZ treatment fell nearly 40 fold as compared to untreated transgenic animals (Figure 4.4C).

Immunocytochemistry staining for insulin and luciferase in transgenic insulin-luciferase pancreata demonstrated that luciferase staining was present only in insulin producing beta cells (Figure 4.4E). Morphometric measurements of insulin and luciferase staining indicate that approximately 20% of beta cells express luciferase. After STZ treatment the number of cells staining for insulin drops approximately 4 hold; the number of cells staining for luciferase shows a similar decrease (Figure 4.4D). Thus, the rate of apoptosis of beta cells expressing luciferase and beta cells that do not express luciferase appears to be similar. Figure 4.4E shows a representative islet from

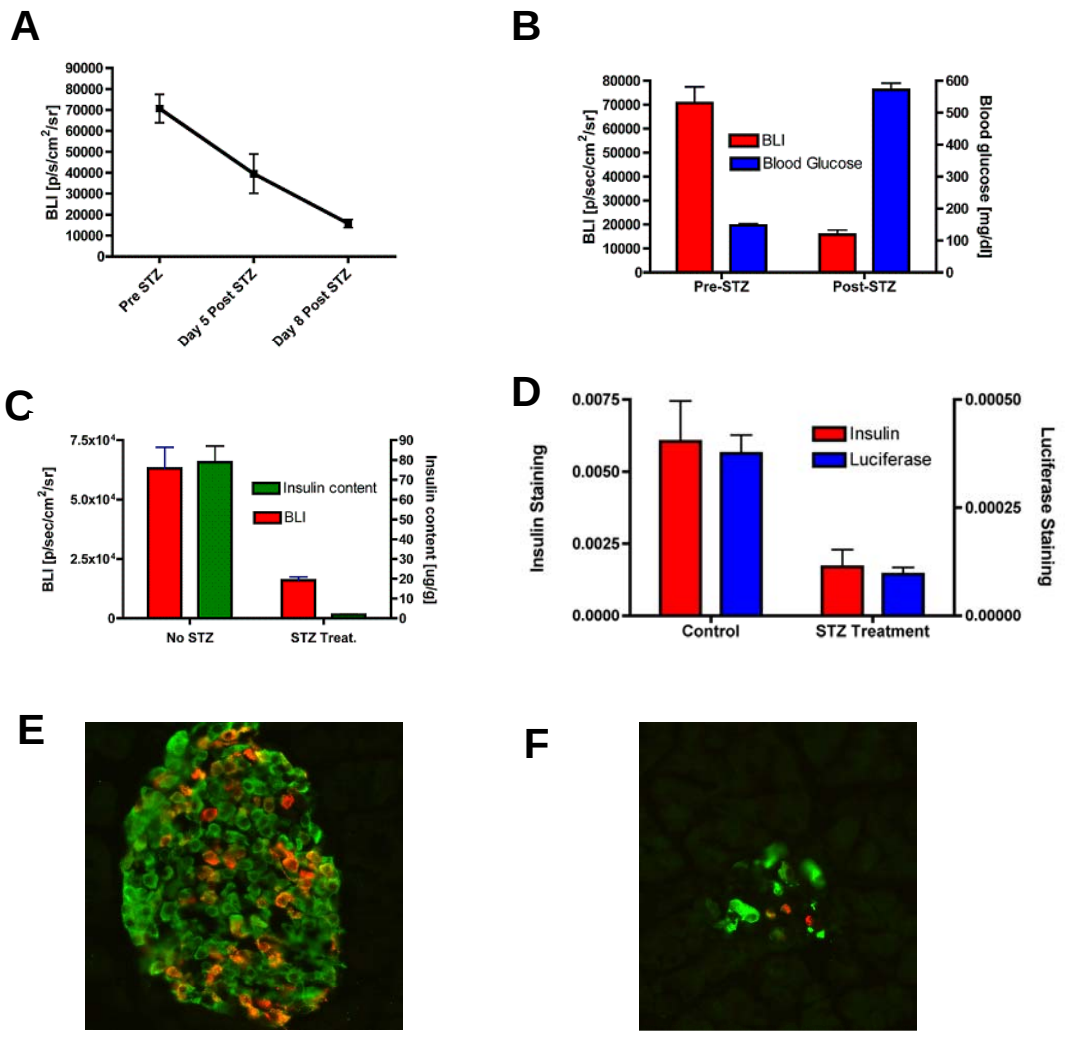

Figure 4.4. Effect of STZ-induced diabetes on bioluminescence. (A) After injection of STZ there is a gradual decrease in BLI values (n = 4). (B) Bioluminescence intensity has dropped 8 days after STZ, whereas blood glucose levels have increased to diabetic levels (n = 4). (C) Mice exposed to STZ treatment for 8 days have reduced bioluminescence intensity and lower pancreatic insulin content compared with untreated control mice (n = 4). (D) Morphometric measurements of insulin and luciferase staining demonstrate that approximately 30% of beta cells express luciferase. After STZ treatment, morphometric measurements of both insulin and luciferase expression drop by the same proportion, indicated that cell death of luciferase-expressing cells is the same as other insulin-producing cells. (E) Immunocytochemistry of control islet stained for insulin in green and luciferase in red. (F) Immunocytochemistry of an islet from 8 days after STZ treatment. There is notable loss of both insulin staining and luciferase staining. Note the higher level of luciferase staining, indicating that the diabetic state induces high luciferase production.

a normal control animal; Figure 4F shows a representative islet from an STZ-treated animal. There is an obvious decrease in both beta cells and luciferase-expressing cells.

However, the luciferase expression in the STZ-treated animal (Figure 4.4F) stains much more intensely, indicated higher levels of luciferase within these cells.

A longer duration study of STZ administration compared a cohort of mice treated with the same STZ dosage as the previous study (175 mg/kg) with a cohort receiving only 100 mg/kg STZ, a concentration insufficient to induce overt hyperglycemia. One month after STZ administration, the fasting blood glucose levels of mice treated with the high STZ dosage rose to 589 ± 18 mg/dl, whereas mice receiving the lower STZ dose reached blood glucose levels of 238 ± 72 mg/dl. Over the course of the study, mice receiving the high STZ dosage demonstrated a drop in BLI intensity, while mice receiving the lower dose had a slight increase in BLI (Figure 4.5). At the end of one month, the pancreata of diabetic mice receiving the high STZ dose contained 5.4 ± 2.3 μg insulin per gram pancreas, while the pancreata of non-diabetic animals contained 100.1 ± 20.4 μg insulin per gram pancreas.

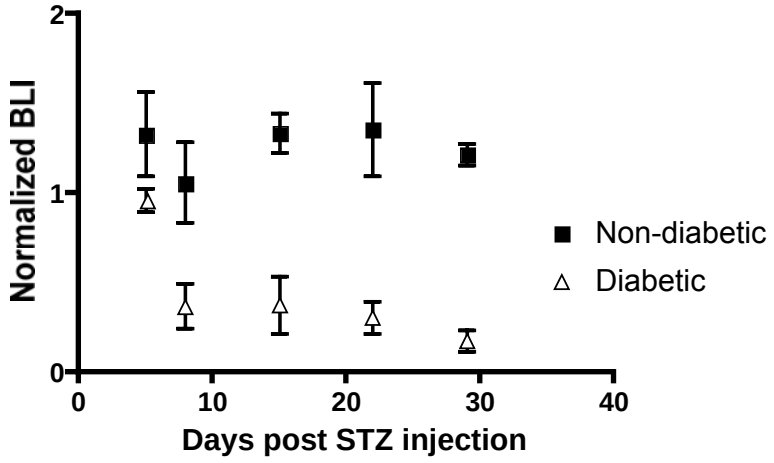

Figure 4.5. Long term effect of STZ-induced diabetes on bioluminescence. Non-diabetic mice treated with a low STZ dose (100 mg/kg) that does not result in diabetes display constant bioluminescence for 1 month after STZ treatment. Mice treated with a high dose of STZ (175 mg/kg) become diabetic and show a sharp loss of bioluminescence intensity at 1 week after STZ treatment.

4.3.5. In Vivo Imaging of Transplanted Islets

Transgenic insulin-luciferase islets transplanted into the renal capsule (Figure 4.6A) or liver via portal vein infusion (Figure 4.6B) were visible in the expected anatomical location. Islets transplanted to the renal capsule continued to emit bioluminescence 5 months after transplantation (data not shown). Three-dimensional reconstruction of transplanted bioluminescent islets was performed for both kidney and liver transplants. Islets transplanted to the renal capsule were reconstructed as smaller, contiguous grafts (Figure 4.6C), consistent with graft appearance upon removal. Islets transplanted through the portal vein were more dispersed: bioluminescent reconstruction revealed the location of these islets scattered throughout the liver (Figure 4.6D).

Transgenic insulin-luciferase islets transplanted to the kidney capsule were imaged 4 weeks after transplantation using BLI; grafts were subsequently excised and assayed for insulin content. The insulin content of islet grafts correlated with the number of islets transplanted ($R^2 = 0.4633$). However, there was a wide range in insulin content at each number of islets (Figure 4.6E). There was stronger correlation between the insulin content of grafts and bioluminescence intensity ($R^2 = 0.6742$). Bioluminescence is a better predictor of graft insulin content than the number of islets transplanted.

4.4. Discussion

A method capable of non-invasively assessing the pancreatic beta cell would enable novel studies of beta cell growth and death in the diabetic state and aid the development of new treatments. Such a technique would also be useful in studies of transplanted islets, facilitating studies of islet engraftment and survival. This manuscript details studies generating and characterizing a transgenic mouse line expressing luciferase under control of the mouse insulin I promoter. The expression of luciferase in

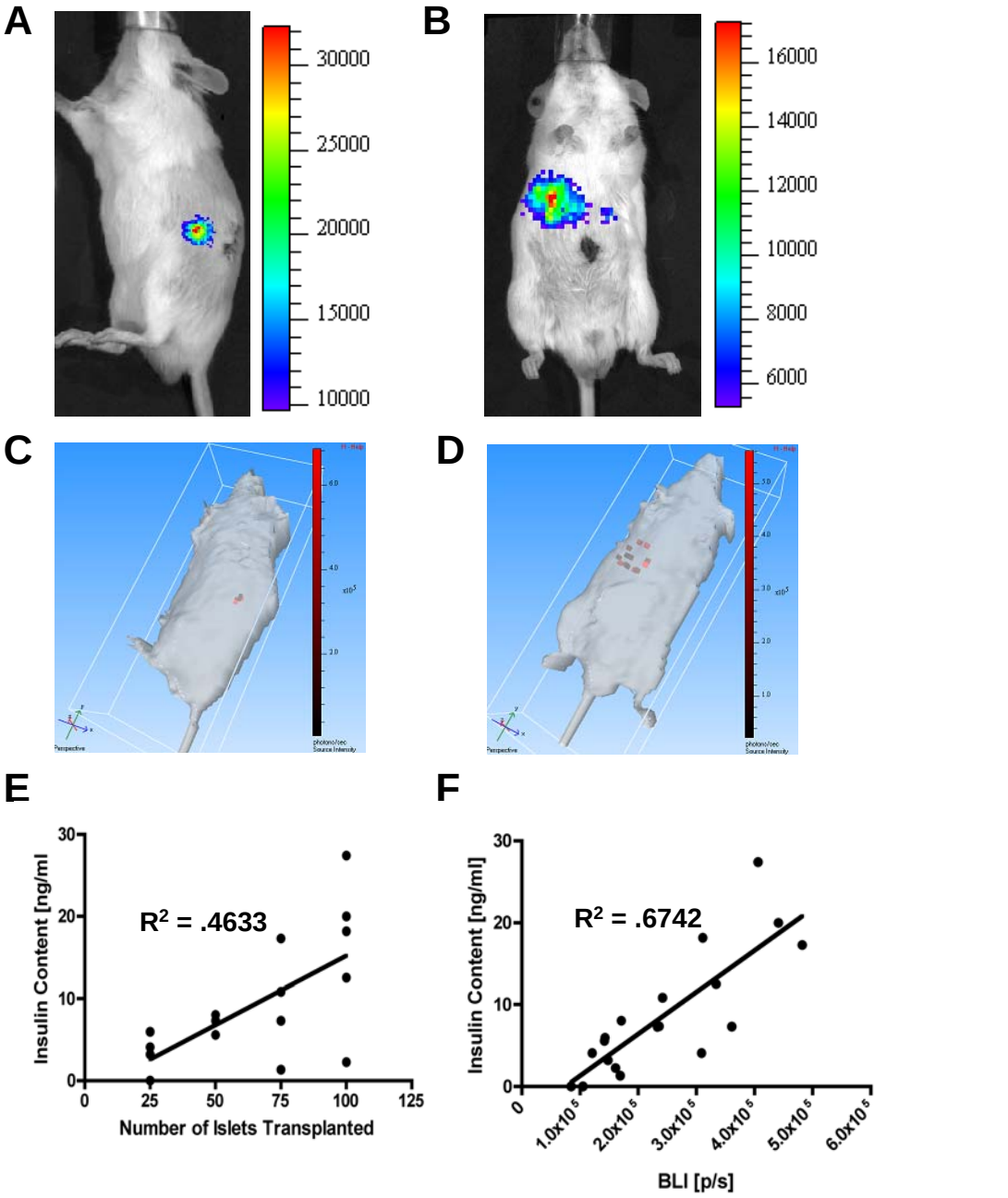

Figure 4.6. Transplantation of transgenic MIP-Luc islets. (A) Seventy five transgenic islets transplanted to the renal capsule emitted light emission from the kidney after injection of luciferin. (B) Two hundred transgenic islets transplanted to the liver via portal vein infusion emitted strong light emission from the liver after injection of luciferin. (C) Three dimensional bioluminescence reconstruction of the mouse pictured in A. The red voxels indicate the location of islets transplanted to the kidney. (D) Three dimensional bioluminescence reconstruction of the mouse pictured in B. The red voxels indicate the location of islets transplanted to the liver. (E) Quantification of bioluminescence from islets transplanted to the renal capsule 4 weeks after transplantation. Islets were transplanted in quantities of 25, 50, 75, and 100 islets (n = 4-5 per group). Bioluminescence correlates with the number of islets transplanted. (F) Bioluminescence shows stronger correlation with the insulin content of islet grafts. Thus bioluminescence is a better metric of the number of islets surviving post transplantation than the number of islets originally transplanted.

the beta cells of these animals provides an optical label which can be imaged non-invasively and repeatedly in small animal models using a technique known as bioluminescence imaging (BLI) [33-35]. While BLI is not applicable to human studies, its use in small animal models provides a link between *in vitro* studies and clinical application. The described studies builds upon our previous work using a viral vector to label islets with luciferase [36,37], achieving beta cell specificity and the abolishing the need for *in vitro* islet labeling. Furthermore, as the transgene is now integrated into the islet genome, this technique can be used to track islet proliferation.

One concern with transgenic animals is whether expression of the transgene alters normal functioning. Rigorous functional testing ensured that transgenic animals exhibited no alteration in islet function. Immunocytochemistry confirmed normal islet architecture and uniform luciferase expression throughout the beta cell population of the islet, with approximately 20% of beta cells expressing luciferase.

Other groups have generated similar transgenic mouse models for studies using bioluminescence [39-41]. Studies published using these islets found increased light emission from islets exposed to hyperglycemic states *in vitro* [39,40]. We encountered similar results: higher glucose levels stimulated higher luciferase expression and thus higher bioluminescence intensity. This finding has implications for studies of diabetic mouse models, as hyperglycemia may affect the bioluminescence signal. Our studies using an STZ-induced model of diabetes indicate that beta cell apoptosis, as evidenced by hyperglycemia and a drop in pancreatic insulin content, is accompanied by a drop in bioluminescence. However, the magnitude of bioluminescence loss is not as great as the decrease in insulin content. Morphometric measurements of insulin and luciferase expression indicate that beta cells labeled with luciferase apoptosis at the same rate as unlabeled beta cells after STZ administration. Thus transgene expression does not seem to alter STZ responsiveness of a beta cell. However, luciferase staining of islets

from STZ treated animals appears much brighter than control animals, indicating higher luciferase content in these islets. Pancreatic insulin content measurements are needed to ensure that hyperglycemia induces higher luciferase expression. The up regulation of luciferase expression due to hyperglycemia is most likely due to glucose-mediated regulation of insulin gene expression. The practical implication of this finding is that while bioluminescence intensity does decline due to beta cell death, the BLI magnitude may not accurately reflect beta cell mass in hyperglycemic states. BLI is rather a measure of beta cell mass incorporating some aspects of islet function.

The application of transgenic bioluminescent islets to transplant studies enables non-invasive tracking of islet grafts. Our studies illustrate a common issue with islet transplantation: the number of islets actually engrafting can differ greatly. Thus the number of islets initially transplanted shows weak correlation with graft insulin content. However, bioluminescence imaging can provide a better metric of surviving islet mass. Bioluminescence measurements correlate more strongly with graft insulin content.

Bioluminescence measurements of transgenic mice expressing luciferase under control of the mouse insulin I promoter can provide non-invasive measures of islet mass. Bioluminescence measurements correlate with the number of transgenic islets. However, luciferase expression is affected by glucose levels, complicating application to diabetic models. Studies applying this model must take hyperglycemia into account for accurate quantification of beta cell mass. This transgenic animal should be useful for future studies of the beta cell in diabetic models and transplant settings and pre-clinical evaluation of treatment interventions.

4.5. Works Cited

1. C. Bernard-Kargar, and A. Ktorza. "Endocrine pancreas plasticity under physiological and pathological conditions." *Diabetes*. 50 Suppl 1(S30-5 (2001).

2. S. Sreenan, A. J. Pick, M. Levisetti, A. C. Baldwin, W. Pugh, and K. S. Polonsky. "Increased beta-cell proliferation and reduced mass before diabetes onset in the nonobese diabetic mouse." *Diabetes*. 48(5), 989-96 (1999).

3. G. C. Weir, S. Bonner-Weir, and J. L. Leahy. "Islet mass and function in diabetes and transplantation." *Diabetes*. 39(4), 401-5 (1990).

4. B. Hirshberg, K. I. Rother, I. B. Digon, J. Venstrom, and D. M. Harlan. "State of the art: islet transplantation for the cure of type 1 diabetes mellitus." *Rev Endocr Metab Disord*. 4(4), 381-9 (2003).

5. C. Ricordi. "Islet transplantation: a brave new world." *Diabetes*. 52(7), 1595-603 (2003).

6. R. P. Robertson. "Islet transplantation as a treatment for diabetes - a work in progress." *N Engl J Med*. 350(7), 694-705 (2004).

7. A. M. Shapiro, J. R. Lakey, E. A. Ryan, G. S. Korbutt, E. Toth, G. L. Warnock, N. M. Kneteman, and R. V. Rajotte. "Islet transplantation in seven patients with type 1 diabetes mellitus using a glucocorticoid-free immunosuppressive regimen." *N Engl J Med*. 343(4), 230-8 (2000).

8. D. K. McCulloch, D. J. Koerker, S. E. Kahn, S. Bonner-Weir, and J. P. Palmer. "Correlations of in vivo beta-cell function tests with beta-cell mass and pancreatic insulin content in streptozocin-administered baboons." *Diabetes*. 40(6), 673-9 (1991).

9. W. Gepts, and P. M. Lecompte. "The pancreatic islets in diabetes." *Am J Med*. 70(1), 105-15 (1981).

10. L. L. Kjems, B. M. Kirby, E. M. Welsh, J. D. Veldhuis, M. Straume, S. S. McIntyre, D. Yang, P. Lefebvre, and P. C. Butler. "Decrease in beta-cell mass leads to impaired pulsatile insulin secretion, reduced postprandial hepatic insulin clearance, and relative hyperglucagonemia in the minipig." *Diabetes*. 50(9), 2001-12 (2001).

11. M. O. Larsen, C. F. Gotfredsen, M. Wilken, R. D. Carr, N. Porksen, and B. Rolin. "Loss of beta-cell mass leads to a reduction of pulse mass with normal periodicity, regularity and entrainment of pulsatile insulin secretion in Gottingen minipigs." *Diabetologia*. 46(2), 195-202 (2003).

12. M. O. Larsen, B. Rolin, M. Wilken, R. D. Carr, and C. F. Gotfredsen. "Measurements of insulin secretory capacity and glucose tolerance to predict pancreatic beta-cell mass in vivo in the nicotinamide/streptozotocin Gottingen minipig, a model of moderate insulin deficiency and diabetes." *Diabetes*. 52(1), 118-23 (2003).

13. K. Saito, N. Yaginuma, and T. Takahashi. "Differential volumetry of A, B and D cells in the pancreatic islets of diabetic and nondiabetic subjects." *Tohoku J Exp Med*. 129(3), 273-83 (1979).

14. S. Bonner-Weir, D. F. Trent, and G. C. Weir. "Partial pancreatectomy in the rat and subsequent defect in glucose-induced insulin release." *J Clin Invest*. 71(6), 1544-53 (1983).

15. A. M. Davalli, Y. Ogawa, L. Scaglia, Y. J. Wu, J. Hollister, S. Bonner-Weir, and G. C. Weir. "Function, mass, and replication of porcine and rat islets transplanted into diabetic nude mice." *Diabetes*. 44(1), 104-11 (1995).

16. A. M. Davalli, Y. Ogawa, C. Ricordi, D. W. Scharp, S. Bonner-Weir, and G. C. Weir. "A selective decrease in the beta cell mass of human islets transplanted into diabetic nude mice." *Transplantation*. 59(6), 817-20 (1995).

17. P. E. Lacy. "The pancreatic beta cell. Structure and function." *N Engl J Med*. 276(4), 187-95 (1967).

18. B. W. Paty, S. Bonner-Weir, M. R. Laughlin, A. J. McEwan, and A. M. Shapiro. "Toward development of imaging modalities for islets after transplantation: insights from the National Institutes of Health Workshop on Beta Cell Imaging." *Transplantation*. 77(8), 1133-7 (2004).

19. B. Gimi, L. Leoni, J. Oberholzer, M. Braun, J. Avila, Y. Wang, T. Desai, L. H. Philipson, R. L. Magin, and B. B. Roman. "Functional MR microimaging of pancreatic beta-cell activation." *Cell Transplant*. 15(2), 195-203 (2006).

20. N. V. Evgenov, Z. Medarova, G. Dai, S. Bonner-Weir, and A. Moore. "In vivo imaging of islet transplantation." *Nat Med*. 12(1), 144-8 (2006).

21. J. Kriz, D. Jirak, P. Girman, Z. Berkova, K. Zacharovova, E. Honsova, A. Lodererova, M. Hajek, and F. Saudek. "Magnetic resonance imaging of pancreatic islets in tolerance and rejection." *Transplantation*. 80(11), 1596-603 (2005).

22. D. Jirak, J. Kriz, V. Herynek, B. Andersson, P. Girman, M. Burian, F. Saudek, and M. Hajek. "MRI of transplanted pancreatic islets." *Magn Reson Med*. 52(6), 1228-33 (2004).

23. Q. Zheng, H. Dai, M. E. Merritt, C. Malloy, C. Y. Pan, and W. H. Li. "A new class of macrocyclic lanthanide complexes for cell labeling and magnetic resonance imaging applications." *J Am Chem Soc*. 127(46), 16178-88 (2005).

24. Y. Lu, H. Dang, B. Middleton, Z. Zhang, L. Washburn, D. B. Stout, M. Campbell-Thompson, M. A. Atkinson, M. Phelps, S. S. Gambhir, J. Tian, and D. L. Kaufman. "Noninvasive imaging of islet grafts using positron-emission tomography." *Proc Natl Acad Sci U S A*. 103(30), 11294-9 (2006).

25. C. Toso, H. Zaidi, P. Morel, M. Armanet, A. Andres, N. Pernin, R. Baertschiger, D. Slosman, L. H. Buhler, D. Bosco, and T. Berney. "Positron-emission

tomography imaging of early events after transplantation of islets of Langerhans." *Transplantation*. 79(3), 353-5 (2005).

26. P. B. Clark, H. D. Gage, C. Brown-Proctor, N. Buchheimer, J. Calles-Escandon, R. H. Mach, and K. A. Morton. "Neurofunctional imaging of the pancreas utilizing the cholinergic PET radioligand [18F]4-fluorobenzyltrozamicol." *Eur J Nucl Med Mol Imaging*. 31(2), 258-60 (2004).

27. A. Moore, S. Bonner-Weir, and R. Weissleder. "Noninvasive in vivo measurement of beta-cell mass in mouse model of diabetes." *Diabetes*. 50(10), 2231-6 (2001).

28. L. Ladriere, F. Malaisse-Lagae, R. Alejandro, and W. J. Malaisse. "Pancreatic fate of a (125)I-labelled mouse monoclonal antibody directed against pancreatic B-cell surface ganglioside(s) in control and diabetic rats." *Cell Biochem Funct*. 19(2), 107-15 (2001).

29. S. Schneider, P. J. Feilen, M. Schreckenberger, M. Schwanstecher, C. Schwanstecher, H. G. Buchholz, O. Thews, K. Oberholzer, A. Korobeynikov, A. Bauman, S. Comagic, M. Piel, E. Schirrmacher, C. Y. Shiue, A. A. Alavi, P. Bartenstein, F. Rosch, M. M. Weber, H. H. Klein, and R. Schirrmacher. "In vitro and in vivo evaluation of novel glibenclamide derivatives as imaging agents for the non-invasive assessment of the pancreatic islet cell mass in animals and humans." *Exp Clin Endocrinol Diabetes*. 113(7), 388-95 (2005).

30. F. Souza, N. Simpson, A. Raffo, C. Saxena, A. Maffei, M. Hardy, M. Kilbourn, R. Goland, R. Leibel, J. J. Mann, R. Van Heertum, and P. E. Harris. "Longitudinal noninvasive PET-based beta cell mass estimates in a spontaneous diabetes rat model." *J Clin Invest*. 116(6), 1506-13 (2006).

31. I. R. Sweet, D. L. Cook, A. Lernmark, C. J. Greenbaum, and K. A. Krohn. "Non-invasive imaging of beta cell mass: a quantitative analysis." *Diabetes Technol Ther*. 6(5), 652-9 (2004).

32. I. R. Sweet, D. L. Cook, A. Lernmark, C. J. Greenbaum, A. R. Wallen, E. S. Marcum, S. A. Stekhova, and K. A. Krohn. "Systematic screening of potential beta-cell imaging agents." *Biochem Biophys Res Commun*. 314(4), 976-83 (2004).

33. C. H. Contag, S. D. Spilman, P. R. Contag, M. Oshiro, B. Eames, P. Dennery, D. K. Stevenson, and D. A. Benaron. "Visualizing gene expression in living mammals using a bioluminescent reporter." *Photochem Photobiol*. 66(4), 523-31 (1997).

34. A. Rehemtulla, L. D. Stegman, S. J. Cardozo, S. Gupta, D. E. Hall, C. H. Contag, and B. D. Ross. "Rapid and quantitative assessment of cancer treatment response using in vivo bioluminescence imaging." *Neoplasia*. 2(6), 491-5 (2000).

35. B. W. Rice, M. D. Cable, and M. B. Nelson. "In vivo imaging of light-emitting probes." *J Biomed Opt*. 6(4), 432-40 (2001).

36. J. Virostko, Z. Chen, M. Fowler, G. Poffenberger, A. C. Powers, and E. D. Jansen. "Factors influencing quantification of in vivo bioluminescence imaging: application to assessment of pancreatic islet transplants." *Mol Imaging*. 3(4), 333-42 (2004).

37. M. Fowler, J. Virostko, Z. Chen, G. Poffenberger, A. Radhika, M. Brissova, M. Shiota, W. E. Nicholson, Y. Shi, B. Hirshberg, D. M. Harlan, E. D. Jansen, and A. C. Powers. "Assessment of pancreatic islet mass after islet transplantation using in vivo bioluminescence imaging." *Transplantation*. 79(7), 768-76 (2005).

38. Y. Lu, H. Dang, B. Middleton, Z. Zhang, L. Washburn, M. Campbell-Thompson, M. A. Atkinson, S. S. Gambhir, J. Tian, and D. L. Kaufman. "Bioluminescent monitoring of islet graft survival after transplantation." *Mol Ther*. 9(3), 428-35 (2004).

39. S. J. Smith, H. Zhang, A. O. Clermont, A. C. Powers, D. B. Kaufman, A. F. Purchio, and D. West. "In Vivo Monitoring of Pancreatic beta-Cells in a Transgenic Mouse Model." *Mol Imaging*. 5(2), (2006).

40. S. Y. Park, X. Wang, Z. Chen, A. C. Powers, M. A. Magnuson, W. S. Head, D. W. Piston, and G. I. Bell. "Optical imaging of pancreatic beta cells in living mice expressing a mouse insulin I promoter-firefly luciferase transgene." *Genesis*. 43(2), 80-6 (2005).

41. X. Chen, X. Zhang, C. S. Larson, M. S. Baker, and D. B. Kaufman. "In vivo bioluminescence imaging of transplanted islets and early detection of graft rejection." *Transplantation*. 81(10), 1421-7 (2006).

42. W. Zhang, J. Q. Feng, S. E. Harris, P. R. Contag, D. K. Stevenson, and C. H. Contag. "Rapid in vivo functional analysis of transgenes in mice using whole body imaging of luciferase expression." *Transgenic Res*. 10(5), 423-34 (2001).

43. M. Brissova, M. Fowler, P. Wiebe, A. Shostak, M. Shiota, A. Radhika, P. C. Lin, M. Gannon, and A. C. Powers. "Intraislet endothelial cells contribute to revascularization of transplanted pancreatic islets." *Diabetes*. 53(5), 1318-25 (2004).

44. T. Wang, I. Lacik, M. Brissova, A. V. Anilkumar, A. Prokop, D. Hunkeler, R. Green, K. Shahrokhi, and A. C. Powers. "An encapsulation system for the immunoisolation of pancreatic islets." *Nat Biotechnol*. 15(4), 358-62 (1997).

45. M. Brissova, M. Shiota, W. E. Nicholson, M. Gannon, S. M. Knobel, D. W. Piston, C. V. Wright, and A. C. Powers. "Reduction in pancreatic transcription factor PDX-1 impairs glucose-stimulated insulin secretion." *J Biol Chem*. 277(13), 11225-32 (2002).

46. M. Brissova, M. J. Fowler, W. E. Nicholson, A. Chu, B. Hirshberg, D. M. Harlan, and A. C. Powers. "Assessment of human pancreatic islet architecture and composition by laser scanning confocal microscopy." *J Histochem Cytochem*. 53(9), 1087-97 (2005).

47. M. Brissova, M. Blaha, C. Spear, W. Nicholson, A. Radhika, M. Shiota, M. J. Charron, C. V. Wright, and A. C. Powers. "Reduced PDX-1 expression impairs islet response to insulin resistance and worsens glucose homeostasis." *Am J Physiol Endocrinol Metab*. 288(4), E707-14 (2005).

CHAPTER V

FACTORS INFLUENCING QUANTIFICATION OF *IN VIVO* BIOLUMINESCENCE IMAGING: APPLICATION TO ASSESSMENT OF PANCREATIC ISLET TRANSPLANTS

John Virostko[1], Zhongyi Chen[2], Michael Fowler[2], Greg Poffenberger[2],

Alvin C. Powers[2,3], E. Duco Jansen[1]

[1]Department of Biomedical Engineering, Vanderbilt University, Nashville, TN 37235

[2]Department of Medicine, Division of Diabetes, Endocrinology, and Metabolism,

Vanderbilt University, Nashville, TN 37232

[3]VA Tennessee Valley Healthcare System, Nashville, TN 37212

Portions of this manuscript have been published in:

"Factors influencing quantification of in vivo bioluminescence imaging:

application to assessment of pancreatic islet transplants,"

Mol Imaging. 3(4), 333-42 (2004).

5.1. Abstract

The aim of this study is to determine and characterize factors influencing *in vivo* bioluminescence imaging (BLI) and apply them to the specific application of imaging transplanted pancreatic islets. Non-invasive, quantitative assessment of transplanted pancreatic islets poses a formidable challenge. Murine pancreatic islets expressing firefly luciferase were transplanted under the renal capsule or into the portal vein of NOD-SCID mice and the bioluminescence was quantified with a cooled CCD camera and digital photon image analysis. The important, but often neglected, effects of wound healing, mouse positioning, and transplantation site on bioluminescence measurements were investigated by imaging a constant emission, isotropic light-emitting bead (λ=600) implanted at the renal or hepatic site. The renal beads emitted nearly 4 times more light than hepatic beads with a smaller spot size, indicating that light absorption and scatter are greatly influenced by the transplant site and must be accounted for in BLI measurements. Detected luminescence decreased with increasing angle between the mouse surface normal and optical axis. By defining imaging parameters such as post-surgical effects, animal positioning, and light attenuation as a function of transplant site, this study develops BLI as a useful imaging modality for quantitative assessment of islets post transplantation.

5.2. Introduction

Pancreatic islet transplantation has great potential for the treatment of type 1 diabetes mellitus [1-3]. However, the number of transplanted islets needed to overcome diabetes presents a major obstacle precluding islet transplantation from being adopted as a routine treatment. In addition, diabetes reversal in most patients requires islets

isolated from at least two donor pancreata [2]; the supply of donor pancreata for islet isolation falls well short of the number needed to treat type 1 diabetics in the United States [2,3]. Thus, significant efforts are focused on preserving or increasing islet mass post transplantation [4-6]. The survival rate of transplanted islets is incompletely defined; in addition to immune factors, studies indicate that hypoxia, nutrient deprivation, and inflammation hamper islet engraftment and survival and result in significant islet loss in the early post-transplantation period [7,8]. Efforts to overcome these obstacles are limited because no suitable method of non-invasively measuring the number of surviving islets or islet mass currently exists. Islet mass is commonly estimated from insulin secretion following glucose tolerance testing, but this method assesses islet function, which does not necessarily correlate with islet mass. Morphometric analysis of histological sections of islet grafts can be used to measure islet mass, but requires removal of the organ containing the islets, preventing any sequential studies [9]. Additionally, this morphometric analysis is difficult to perform when islets are scattered, as they are when embolized throughout the liver, the most common site of transplant [2,3].

This study seeks to further develop *in vivo* bioluminescence imaging (BLI) as a method to quantify the number of islets surviving post transplantation. BLI refers to the generation of photons by a biologic source such as cells or bacteria as a result of an ATP- and oxygen-dependent enzyme reaction (usually luciferase) with the enzyme substrate [10,11]. BLI has been utilized to assess a number of biologic processes such as inflammation, wound healing, and tumor cell growth in vivo [12-15]. As recently described by Lu and colleagues [16] and by our group [Fowler et al, manuscript submitted], BLI has recently shown promise for monitoring transplanted pancreatic islets. However, a number of imaging parameters remain undefined and these must be addressed before BLI can be used to accurately quantify transplanted islet mass. For

example, islets are commonly transplanted to different anatomical locations in animal models. Correlation of light emission and transplanted islet mass must take into account the factors that influence light transmission from the bioluminescent source to the CCD camera aperture. Light transmission is determined by the optical properties of the tissue through which the light must pass [17]; different islet graft locations are subject to different degrees of light attenuation. In this report, constant emission, isotropic light-emitting beads with spectral emission similar to the luciferase reaction were implanted beneath the renal capsule or into the liver of mice to serve as a model of transplanted islet bioluminescence. The luminescent beads provide a constant, known light intensity that is reliable and reproducible, allowing for validation and calibration of the imaging method. In contrast, bioluminescent islets are subject to biological variability as islet light emission depends on the health and size of the islets and survival of islets post transplantation. The effects of wound healing, mouse positioning, and light attenuation by tissues overlying the islet grafts were determined by imaging these bead-bearing mice to identify factors that must be taken into account when correlating light emission with islet mass. While applied to the BLI of transplanted islets, the findings in this study are relevant for quantitative BLI in general where subtleties of confounding factors that may alter the amount of light detected are often ignored.

5.3. Materials & Methods

5.3.1. Animal Model

NOD-SCID mice from Jackson Laboratories (Bar Harbor, Maine) were used for transplant studies as previously described [18]. The NOD-SCID strain is homozygous for the severe combined immune deficiency (SCID) spontaneous mutation,

characterized by an absence of functional T cells and B cells. The NOD-SCID strain accepts allografts without immune rejection.

5.3.2. Mouse Islet Isolation and Luciferase Expression

Murine pancreatic islets were isolated from adult B6D2 mice as previously described [18]. Briefly, mouse pancreata were digested with collagenase P (Roche Molecular Biochemicals, Indianapolis, IN) in Hanks buffered saline (0.6 mg/ml) using a wrist action shaker. Some islets were then handpicked under microscopic guidance. Others were purified by histopaque gradient centrifugation and washed 3 times with 10 mM PBS containing 1% mouse serum. Islets were suspended in 30 μL of 10 mM PBS with 1% mouse serum for transplantantion. Murine islets were cultured in RPMI 1640 (Invitrogen, Carlsbad, CA) with 10% Fetal Bovine Serum (Invitrogen, Carlsbad, CA) and 11 mM glucose. Islets were infected with a recombinant adenovirus that bicistronically encodes the dual reporter genes luciferase and green fluorescence protein (Adv-luciferase) under control of the CMV promoter at a multiplicity of infection (MOI) of 1000 for 16 hours using techniques previously described [19]. Luciferase activity of extracts from islets transduced with Adv-luciferase was measured in a Pharmingen Monolight 3010 Luminometer.

5.3.3. Islet Transplantation

Murine islets were transplanted beneath the renal capsule or infused into the portal vein of NOD-SCID mice as previously described [18]. Briefly, the islet suspension was injected in a 30 μL volume just beneath the renal capsule with a 23-gauge butterfly needle. The needle was withdrawn and the insertion point was cauterized. For the hepatic transplants, islets were infused into the portal vein via PE10 tubing attached to a

30-gauge needle. Slight pressure was applied to the insertion point to stop blood loss. Incisions were closed with black subcutaneous sutures (Prolene, Ethicon, Somerville, NJ) and aluminum skin staples (Autoclips, 9 mm size, Clay Adams, Parsippany, NJ). Clips were removed six days after surgery.

5.3.4. Luminescent Beads

As a surrogate for luciferase-expressing islets, we used luminescent beads (Mb-Microtec, Bern, Switzerland) that consisted of glass capillaries (0.9 mm diameter and 2 mm long). These beads are filled with tritium (a β-emitter with a half life of over 10 years) that excites a phosphor and isotropically emits constant intensity light (Figures 5A, 5B). The spectral emission of these beads was measured using a fiber optic probe attached to a spectrometer (Ocean Optics Inc., Dunedin, FL) equipped with a 360 nm cutoff filter. Spectral emission of a single bead within a centrifuge tube was measured with one-second integration time. An attached laptop computer was used to record the spectral data. To implant a luminescent bead in a NOD-SCID mouse, an incision was made above either the kidney or liver, as described previously for the islet transplantations [18]. The luminescent bead was glued onto the kidney or liver at a site that was deemed anatomically similar to the site of islet engraftment using Vetbond™ tissue adhesive (3M, St. Paul, Minnesota). The incision was closed with subcutaneous sutures and skin staples as previously described [18].

5.3.5. Bioluminescence Imaging

For luminescence imaging of islets and beads, we used a liquid nitrogen cooled, back thinned, back illuminated charge coupled device (CCD) camera with a 1300x1340 pixel chip (EEV 1300 series, Roper Scientific, Trenton, NJ). Prior to luminescent imaging a black and white image of the field of view was taken to allow correlation of the

bioluminescent signal to anatomical sites on the animal. A one-millisecond background image (shutter closed) was taken prior to each bioluminescence image. Background subtraction was performed on all images. Metamorph software (Version 4.6r6, Universal Imaging Corporation, Downingtown, PA) was used to analyze the bioluminescence image with peak intensity [regions of equal area were drawn around the region of interest (ROI)]. On chip binning of 5 was used for imaging to increase signal to noise ratio. Pixel intensities within the ROI were summed to yield integrated intensity of luminescence.

5.3.6. Islet Bioluminescence Imaging

For in vitro imaging, the luciferase substrate D-Luciferin (Biosynth International, Naperville, IL) was added in excess (10 μL of 0.15 mg/ml concentration) to murine islets in 6 well plates with 100 μl of phosphate-buffered saline (PBS). After placing the plate in the imaging chamber, bioluminescence was imaged with a four-minute exposure taken with the CCD camera. Light emission was integrated from 2 minutes to 6 minutes after luciferin addition to capture peak bioluminescence activity. To image mice bearing transplants of luciferase-expressing pancreatic islets, the hair overlying the islet graft was shaved in the anesthetized mice (intra-peritoneal injection of 50 mg/kg body weight sodium pentobarbital). The substrate D-luciferin, dissolved in sterile de-ionized water, was injected intra-peritoneally (150 mg/kg body weight). Mice were gently secured to a black felt pad to minimize any motion artifacts in lateral decubitis orientation (graft facing up) for renal grafts and supine orientation for hepatic grafts. This pad was then placed in the light-tight imaging chamber. Bioluminescence images were taken with four-minute integration time. Luminescence emission was found to peak/plateau approximately 8

minutes post substrate administration, hence images used for quantification was taken from approximately 6 minutes post luciferin administration to 10 minutes post injection.

5.3.7. Imaging of Luminescent Beads

Prior to implantation, a black felt pad holding the luminescent beads was imaged with the CCD camera. Beads were first imaged with a 1 second exposure time and then re-imaged 4 times, reorienting the bead between each image, in order to quantify variability in bead light emission. Bead luminescence was quantified using circles of equal area drawn around the ROI. Luminescence was quantified by summing pixel intensities within the ROI to yield integrated intensity.

Imaging of mice with an implanted bead was performed as described above for mice bearing islet transplants except no luciferin was injected. A one second exposure was taken for all images. Background subtraction was performed and implanted bead luminescence was quantified by photon counting of the ROI. Spot size was determined using Metamorph. The maximum intensity pixel from each bead was found and measured. A threshold was then applied at half the maximum intensity for all pixels above that value. The number of pixels exceeding threshold was determined. This area is the spot size; full width at half maximum (FWHM) was calculated as the diameter of this circular spot size.

$$FWHM = \sqrt{\frac{4 \cdot Area_{threshold}}{\pi}} \tag{5.1}$$

5.3.8. Rotational Variability Study

The effect of mouse rotation (relative to the imaging axis) on the measured photon flux from an implanted bead was measured using a rotational stage (Figure 5A, 5B). This stage consisted of a hinged black felt platform that allowed 50-degree rotation

in either direction. An anesthetized mouse with a luminescent bead was placed on the stage with the mouse gently secured in position with a black strap; the stage was then placed in the light-tight imaging box of the CCD camera. Mice with the bead on the renal capsule were placed in a lateral decubitis position (bead facing up); mice with a hepatic bead were placed in the supine position. The stage was rotated in ten-degree increments from –50 degrees to 50 degrees (with 0 degrees indicating parallel to the floor). Positive rotation was defined as clockwise rotation when viewed from the head of the mouse. Thus for renal beads, positive rotation was defined as rotation toward the prone orientation, while negative rotation indicated rotation towards the supine orientation. One-second camera exposures were taken at each angle. Luminescence was quantified using Metamorph's photon counting ROI analysis, as previously described. Luminescence at each angle was normalized to the measured luminescence at 0 degrees.

5.3.9. Monte Carlo Simulation

Monte Carlo simulation was used to model the propagation of photons from the luminescent bead to the aperture of the CCD camera. Monte Carlo simulation provides a well-accepted numerical simulation of light transport in multi-layer tissues close to tissue boundaries. Monte Carlo simulation has been used to model light propagation in a variety of applications [20-22]. The Monte Carlo code used was based on the MCML code developed by Steven Jacques and others, modified for isotropic sources [23]. Transmission of light through the tissue was determined as a function of radial position; photon transmission reaching the camera aperture was calculated as the photon weight transmitted within the radius of the camera aperture. Monte Carlo simulation was run for three conditions: the bead alone, the bead implanted in the renal capsule, and the bead implanted beneath the liver (Figure 5.3). The bead simulation consisted of a single layer

of non-absorbing, non-scattering media corresponding to the air between the camera stage and aperture. The renal bead simulation added a layer of skin to the air layer. The hepatic bead simulation added a layer of liver tissue to the skin and air layers for a three-layer model. Thickness of the tissue layers was determined by sacrificing the animal and measuring tissue thickness overlying the bead using calipers. Tissue optical properties used in the simulations were obtained from work by Cheong, et al. [24]. The following optical properties were used in simulation: Air layer: n = 1, g = 1, $\mu_a = 10^{-9}$ cm^{-1}, $\mu_s = 0$ cm^{-1}; Skin layer: n = 1.37, g = 0.9, $\mu_a = 10$ cm^{-1}, $\mu_s = 20$ cm^{-1}; Liver layer: n = 1.37, g = 0.9, $\mu_a = 9.6$ cm^{-1}, $\mu_s = 89$ cm^{-1}.

5.4. Results

5.4.1. Bioluminescence of Luciferase-Expressing Islets

Pancreatic islets transduced with an increasing MOI of Adv-luciferase expressed increasing luciferase activity (Figure 5.1A). For subsequent studies, a MOI of 1000 was used. Adenovirus infection of murine islets did not alter glucose-stimulated insulin secretion of islets in a cell perifusion system (data not shown). Luminescence of luciferase-expressing murine islets in culture was easily detected (Figure 5.1B) after addition of luciferin to the culture media. Bioluminescence intensity increased linearly with the number of islets/well. Two different anatomical sites are typically used for murine islet transplantation. Islets transplanted beneath the renal capsule form an islet graft localized in a small area; this site is widely used in murine models of islet transplantation. However, liver transplantation is more applicable to clinical studies, as the liver is the site of human islet transplantations. Following an intra-peritoneal

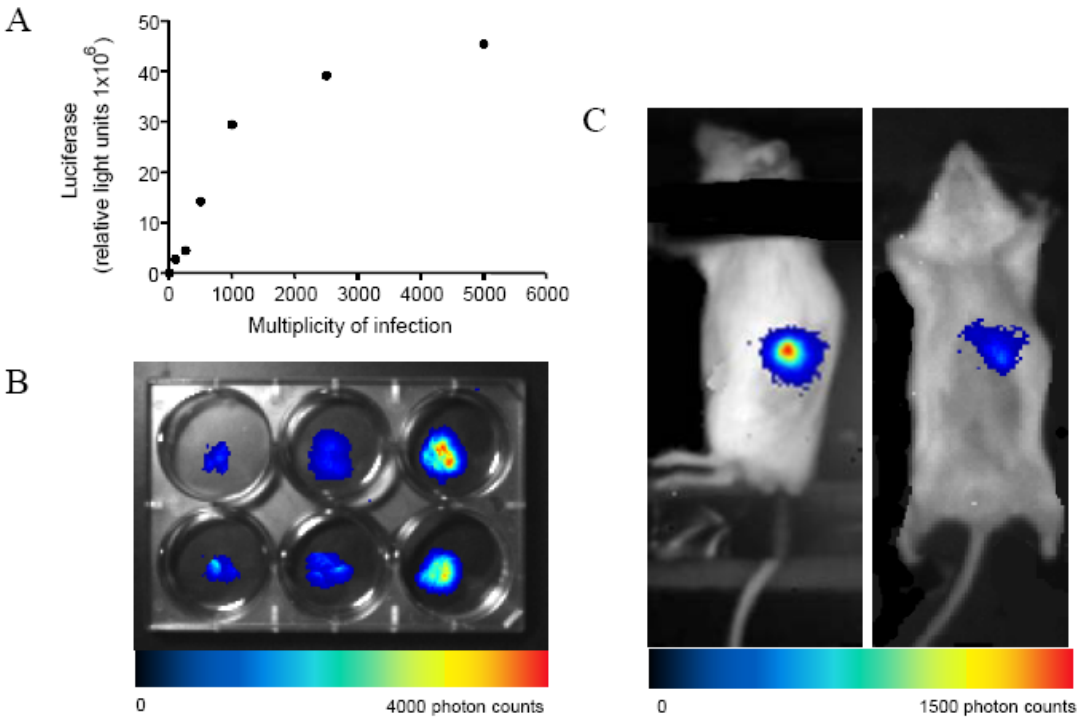

Figure 5.1. Luminescence of pancreatic islets expressing luciferase. (A) Luciferase activity of murine islets transduced with an increasing multiplicity of infection of Adv-luciferase (50 islets/point; expressed as number of viral particles/cell with the assumption of 500 cells/islet) was measured in a luminometer. (B) Luciferase-expressing murine islets in a six-well plate. Islets in quantities of 50, 100, and 200 islets from left to right; upper and lower rows duplicates. (C) Luciferase-expressing murine islets (100) transplanted beneath the renal capsule (left) or transplanted into liver (right).

injection of luciferin, bioluminescence emission was detected in mice bearing luciferase-expressing islets transplanted beneath the renal capsule or into the liver (Figure 5.1C).

5.4.2. Luminescent Beads In Vitro

Light emission from the luminescent beads was quantified using a CCD camera and integrated photon measurements (Figures 5.2A, 5.2B). Multiple images of the same bead resulted in similar photon measurements with less than 3% variation from mean (n=10). Additionally, photon measurements of the same bead did not change over a period of several months. Luminescent beads provide a constant light source with a half-life of 10 years and hence they can be considered isotropic and constant intensity emitters for the duration of the experiment. The spectral emission of these beads

measured using a fiber optic probe attached to a spectrometer was similar to that of light generated by the firefly luciferase reaction (Figure 5.2C).

5.4.3. Luminescent Beads In Vivo

Luminescent beads were implanted at the sites used for islet transplantation: the renal capsule and the liver (Figures 5.2D, 5.2E). The renal beads show a brighter, more concise region of luminescence. Light emission from the hepatic beads is less bright and spread over a larger area. Note the difference in scale between the two images.

Mice (n = 4) with luminescent beads implanted at the renal capsule were imaged weekly for 6 weeks post implantation to determine the temporal variation in luminescence intensity (Figure 5.2F). Bead intensity is quantified as the ratio of bead light luminescence in vivo (implanted bead) to the constant light emission of the bead in vitro (pre-implantation). At one-week post implantation, the mice with renal beads showed significantly lower luminescence than in later weeks (t-test, $\alpha = 0.05$). The detected luminescence increased two-fold over the week one measurement. Six weeks post implantation, the ratio of implanted bead luminescence to pre-implantation bead luminescence was 0.2394 +/- 0.0261. The renal beads also showed the greatest mouse to mouse difference in detected light the week immediately post implantation. By the second week post implantation the spread in detected light among different mice had decreased.

Luminescent beads implanted beneath the liver showed lower light emission (Figure 5.2F). In the first week post implantation, the detected luminescence was lower than in later weeks. At six weeks, the ratio of implanted bead intensity to pre-implantation bead intensity was at a steady state value of 0.0645 +/- 0.0140.

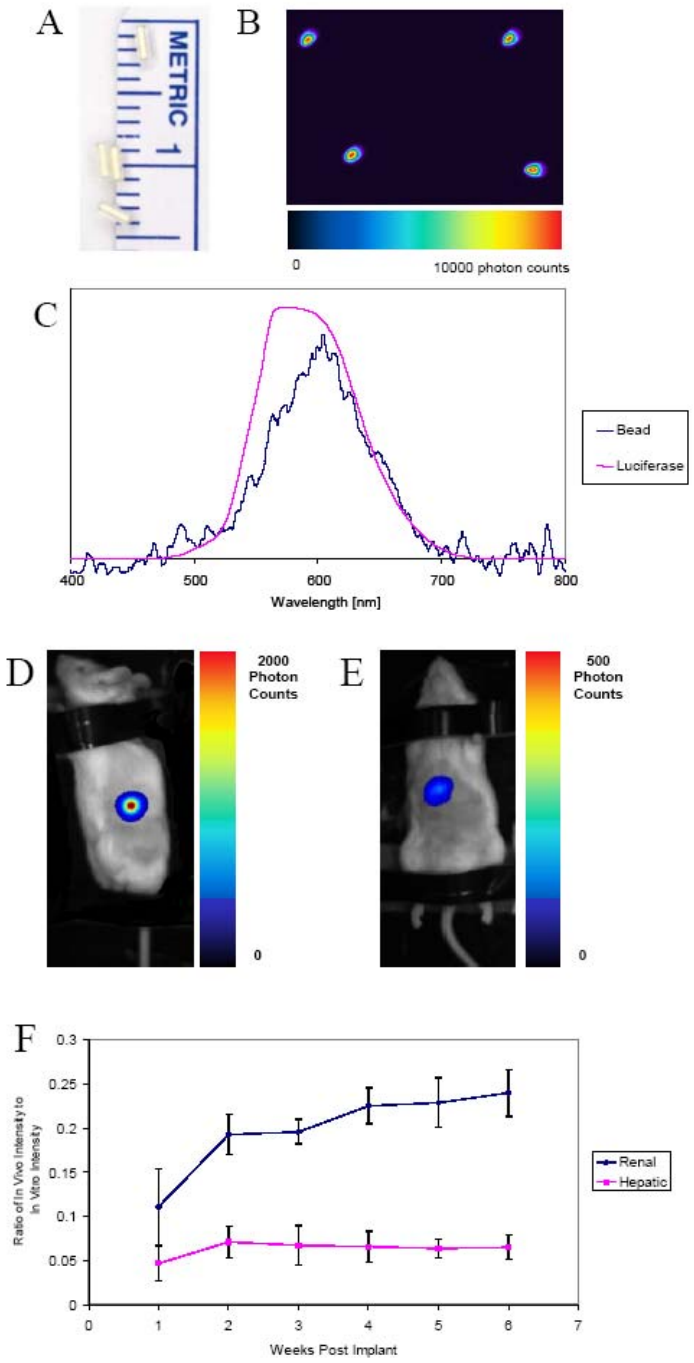

Figure 5.2. (A) Luminescent beads shown next to a ruler (each mark corresponds to one millimeter). (B) A CCD camera image taken of four luminescent beads with a one-second exposure. (C) The emission spectrum of the luminescent bead (shown in blue) plotted with the emission spectrum of the luciferase reaction (shown in magenta). (D) Luminescent bead implanted beneath renal capsule. (E) Luminescent bead implanted in liver. (F) Quantification of luminescence from mice with renal or hepatic bead weekly post implantation. Data is shown as the ratio of implanted bead luminescence to bead luminescence pre-implantation. Each point represents average of 3-4 mice. Error bars indicate the standard error of the mean.

The luminescence from the renal and hepatic implanted beads was also analyzed for light scattering. Spot size, full width at half maximum (FWHM), was determined each week post implantation. There was no statistically significant change in spotsize over the six weeks post transplantation. The FWHM of the liver implanted beads was 17% larger than the FWHM of the renal beads. As in the intensity measurements, the greatest variability was seen one week following surgery.

5.4.4. Monte Carlo Simulation

Light propagation from the luminescent bead to the camera aperture was modeled using Monte Carlo simulation. Simulation was run for the bead alone, for the bead implanted on the renal capsule, and for the bead implanted beneath the renal capsule. Geometry and optical properties used in simulation are listed in the caption of Figure 5.3. The results of this simulation are in agreement with experimental values found using the constant light-emitting bead (Table 5.1).

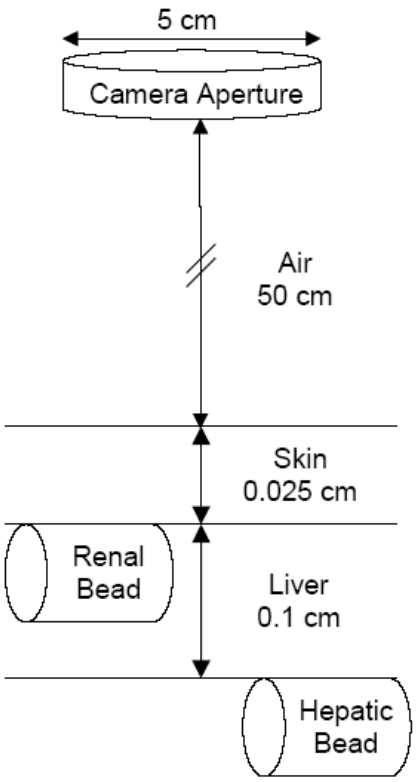

Figure 5.3. Geometry used for Monte Carlo simulation of light propagation from either the renal or hepatic bead to the camera aperture. Modeling of the bead alone included only the non-absorbing, non-scattering air layer. The following optical properties were used in simulation: Air layer: n = 1, g = 1, μa = 10^{-9} cm-1, μs = 0 cm^{-1}; Skin layer: n = 1.37, g = 0.9, μa = 10 cm^{-1}, μs = 20 cm^{-1}; Liver layer: n = 1.37, g = 0.9, μa = 9.6 cm^{-1}, μs = 89 cm^{-1}.

5.4.5. Rotational Variation

Figure 5.4 shows the luminescence intensity from the implanted beads as a function of rotational angle. As the mouse was rotated from a normal (i.e. surface of animal normal to

the optical axis of the imaging system) position (lateral decubitis for renal beads, supine for hepatic beads), the luminescence intensity decreased. At small deviation from the optical axis, intensity decreased only slightly. But at 50-degree rotation from flat, luminescence intensity decreased to approximately one quarter (0.27) of the normal angle intensity for the renal bead (Figure 5.4D) and half (0.48) of the normal angle intensity for the hepatic bead (Figure 5.4C). The angular dependence was stronger for beads at the renal capsule site than for hepatic beads.

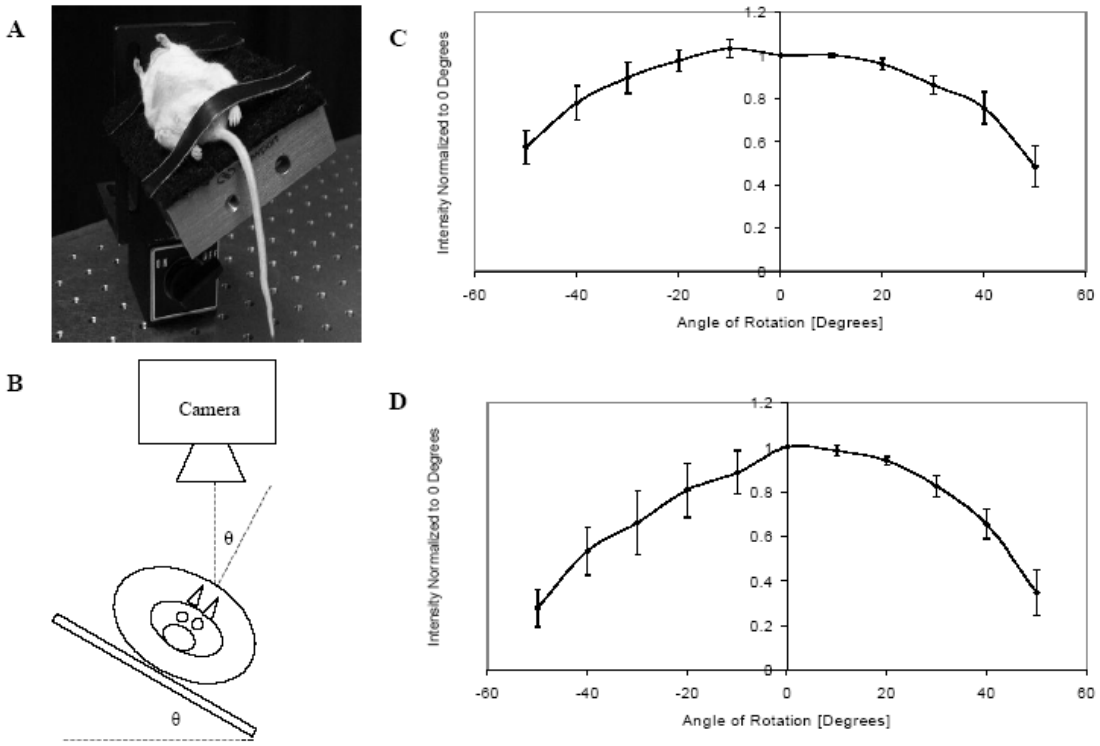

Figure 5.4. (A) Image of a mouse with an implanted hepatic bead. The mouse was secured to the rotational stage. (B) Schematic of the rotational stage, showing the relationship between the rotational angle of the stage and the angle between the camera optical axis and surface normal of the mouse. (C) Change in hepatic bead luminescence intensity with angle of rotation. Bioluminescence intensity at each angle is normalized to normal position ($\theta = 0°$) (supine for hepatic implantation). Shown is the mean of 4 mice; error bars indicate the standard error of the mean. (D) Change in renal bead luminescence intensity with angle of rotation. Bioluminescence intensity at each angle is normalized to normal position ($\theta = 0°$) (lateral decubitis for renal implantation). Shown is the mean of 4 mice; error bars indicate the standard error of the mean.

5.4.6. Bioluminescence of Islets In Vivo

Bioluminescence intensity correlates linearly with the number of islets transplanted [25]. As expected from the studies with the luminescent bead, light emission from hepatical transplanted islets is less than that from renally transplanted islets (Table 5.1). The spot size of hepatic islet grafts is greater than the spot size of renal islet grafts.

To investigate the survival of transplanted islets, we calculated the in vivo / in vitro luminescence ratio of the luminescent beads and the luciferase-expressing islets for both the hepatic and renal sites. Since the effects of the surrounding tissue on light transmission should be similar for beads and islets, the in vivo / in vitro luminescence ratio provides an estimate of the amount of luciferase expression that has survived post transplant. As mentioned above, the in vivo / in vitro luminescence ratio for hepatic bead implants was nearly 4 times lower than the ratio for renal bead implants (0.0645 +/- .0140 vs. 0.239 +/- 0.0261). Transplanted islets show a similar relationship, with higher light emission from renal islet grafts than hepatic grafts. However, the in vivo / in vitro luminescence ratio for transplanted islets was markedly less than the ratio for implanted beads at both the renal and hepatic sites (Table 5.1). This suggests that only a minority of the luciferase-expressing islets survive after transplantation.

Table 5.1. The ratio of in vivo to in vitro bioluminescence intensity for renal transplantation site (left column) and hepatic transplantation site (right column). Top row: Monte Carlo simulation; Second row: results from constant light-emitting bead (values expressed as mean +/- SEM); Third row: 100 islets; Fourth row: 200 islets.

	Renal In Vivo Intensity / In Vitro Intensity	**Hepatic In Vivo Intensity / In Vitro Intensity**
Monte Carlo Simulation	0.2744	0.0495
Bead	0.2394 +/- 0.0261	0.0645+/ - 0.0140
100 Islets	0.0476	0.0116
200 Islets	0.0284	0.0112

5.5. Discussion

In this report we characterized imaging parameters that must be understood and accounted for to accurately quantify bioluminescence imaging and applied these findings to BLI of transplanted islets. Bioluminescence from islet grafts was simulated by implanting a constant light-emitting bead, allowing investigation of important imaging parameters, including the effect of geometric features and tissue optical properties on bioluminescence measurements. Using this constant light-emitting source, we have shown that post-surgical effects (i.e. wound healing), animal positioning, and the anatomic location of the light source influence bioluminescence measurements.

A major parameter of interest when tracking transplanted islets is the number of islets surviving post-transplantation. The relationship between number of bioluminescent islets and emitted light intensity could be useful for monitoring the survival of transplanted islets. However, a number of biologic variables and imaging parameters influence bioluminescence. For example, the measured light intensity depends on the transduction efficiency of the adenovirus, the size of the islets, and various other geometric and biological factors such as thickness of overlying tissue (and changes in tissue thickness due to for example wound healing and/or scar formation), optical properties of tissue, perfusion/hemoglobin content, and substrate availability. The implanted beads mimic bioluminescence by emitting a constant and known intensity light from the site used for islet transplantation. The emission spectrum of the beads closely mimics that of firefly luciferase induced bioluminescence (Figure 5.2C). The peak bead luminescence (600 nm) is slightly higher than the peak emission of the luciferase reaction (563 nm). However, studies indicate that the firefly luciferase reaction shows temperature dependence, with peak emission at 590 nm at physiological temperatures [personal communication with Dr. Brad Rice, Xenogen Corp.]. The strategy of

measuring light emission from the beads in vivo allows us to distinguish changes in measured bioluminescence owing to actual changes in islet light emission from changes caused by other factors that may influence light transport in the animal and toward the imaging detector.

Light transmitted to the CCD camera is dependent on transplantation site. Use of the constant light-emitting bead implanted at a transplantation site allowed quantification of light attenuation at each implantation site. Comparison of renally implanted beads to hepatically implanted beads showed a marked difference between light transmission from each site. Bioluminescence signals collected from renal implants are brighter and spatially more concise than signals from implants in the liver. Monte Carlo modeling of light propagation supports the finding that light is attenuated 4 times more strongly from the hepatic site. The renal capsule implantation site is more superficial; the mean optical path length for light emitted from this site is shorter than that for light emitted from the liver. Light emanating from the hepatic transplants must pass through liver tissue, a highly perfused tissue that contributes significant light scattering and absorption, resulting in lower light emission and increased spatial spread of light at the skin surface.

The spot size of luminescence differed between hepatic islets and renal islets. Islets infused into the portal vein are thought to embolize throughout the liver, leading to a more diffuse light source. Renally transplanted islets are typically confined to a contiguous and highly localized graft. However, spot size is also a function of the tissue optics through which propagating photons pass. Bioluminescence from the liver passes through hepatic tissue, leading to increased scattering and thus a larger spot size than renal grafts. The extent to which increased hepatic light scattering leads to larger spot size was analyzed using the mice with implanted beads. The full width at half maximum (FWHM) for the hepatic beads was 17% higher than the renal bead implants. The islet

transplants showed a much greater difference in spot size between hepatic and renal sites than the bead implantations. This indicates that hepatic islet dispersion is likely the primary reason for larger hepatic islet spot size. Intra-hepatic islets are more spatially dispersed throughout the organ than those beneath the renal capsule where the graft is clustered in a contiguous area.

The luminescence from implanted beads was tracked temporally to investigate post-surgical effects on light transmission. Our results with the light-emitting beads demonstrate that the effect of the inflammatory response on bioluminescence measurements is dynamic as the wound healing progresses. The metal clips interfered with imaging less than one-week post surgery by blocking underlying light emission, preventing accurate measurement of bioluminescence. After surgical clip removal, tissue changes at the surgical site also effected light emission for 1-2 weeks post implantation before stabilizing to consistent measurements in later weeks. Both the renal and hepatic bead implants showed less luminescence the first week post transplantation, with the renal implants showing the greatest variation in light transmission one week post-op. This finding emphasizes that the surgical site may induce imaging artifacts that must be considered when BLI is used to quantitatively assess biological processes. Lu and colleagues [16] found that islet bioluminescence decreased considerably the week immediately following surgery. It was postulated that insufficient vascularization of the islets one-week post-op could hamper delivery of the substrate luciferin to the islet graft. Thus, dynamic changes in light transport by surgery-related edema, angiogenesis, or scar tissue overlying the bioluminescent source or even the presence of tissue ridges and/or sutures or clips at the suture site can significantly decrease bioluminescence measurements by increasing optical path length, resulting in light quantification that does not accurately reflect light emission from the bioluminescent source. For accurate quantitative use of bioluminescence as a surrogate marker for

biological processes, whether these by islet mass, tumor volume, gene transcription, or one of many other uses of this technology, these effects must be taken into consideration.

Bioluminescence measurements can also be affected by rotation of the sample. Detected photon emission depends on the angle the surface normal makes with the optical axis of the camera system. The practical implication of this finding is that the exact positioning of the mouse relative to the camera axis is an important parameter that must be carefully controlled. Failure to do so can induce variations in the photon counting measurements that are not representative of the biological processes for which bioluminescence is the surrogate marker. The application of tomographic analysis to bioluminescence imaging, thus far still in a developmental state, must take into account these rotational effects. The effect of rotation on luminescence measurements was determined for both the renal and hepatic implanted beads. Both implantation sites showed a parabolic relationship between angle and luminescence, with luminescence decreasing with an increasing angle from normal. At rotations of 50 degrees from normal, measured luminescence decreased to approximately a quarter compared to the normal measurement for renal beads. For hepatic beads, the decrease at 50 degrees from normal was less, resulting in measured intensity less than half of the normal measurement. The drop in renal intensity was sharper and more pronounced than that seen from the hepatic bead. Supine orientation served as normal placement for hepatic bead imaging while lateral orientation was used for renal imaging to minimize the optical path length of light through tissue. The animal surface overlying the liver bead thus has more surface area normal to the camera axis than the animal surface overlying the renal bead. This, in turn, results in a slower decrease in luminescence with increasing rotation for the hepatic implantation.

Light emitted from islet grafts is significantly lower than light emission from islets in vitro. However, it was unclear how much of this decrease in luminescence was due to islet death post-transplantation and how much could be attributed to light attenuation by tissues overlying the implants. The light-emitting beads transplanted at the site of islet grafts were used to quantify light transmission through the tissues overlying the luminescent source. For renal implantation, the ratio between luminescence after implantation (in vivo) to luminescence of the bead alone (prior to implantation) stabilized at a constant value two weeks post-implantation. Experimental results for both renal and hepatic implanted beads are in agreement with Monte Carlo modeling of photon propagation. Light attenuation by tissue overlying hepatic transplants results in a nearly four-fold less light transmission from hepatic islets than renal islets. This is in agreement with the ratio found using the constant light-emitting bead, suggesting that the survival rate of islets at the renal and hepatic site is similar. Interestingly, the ratio between in vivo and in vitro luminescence of the beads was much greater than the ratio for islets, suggesting a large (six to eight fold) drop in viable islets post transplantation (Table 5.1). This conclusion assumes that the BLI of islets reflects islet survival of luciferase-expressing islet cells. However, bioluminescence measurements could be affected by loss of the luciferase transgene and differences in substrate availability. Additional work is needed to conclusively prove that transplanted islet mass, assessed by morphologic and histologic approaches, correlates with BLI.

Bioluminescence measurements are subject to some inherent limitations. In vivo BLI can be applied only to small animal models; the tissue thickness of larger animal models or humans currently prevents BLI studies. Additionally, islets transduced with our adenovirus constitutively express the reporter gene luciferase in all islet cell types, not just β-cells. This limitation can be circumvented by the using a beta-cell specific promoter or by creating transgenic islets that express luciferase solely in the β-cells.

The adenovirus system used for islet transduction also has a limitation in that dividing cells the transgene is passed to only one of the daughter cells and thus β-cell replication post transplantation would not be reflected in bioluminescence measurements. As reported by Lu and colleagues [16], the use of lentivirus-mediated gene transfer may allow for integration of the luciferase DNA into the genome before cell division but typically has much lower transfection efficiency compared to the adenovirus.

The correlation of light emission to islet number in vivo enables the use of BLI as a non-invasive means of islet assessment in mouse models of diabetes and islet transplants. In turn, these models may be used as models for assessing and screening of novel therapeutic approaches to improve islet survival. Information regarding relative islet mass or number as function of time or in response to pharmacological intervention should be readily obtainable from the bioluminescence measurements (i.e. increase or decrease of signal). Absolute information regarding the number of islets surviving requires additional investigation correlating islet histology with BLI using the imaging parameters optimized in this study. In conclusion, BLI is shown to be a valuable method to assess transplanted islet mass in vivo. However, we have shown using our luminescent bead studies that post-surgical dynamics, animal positioning, and light source location can significantly alter the measured bioluminescence. Clearly these findings are not unique to the application of transplanted islet imaging, but hold important clues for the field of BLI in general. Our findings suggest that for accurate use of BLI as a quantitative surrogate marker for biological processes, detailed and careful system characterization and calibration is required.

5.6. Works Cited

1. A. M. Shapiro, J. R. Lakey, E. A. Ryan, G. S. Korbutt, E. Toth, G. L. Warnock, N. M. Kneteman, and R. V. Rajotte. "Islet transplantation in seven patients with type

1 diabetes mellitus using a glucocorticoid-free immunosuppressive regimen." *N Engl J Med*. 343(4), 230-8 (2000).

2. B. Hirshberg, K. I. Rother, I. B. Digon, J. Venstrom, and D. M. Harlan. "State of the art: islet transplantation for the cure of type 1 diabetes mellitus." *Rev Endocr Metab Disord*. 4(4), 381-9 (2003).

3. A. M. Morawski, P. M. Winter, K. C. Crowder, S. D. Caruthers, R. W. Fuhrhop, M. J. Scott, J. D. Robertson, D. R. Abendschein, G. M. Lanza, and S. A. Wickline. "Targeted nanoparticles for quantitative imaging of sparse molecular epitopes with MRI." *Magn Reson Med*. 51(3), 480-6 (2004).

4. J. C. Ferrer-Garcia, J. F. Merino-Torres, G. Perez Bermejo, C. Herrera-Vela, J. L. Ponce-Marco, and F. Pinon-Selles. "Insulin-induced normoglycemia reduces islet number needed to achieve normoglycemia after allogeneic islet transplantation in diabetic mice." *Cell Transplant*. 12(8), 849-57 (2003).

5. N. S. Kenyon, L. A. Fernandez, R. Lehmann, M. Masetti, A. Ranuncoli, M. Chatzipetrou, G. Iaria, D. Han, J. L. Wagner, P. Ruiz, M. Berho, L. Inverardi, R. Alejandro, D. H. Mintz, A. D. Kirk, D. M. Harlan, L. C. Burkly, and C. Ricordi. "Long-term survival and function of intrahepatic islet allografts in baboons treated with humanized anti-CD154." *Diabetes*. 48(7), 1473-81 (1999).

6. L. Visser, S. Poppema, B. De Haan, P. Klok, J. Van Der Leij, A. Van Den Berg, and P. De Vos. "Prolonged survival of rat islet xenografts in mice after CD45RB monotherapy." *Transplantation*. 77(3), 386-91 (2004).

7. A. M. Davalli, L. Scaglia, D. H. Zangen, J. Hollister, S. Bonner-Weir, and G. C. Weir. "Vulnerability of islets in the immediate posttransplantation period. Dynamic changes in structure and function." *Diabetes*. 45(9), 1161-7 (1996).

8. S. T. Grey, C. Longo, T. Shukri, V. I. Patel, E. Csizmadia, S. Daniel, M. B. Arvelo, V. Tchipashvili, and C. Ferran. "Genetic engineering of a suboptimal islet graft with A20 preserves beta cell mass and function." *J Immunol*. 170(12), 6250-6 (2003).

9. H. Yamauchi, J. Chiba, K. Kakizaki, M. Maeda, K. Miyagawa, and R. Nakamura. "Effect of islet transplantation on diabetes mellitus after subtotal pancreatectomy in rat: a quantitative analysis of islet tissue." *Tohoku J Exp Med*. 147(4), 365-77 (1985).

10. J. W. Hastings. "Chemistries and colors of bioluminescent reactions: a review." *Gene*. 173(1 Spec No), 5-11 (1996).

11. C. H. Contag, and B. D. Ross. "It's not just about anatomy: in vivo bioluminescence imaging as an eyepiece into biology." *J Magn Reson Imaging*. 16(4), 378-87 (2002).

12. M. Edinger, Y. A. Cao, Y. S. Hornig, D. E. Jenkins, M. R. Verneris, M. H. Bachmann, R. S. Negrin, and C. H. Contag. "Advancing animal models of

neoplasia through in vivo bioluminescence imaging." *Eur J Cancer*. 38(16), 2128-36 (2002).

13. A. Wetterwald, G. van der Pluijm, I. Que, B. Sijmons, J. Buijs, M. Karperien, C. W. Lowik, E. Gautschi, G. N. Thalmann, and M. G. Cecchini. "Optical imaging of cancer metastasis to bone marrow: a mouse model of minimal residual disease." *Am J Pathol*. 160(3), 1143-53 (2002).

14. R. T. Sadikot, E. D. Jansen, T. R. Blackwell, O. Zoia, F. Yull, J. W. Christman, and T. S. Blackwell. "High-dose dexamethasone accentuates nuclear factor-kappa b activation in endotoxin-treated mice." *Am J Respir Crit Care Med*. 164(5), 873-8 (2001).

15. J. Y. Adams, M. Johnson, M. Sato, F. Berger, S. S. Gambhir, M. Carey, M. L. Iruela-Arispe, and L. Wu. "Visualization of advanced human prostate cancer lesions in living mice by a targeted gene transfer vector and optical imaging." *Nature Medicine*. 8(8), 891-896 (2002).

16. R. Bhargava, P. A. Senior, T. E. Ackerman, E. A. Ryan, B. W. Paty, J. R. Lakey, and A. M. Shapiro. "Prevalence of hepatic steatosis after islet transplantation and its relation to graft function." *Diabetes*. 53(5), 1311-7 (2004).

17. A. J. Welch, and M. J. C. van Gemert. "Optical-Thermal Respoonse of Laser-Irradiated Tissue." Plenum Press. (1995).

18. M. Brissova, M. Fowler, P. Wiebe, A. Shostak, M. Shiota, A. Radhika, P. C. Lin, M. Gannon, and A. C. Powers. "Intraislet endothelial cells contribute to revascularization of transplanted pancreatic islets." *Diabetes*. 53(5), 1318-25 (2004).

19. L. Wu, W. Nicholson, S. M. Knobel, R. J. Steffner, J. M. May, D. W. Piston, and A. C. Powers. "Oxidative stress is a mediator of glucose toxicity in insulin-secreting pancreatic islet cell lines." *J Biol Chem*. 279(13), 12126-34 (2004).

20. S. T. Flock, M. S. Patterson, B. C. Wilson, and D. R. Wyman. "Monte Carlo modeling of light propagation in highly scattering tissue--I: Model predictions and comparison with diffusion theory." *IEEE Trans Biomed Eng*. 36(12), 1162-8 (1989).

21. M. Keijzer, S. L. Jacques, S. A. Prahl, and A. J. Welch. "Light distributions in artery tissue: Monte Carlo simulations for finite-diameter laser beams." *Lasers Surg Med*. 9(2), 148-54 (1989).

22. B. C. Wilson, and G. Adam. "A Monte Carlo model for the absorption and flux distributions of light in tissue." *Med Phys*. 10(6), 824-30 (1983).

23. L. Wang, S. L. Jacques, and L. Zheng. "MCML--Monte Carlo modeling of light transport in multi-layered tissues." *Comput Methods Programs Biomed*. 47(2), 131-46 (1995).

24. W. F. Cheong, S. A. Prahl, and A. J. Welch. "A Review of the Optical-Properties of Biological Tissues." *Ieee Journal of Quantum Electronics*. 26(12), 2166-2185 (1990).

25. M. Fowler, J. Virostko, Z. Chen, G. Poffenberger, A. Radhika, M. Brissova, M. Shiota, W. E. Nicholson, Y. Shi, B. Hirshberg, D. M. Harlan, E. D. Jansen, and A. C. Powers. "Assessment of pancreatic islet mass after islet transplantation using in vivo bioluminescence imaging." *Transplantation*. 79(7), 768-76 (2005).

CHAPTER VI

VALIDATION OF LUMINESCENT SOURCE RECONSTRUCTION USING SINGLE-VIEW SPECTRALLY RESOLVED BIOLUMINESCENCE IMAGES

John Virostko[1], Alvin C. Powers[2,3], E. Duco Jansen[1]

[1]Department of Biomedical Engineering, Vanderbilt University, Nashville, TN 37235

[2]Department of Medicine, Division of Diabetes, Endocrinology, and Metabolism, Vanderbilt University, Nashville, TN 37232

[3]VA Tennessee Valley Healthcare System, Nashville, TN 37212

Portions of this manuscript have been submitted for publication in *Applied Optics.*

6.1. Abstract

The application of three-dimensional techniques to bioluminescence imaging (BLI) has the potential to vastly improve the image quality and information available. The recently developed Living Image® Software 3D Analysis Package (Xenogen, Alameda, CA) employs the diffusion model of light propagation to reconstruct bioluminescent source position and intensity from single view, multi-spectral images. The purpose of this study was to independently characterize the capabilities and limitations of this technique. Light-emitting beads with spectral emission similar to that emitted by the firefly luciferase reaction provided constant, known light emission from a controllable and known location. Reconstruction of light sources placed within optically homogenous tissue had an average inaccuracy of 17% for the actual depth and intensity across all depths tested. The greatest error in reconstruction was found for shallow sources less than the mean free path, for which the diffusion approximation breaks down. For sources deeper than the mean free path depth, the error in depth reconstruction was less than 4% and error in intensity reconstruction less than 12%. Reconstruction of luminescent beads implanted within an optically heterogeneous mouse abdomen proved less accurate, with accuracy dependent on input tissue optical properties. The ability to distinguish multiple sources was a function of source depth: sources spaced by a distance approximately equal to twice the depth could be resolved. The current depth and optical heterogeneity limitations of 3D bioluminescence reconstruction establish the need for advancements in instrumentation and modeling.

6.2. Introduction

Advances in small animal imaging are transforming the face of biomedical research. Small animal models of disease and treatment responses are emerging as

key bridges between *in vitro* investigation and clinical trials, accelerating the pace of research and drug development. Bioluminescence imaging (BLI) has recently emerged as a valuable small animal imaging modality. While firefly luciferase was characterized decades ago [1], early attempts to harness luciferase as an optical reporter gene were confined to *in vitr*o cell work and immunoassays [2]. The development of cooled charge-coupled device (CCD) cameras and progress in efficient methods of viral luciferase transfection permitted imaging of bioluminescent sources located deep within small animal models [3]. As the technology has become commercially available, application of *in vivo* BLI has enabled researchers to track cell migration and distribution [4], quantify tumor growth and assess treatment response [5], and track gene expression using transgenic animals [6].

BLI holds many advantages as a small animal imaging modality. Bioluminescence analysis is relatively straightforward for providing quantitative information on the number of metabolically active cells or relative amounts of gene expression [6-9]. BLI benefits from high sensitivity with inherently low background. The technology can be easy to implement, as BLI instrumentation is typically less expensive and easier to perform by a non-specialist than other imaging modalities. Lastly, BLI is a high throughput imaging modality: several animals can be imaged in a single imaging session, with imaging times generally on the order of several minutes.

The primary limitations of bioluminescence imaging stem from fundamental optical phenomena. Photons are absorbed by biological tissue, with the attenuation being a non-linear function of tissue depth. Thus, quantification of a bioluminescent signal is subject to signal location. In studies of luciferase-labeled cells transplanted into either a superficial renal location or hepatic site, we have observed a four-fold difference in light quantification due solely to source depth [10]. This can lead to erroneous interpretation of BLI quantification if these depth effects are not corrected. Photons are

also subject to scattering by biological tissue overlying the source location. The low spatial resolutions caused by optical scatter results in planar images of bioluminescence that typically appear as a diffuse cloud of photons overlying the actual light source. Studies seeking to track stem cell migration to specific organs, locate tumor metastasis, or spatially localize transgene expression are hampered by the inability to spatially reconstruct bioluminescent sources.

The development of bioluminescence tomography (BLT) capable of reconstructing source location and intensity would overcome these current limitations of BLI. A number of groups have published algorithms for three dimensional bioluminescence reconstruction [11-20]. The first commercially available software package that reconstructs three-dimensional bioluminescent source information was recently developed by Xenogen Corporation (Alameda, CA). This Living Image® Software 3D Analysis Package performs reconstruction of source location and intensity using the diffusion model of light propagation [21]. The diffusion approximation is applied to spectrally-filtered bioluminescent image information to reconstruct the bioluminescent source location and intensity. The algorithm first determines the subject topography from a structured light image and divides the subject volume into a mesh of voxels. A Green's function relates the light source intensity in each voxel to the photon density at each surface element. This Green's function incorporates tissue optical properties to analytically solve the diffusion equation for spectrally filtered bioluminescent data. The result is a three-dimensional subject mesh mapping light source localization and intensity. Further details regarding the algorithm used by the Living Image® Software 3D Analysis Package can be found in the conference proceedings [22,23] and the manuscript by Kuo, et al [24].

The purpose of this study was to independently determine the accuracy of the Living Image® Software 3D Analysis to reconstruct light source location and intensity.

Constant intensity light-emitting beads with spectral emission similar to the firefly luciferase (*luc*) reaction provided constant, known light emission from a controllable and known location. The effect of source depth on the accuracy of reconstructed source location, intensity, and ability to distinguish multiple sources was investigated in an optically homogeneous tissue slab. As the reconstruction algorithm assumes homogeneous subject optical properties, the effects of tissue heterogeneity on reconstruction accuracy were investigated using luminescent bead implantation within a live mouse. This research demonstrates practical implementation of the Living Image® Software 3D Analysis to establish the capabilities and limitations of bioluminescent source reconstruction.

6.3. Materials & Methods

6.3.1. Tissue Slab Setup

Uncooked chicken breast was used as a representative biological tissue, as it could be divided into large slabs of tissue with uniform optical properties. Square slabs approximately 6 cm on each side were cut from the chicken breast using a scalpel. These slabs were then cut to a thickness of 2.5 mm, 5.0 mm, 7.5 mm, 10.0 mm, 12.5 mm, and 15.0 mm, as assessed by micrometer. Another slab with a thickness of 20 mm was placed on a 10 cm petri dish to serve as the bottom tissue layer. Luminescent beads (Mb-Microtec, Bern, Switzerland) were used as a surrogate bioluminescent source. These beads consisted of glass capillaries (0.9 mm diameter and 2 mm long) filled with tritium (a β-emitter with a half life of over 10 years) that excites a phosphor and isotropically emits constant and known intensity light. The bead was placed on top of the bottom tissue slab and maintained at the same distance relative to the camera aperture for all images. For each tissue thickness, the prescribed tissue slab was placed over the

bead, centering the bead underneath the tissue slab. Each experiment was performed four times with results presented as mean ± standard deviation. For the spatial resolution experiments, two luminescent beads were placed the specified distance apart and covered with the corresponding tissue slab thickness.

6.3.2 Mouse Luminescent Bead Implantation

Luminescent beads were implanted in NOD-SCID mice, a mouse model with white fur to limit photon scatter and absorption. Briefly, an incision was made in the abdomen of an anesthetized mouse to expose the viscera. The luminescent bead was secured at various locations within the abdomen using Vetbond™ tissue adhesive (3M, St. Paul, Minnesota). The depth and bead location was varied for each of five mice. Care was taken to implant the beads in various tissues of with widely varying optical properties. The incision was closed with subcutaneous sutures and allowed to heal for two weeks to prevent surgical artifacts from affecting light transmission [10].

6.3.3. Luminescence Imaging

All imaging was performed using an IVIS® 200 Imaging system (Xenogen, Alameda, CA). Luminescent bead intensity was measured by integrating light intensity over the surface area and multiplying by 2π steradians to convert to absolute flux over the entire sphere. The tissue phantom or mouse was placed on the imaging platform within the light-tight chamber. For mouse imaging the animal was anesthetized with 2% isoflurane via a nose cone within the imaging chamber. Spectral imaging was obtained by imaging the implanted bead through six 20 nm bandpass filters at wavelengths from 560 to 660 nm. Additionally, a structured light image was taken to reconstruct the surface topography of the imaged object.

6.3.4. Image reconstruction

Reconstruction was performed using the Living Image® Software 3D Analysis software package. For tissue slab studies, tissue properties were set to 'chicken breast' (with corresponding optical properties as shown in Table 6.1). The source spectrum was set to 'Tritium Bead 5' with spectral emission as previously determined using a spectrometer [10]. For mouse bead implantation studies, various tissue properties were used for reconstruction. The tissue optical properties used in reconstruction are shown in Table 6.1. Internal medium index of refraction was set to 1.40. Six wavelengths, ranging from 560 to 660 nm in 20 nm increments, were used for reconstruction.

Table 6.1. Tissue optical properties used in reconstruction. Listed are the absorption coefficients (μ_a) and reduced scattering coefficients (μ_s') for each of the four tissues used in reconstruction: chicken breast, muscle, skin, and liver. The optical properties are shown for each of the six wavelengths used in reconstruction.

	Chicken Breast		**Muscle**		**Skin**		**Liver**	
Wavelength [nm]	μ_a [cm^{-1}]	μ_s' [cm^{-1}]	μ_a [cm^{-1}]	μ_s' [cm^{-1}]	μ_a [cm^{-1}]	μ_s' [cm^{-1}]	μ_a [cm^{-1}]	μ_s' [cm^{-1}]
560	0.47	3.03	5.07	9.84	4.22	19.20	19.37	8.91
580	0.36	2.87	4.63	9.75	3.73	18.16	14.05	8.65
600	0.21	2.73	1.87	9.29	2.75	17.11	5.98	8.42
620	0.12	2.64	1.07	9.22	1.69	16.25	2.62	8.19
640	0.09	2.51	0.88	9.13	1.35	15.78	1.82	7.97
660	0.06	2.26	0.80	9.02	1.25	15.35	1.43	7.77

6.3.5 Computed Tomography

Computed tomography (CT) imaging was used to determine the actual location of the implanted bead within the mouse abdomen. As the luminescent bead is radiopaque, the implanted beads were visible as hyperintense voxels on the CT image. Mice were scanned using an Imtek MicroCAT II small animal CT scanner and immobilized on an imaging platform for both CT and bioluminescence imaging to prevent

animal movement. CT scans were analyzed using AMIRA™ image visualization software (Mercury Computer Systems, Chelmsford, MA). The distance between the centroid of the luminescent bead and the mouse surface was measured using AMIRA™.

6.4. Results

6.4.1. Tissue Slab

Representative three-dimensional luminescence reconstructions from the tissue slab experiments are shown in Figure 6.1. The reconstructed source voxel is shown in red within the subject volume. The depth of the source voxel was determined by measuring a line inserted between the center of this pixel and the upper surface of the tissue slab, as indicated in the left panels of Figure 6.1. The effect of source depth on reconstruction accuracy was determined by varying the thickness of the tissue slab overlying the luminescent bead. The depth reconstruction for the tissue slab is plotted as a function of true depth in Figure 6.2. The line indicates ideal depth reconstruction for reference. As Figure 6.2 shows, the depth reconstruction displays a high degree of linearity (correlation coefficient, $r^2 = 0.98$). The accuracy of reconstruction is a function of source depth. At the most shallow depths of 2.5 mm and 5.0 mm, the depth is overestimated by 1.7 ± 0.7 mm (68%) and 1.1 ± 0.6 mm (22%), respectively. However, at further depths (7.5 mm to 15 mm) the error in depth reconstruction averages less than 0.4 mm (3%).

Surface light flux decreases as the source depth is increased, in accordance with Beer's law, as plotted in Figure 6.3. An ideal reconstruction of source intensity would reconstruct source intensity at a constant value equal to the actual light emission of the bead, indicated by the dashed line in Figure 6.3. The accuracy of three-dimensional

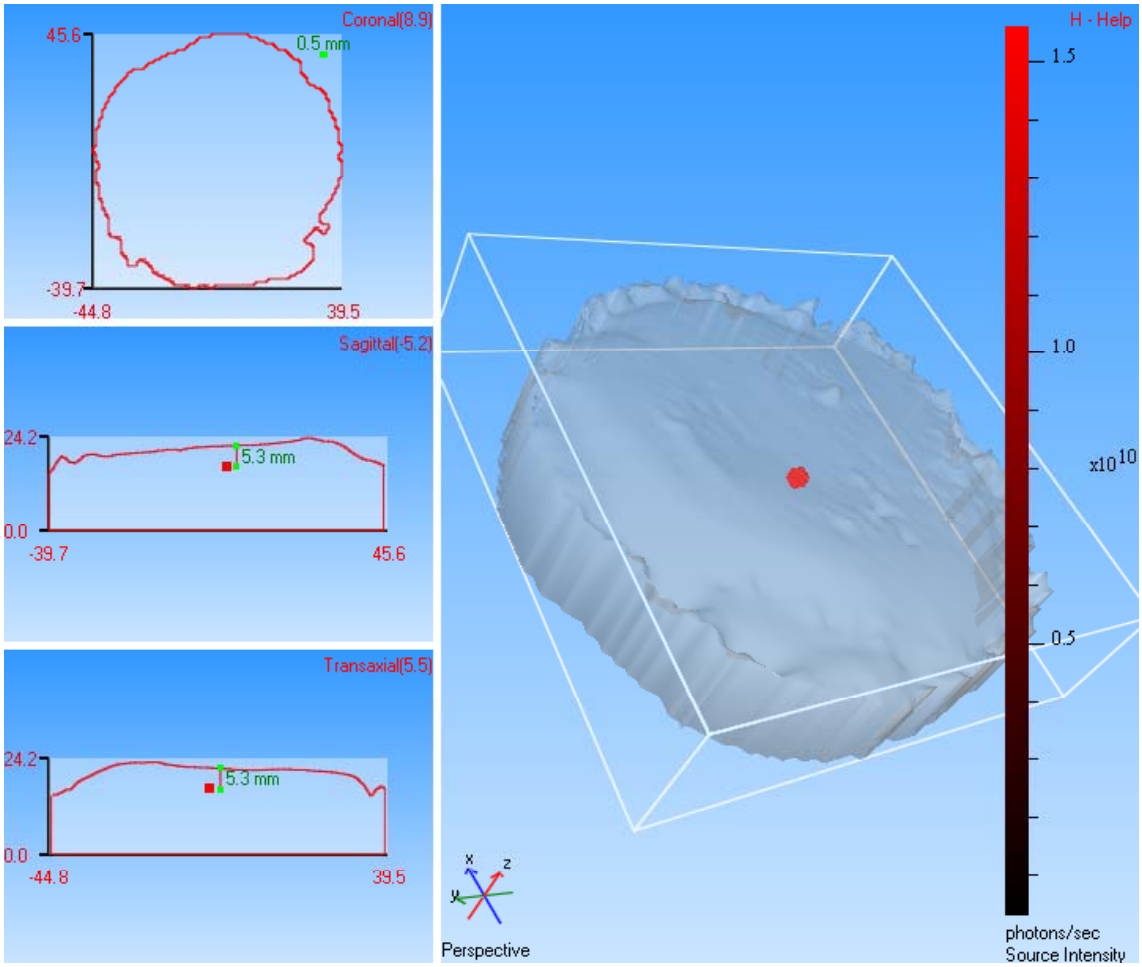

Figure 6.1. Representative output of Living Image® Software 3D Analysis Package reconstruction from a luminescent bead beneath 5 mm of chicken breast. Pictured in the large right panel of the image is the reconstructed subject volume, with the light source indicated by the highlighted pixel. The left panels show cut-away views indicating the position of the light source and demonstrating the manner in which source depth was measured. The axis labels show dimensions in millimeters.

reconstruction of source intensity (Figure 6.3) is a function of source depth. At the most shallow depth of 2.5 mm the surface flux was actually closer to the actual intensity, underestimating it by 8%, whereas the reconstruction overestimates the actual intensity, underestimating it by 31%. At 5.0 mm depth the reconstruction accuracy was slightly more accurate (22% overestimation) than the surface flux (27% underestimation). The intensity reconstruction was most accurate for intermediate depths of 7.5 mm and 10.0 mm for which intensity was overestimated by only 3% and 1% respectively. For depths above 10.0 mm increasing depth led to increased error in intensity reconstruction.

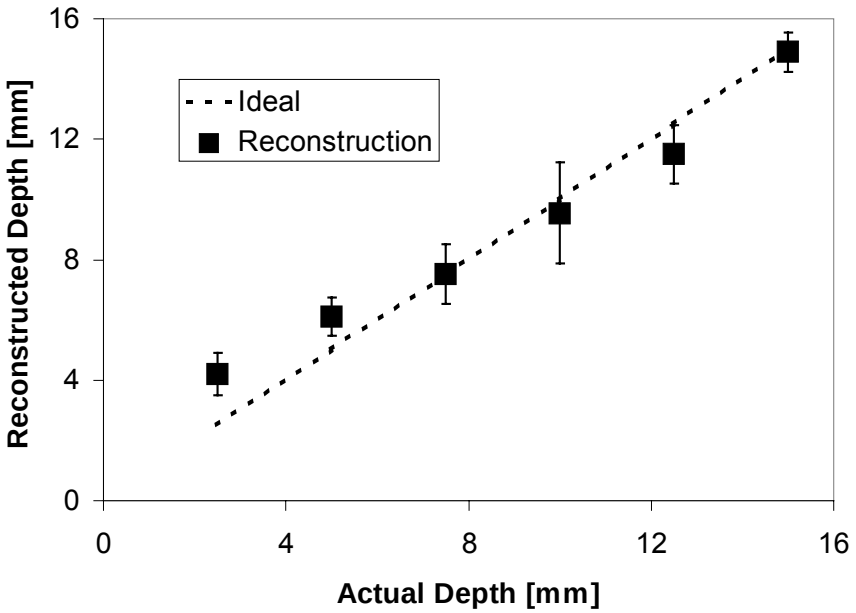

Figure 6.2. Reconstructed source depth as a function of actual source depth under a tissue slab. A luminescent bead was placed beneath the prescribed thickness of muscle tissue (chicken breast). Source depth was reconstructed using the Living Image® reconstruction software. Shown is the mean of four experiments ± the standard deviation. The dashed line indicates ideal reconstruction of the correct source depth.

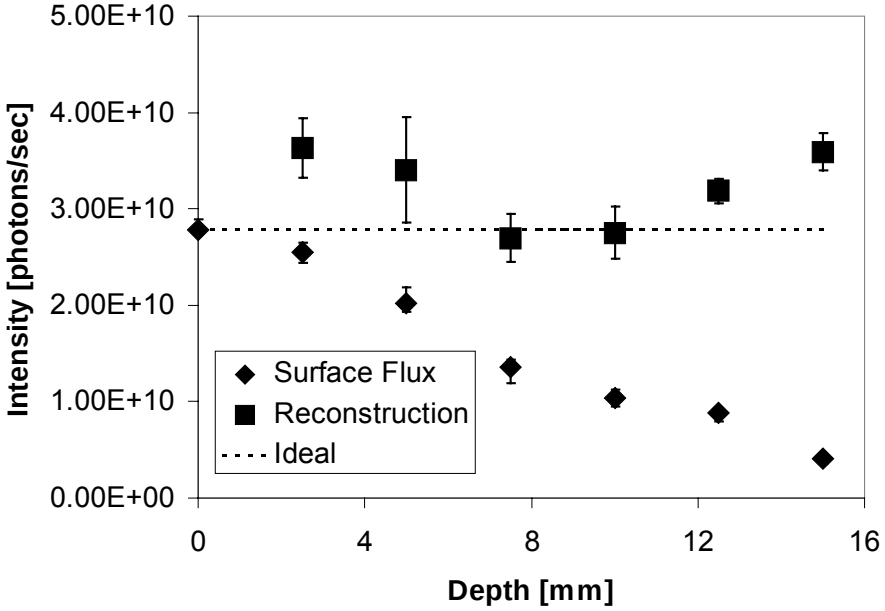

Figure 6.3. Reconstructed source intensity as a function of source depth under a tissue slab. A luminescent bead was placed beneath the prescribed thickness of chicken breast. Source intensity was reconstructed using the Living Image® software package. The mean of four experiments ± the standard deviation is plotted. The dashed line indicates the true light source intensity, as determined by imaging the luminescent bead with no tissue above the bead.

The ability of the reconstruction algorithm to distinguish between two co-planar equal intensity light sources is a function of source separation and source depth, as shown in Table 6.2. At 2.5 mm tissue depth, sources separated by 5.0 mm can be discriminated. For deeper sources, higher separation distances are needed to distinguish multiple sources. Our results indicate that the reconstruction algorithm has the ability to reconstruct two sources separated by a distance approximately equal to twice the source depth. Two exceptions are the beads at 10 mm and 15 mm depth that could be distinguished with 15 mm and 25 mm spatial separation, respectively. Light emitting beads separated by a distance too small to be distinguished were reconstructed as a single diffuse source, centered between the two beads. The distance between the two sources was determined by measuring a line between the two brightest source voxels. These reconstructed source separation distances are similar to the true separation gaps, as shown in Table 6.2.

Table 6.2. The ability of the Living Image® reconstruction algorithm to accurately distinguish two separate luminescent beads separated by the indicated spatial separation is a function of the source depth. Three asterisks (***) indicate that the algorithm was unable to differentiate the two light sources. Numerical values indicate the reconstructed source separation, as determined by measuring the distance between the two highest intensity voxels.

Depth [mm]	Spatial Separation [mm]					
	5	**10**	**15**	**20**	**25**	**30**
2.5	5.1	9	17.6	19.4	27.7	30.7
5	***	7.7	17.8	19.8	26.4	31.5
7.5	***	***	18.3	21.1	24.4	27.5
10	***	***	13.7	17.5	28.1	33.7
12.5	***	***	***	***	23.9	27.5
15	***	***	***	***	24.4	28.5

6.4.2. Mouse Bead Implantation

The tissue slab experiments allow for easily controllable source location, but the chicken breast tissue used has uniform optical properties, which greatly simplifies three-dimensional reconstruction. The Living Image® Software 3D Analysis Package assumes a single tissue with uniform optical properties. However, light propagation in small animal models must traverse tissues with widely varying optical properties. To test the effect of optical heterogeneity on source reconstruction, constant light emitting beads were implanted into various locations within a mouse abdomen. The bead location was varied in depth, ranging from approximately 2 mm depth to 6 mm depth. As the true tissue optical properties vary through a mouse

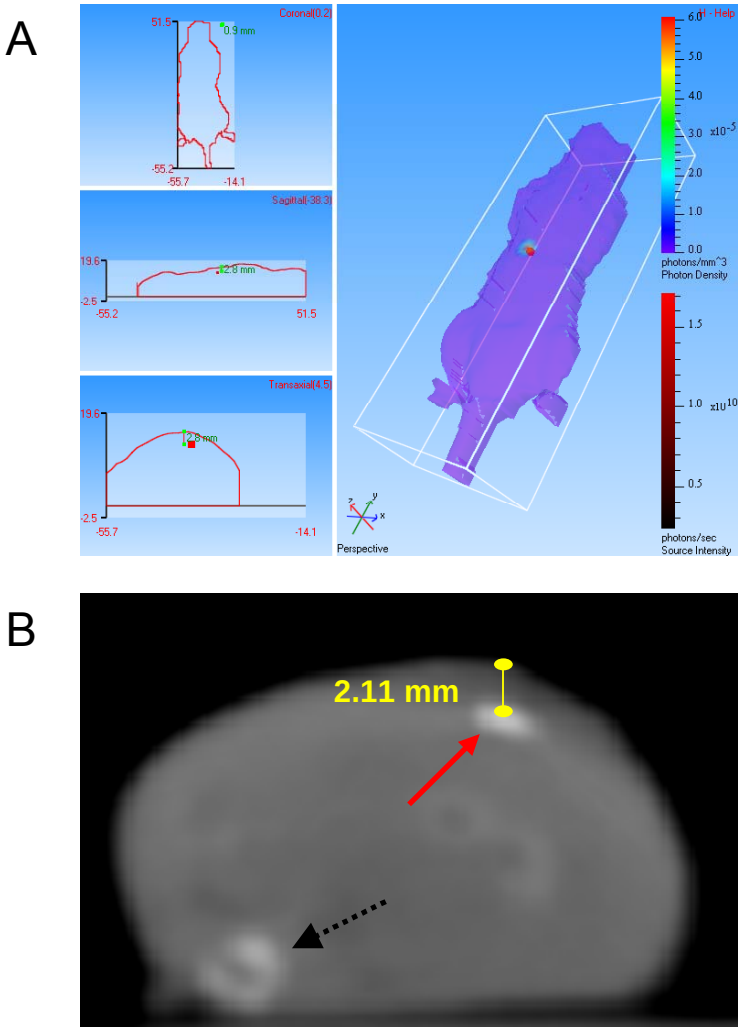

Figure 6.4. Three-dimensional bioluminescence reconstruction of a bead implanted in the liver of a mouse (A) and corresponding CT scan (B) showing the actual location of the luminescent (and radio-opaque) bead. Three-dimensional BLI image was reconstructed using the Living Image® algorithm; the reconstructed light source is shown as the highlighted voxel within the mouse volume. On the CT scan the solid arrow indicates the luminescent bead, with the measured depth indicated. The dashed arrow indicates the spine of the mouse.

abdomen, a number of tissue optical properties were tested to determine the optimum input for reconstruction. The tissue optical properties of the liver, skin and muscle were used for reconstruction (see Table 6.1).

Source depth of the implanted beads was reconstructed using the Living Image® Software 3D Analysis Package. Figure 6.4 shows a representative 3D BLI reconstruction of a luminescent bead in a mouse abdomen (Panel A). Also shown in Figure 6.4 (Panel B) is a CT slice through the mouse abdomen showing the implanted bead, illustrating the method used to determine actual bead depth. As shown in Figure 6.5, accuracy of reconstruction depth was a function of the optical properties used for reconstruction. There was a general tendency for the algorithm to overestimate the source depth, especially at the two most shallow bead locations. Liver optical properties led to severe underestimation of the deepest source (6.0 mm depth reconstructed as 2.8 mm deep). Overall, reconstruction using the optical properties of skin yielded the most accurate depth estimation with an average error of 0.6 mm (15%) while muscle had an average error of 1.0 mm and liver had an average error of 1.3 mm.

The reconstructed intensity of beads implanted within the mouse abdomen is shown in Figure 6.6. Again, accuracy of reconstruction was a function of the optical properties used in reconstruction. Using the optical properties of skin for reconstruction yielded significant overestimation of the source intensity, especially for the deeper sources. Overall, the optical properties of liver yielded the most accurate intensity reconstruction (18% average error), followed by muscle tissue (41%), and skin (95%).

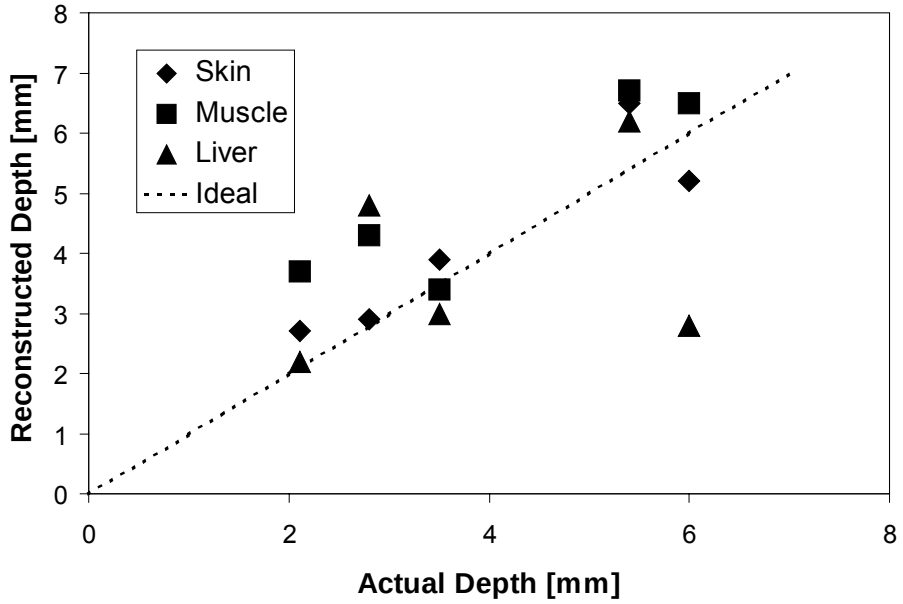

Figure 6.5. Reconstructed source depth as a function of actual source depth. The actual depth of luminescent beads implanted in the abdomen of mice was determined by CT. Source location was reconstructed using the Living Image® algorithm inputting three different tissue optical properties. The dashed line indicates correct source depth reconstruction.

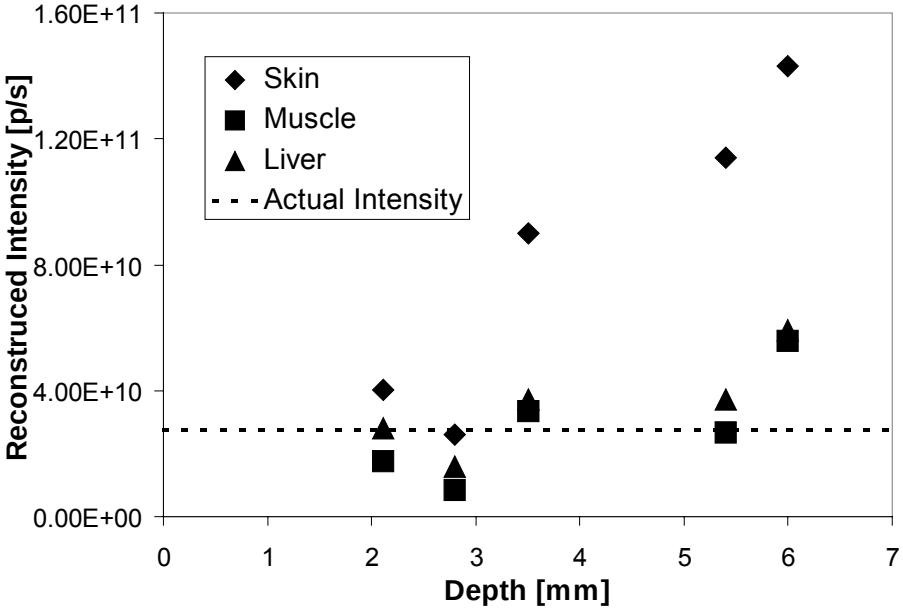

Figure 6.6. Reconstructed source intensity as a function of source depth. Source intensity was reconstructed with the Living Image® software reconstruction using three different tissue optical properties for reconstruction. The actual source intensity is plotted as a dashed line.

6.5. Discussion

The ability to create three dimensional tomographic bioluminescence images will greatly enhance the information available from bioluminescence imaging. Accurate source localization will aid cell-tracking studies of stem cell migration, tumor metastases, and transgene expression. Accurate intensity reconstruction will correct for the source depth dependency of BLI measurements and lead to more accurate quantitative measurements, in particular in longitudinal studies (i.e., BLI as a surrogate marker for biological processes in a single growing animal over time).

In this study we performed practical implementation of the commercially available Living Image® Software 3D Analysis Package to assess the accuracy of source depth and intensity reconstruction. This software performs rapid reconstruction of bioluminescence source and location information using spectrally resolved images and the diffusion approximation of light propagation. In a homogeneous tissue slab the accuracy of both location and intensity reconstruction are functions of source depth. At the most superficial depths (2.5 and 5.0 mm) the source depth and intensity are overestimated. This error likely stems from an inherent limitation in the use of the diffusion approximation: at depths shorter than the mean free path ($1/\mu_a+\mu_s'$) diffusion theory tends to fail. The mean free path using the optical properties of the tissue slab ranges from 2.8 mm (at 560 nm) to 4.3 mm (at 660 nm), consistent with the depths at which the reconstruction is least accurate. Comsa, et al. found similar breakdown of the diffusion approximation at shallow depths [25]. At depths greater than the mean free path the algorithm accurately reconstructed source depth with an average error of less than half a millimeter. While this spatial resolution falls short of the 50 micron resolution currently achieved by MRI and CT [26], it is superior to the millimeter resolution of PET [26]. Source intensity reconstruction was accurate (less than 3% error) at 7.5 mm and 10 mm source depth, but at increasing depth overestimated the actual intensity. The

depth limitation on the accurate reconstruction of both source depth and source intensity restricts the utility of 3D reconstruction using diffusion theory to sources

The Living Image® reconstruction algorithm used in this study assumes homogeneous optical properties throughout the subject volume. This simplifying assumption clearly induces error in source reconstruction, as evident from comparing accuracy in the optically homogeneous tissue slab and heterogeneous mouse abdomen. The luminescent bead depth is reconstructed more accurately for the homogeneous tissue slab than the mouse abdomen implantations. The average error in depth reconstruction across all depths tested was 17% for the homogeneous tissue slab; the beads implanted within the mouse abdomen had an average error of 27% across all depths and tissue properties used for reconstruction. The average error in intensity was reconstruction was even more drastic: the homogeneous tissue again had an average error of 17% while the heterogeneous mouse reconstruction resulted in a 51% average error. The accuracy of reconstruction within the mouse abdomen was greatly influenced by the choice of optical properties used for reconstruction. Indeed, the optical properties that govern light transmission through biological tissue can differ by over an order of magnitude depending on the density and composition of the tissue [27]. The failure to account for optical heterogeneity has been previously shown to adversely affect reconstruction accuracy [17,28]. However, as the Living Image® software assumes homogeneous optical properties, a single set of optimal optical properties must be input for reconstruction. In this study, the optimal choice of optical properties for reconstruction was dependent on which reconstruction metric was optimized. Using the optical properties of skin resulted in the most accurate depth reconstruction, but the greatest overestimation of intensity. The use of liver optical properties resulted in the more accurate intensity reconstruction, but gave the least accurate depth reconstruction. The use of muscle optical properties represents a compromise between these two

extremes, yielding decent reconstruction of both depth (average error of 1.0 mm) and intensity (41% average error). As muscle tissue has fairly average optical properties its use as an average of the heterogeneous optical properties of the mouse abdomen is warranted. There is considerable potential for improvement by implementing a compartmentalized model of a mouse with varying optical properties, as previously demonstrated [17,29].

The ability of the Living Image® Software 3D Analysis Package to accurately resolve two equal intensity point sources in homogeneous tissue is a function of source depth and source separation. The ability to distinguish multiple sources decreases as the source depth increases. We have shown here that the discrimination criterion for homogeneous tissue is that source separation must be approximately twice the source depth. At smaller source separation, two sources are reconstructed as a single source. This finding establishes a key limitation to luminescent source reconstruction using the Living Image® algorithm for single view tomography. The practical implication is that using BLI to distinguish two closely spaced cell populations at deep tissue depths (for instance, tumor metastases within the liver) may be difficult using currently available technology.

Novel methods for bioluminescence tomography using multiple viewing angle hardware are under development [14,17,19]. Models of photon propagation indicate that these methods will improve upon the reconstruction accuracy presented in this manuscript that used single-view images to reconstruct tomographic information. However, these multiple view techniques will sacrifice a major advantage of bioluminescence imaging, high throughput, by limiting images to a single subject and requiring multiple images of that mouse thus increasing imaging time. The techniques described herein allow for simultaneous imaging of multiple animals, and hence represent a compromise between imaging throughput and accuracy. Furthermore,

multiple angle imaging will require new imaging systems, while single view tomographic reconstruction can be performed with any of several commercially available CCD cameras. Advancements in bioluminescent tomography will be aided by incorporation of fluorescence tomographic principles, as bioluminescence can be modeled as fluorescence in the steady state domain [16]. However, any bioluminescent tomography algorithms will require solution of a mathematically difficult inverse problem due to a lack of source-detector pairs [30]. Further work is needed both in instrumentation as well as modeling of photon propagation and incorporation of optical heterogeneity.

6.6. Works Cited

1. W. D. McElroy, H. H. Seliger, and E. H. White. "Mechanism of bioluminescence, chemiluminescence and enzyme function in the oxidation of firefly luciferin." *Photochem Photobiol*. 10(3), 153-70 (1969).

2. L. J. Kricka, J. Stroebel, and P. E. Stanley. "Bioluminescent fusion conjugates and bioluminescent immunoassays: 1988-1998." *Luminescence*. 14(1), 39-46 (1999).

3. C. H. Contag, S. D. Spilman, P. R. Contag, M. Oshiro, B. Eames, P. Dennery, D. K. Stevenson, and D. A. Benaron. "Visualizing gene expression in living mammals using a bioluminescent reporter." *Photochem Photobiol*. 66(4), 523-31 (1997).

4. M. Edinger, Y. A. Cao, Y. S. Hornig, D. E. Jenkins, M. R. Verneris, M. H. Bachmann, R. S. Negrin, and C. H. Contag. "Advancing animal models of neoplasia through in vivo bioluminescence imaging." *Eur J Cancer*. 38(16), 2128-36 (2002).

5. A. Rehemtulla, L. D. Stegman, S. J. Cardozo, S. Gupta, D. E. Hall, C. H. Contag, and B. D. Ross. "Rapid and quantitative assessment of cancer treatment response using in vivo bioluminescence imaging." *Neoplasia*. 2(6), 491-5 (2000).

6. C. H. Contag, and M. H. Bachmann. "Advances in in vivo bioluminescence imaging of gene expression." *Annu Rev Biomed Eng*. 4(235-60 (2002).

7. J. F. Mercier, A. Salahpour, S. Angers, A. Breit, and M. Bouvier. "Quantitative assessment of beta 1- and beta 2-adrenergic receptor homo- and heterodimerization by bioluminescence resonance energy transfer." *J Biol Chem*. 277(47), 44925-31 (2002).

8. G. R. Rettig, M. McAnuff, D. Liu, J. S. Kim, and K. G. Rice. "Quantitative bioluminescence imaging of transgene expression in vivo." *Anal Biochem*. 355(1), 90-4 (2006).

9. Z. Paroo, R. A. Bollinger, D. A. Braasch, E. Richer, D. R. Corey, P. P. Antich, and R. P. Mason. "Validating bioluminescence imaging as a high-throughput, quantitative modality for assessing tumor burden." *Mol Imaging*. 3(2), 117-24 (2004).

10. J. Virostko, Z. Chen, M. Fowler, G. Poffenberger, A. C. Powers, and E. D. Jansen. "Factors influencing quantification of in vivo bioluminescence imaging: application to assessment of pancreatic islet transplants." *Mol Imaging*. 3(4), 333-42 (2004).

11. G. Alexandrakis, F. R. Rannou, and A. F. Chatziioannou. "Effect of optical property estimation accuracy on tomographic bioluminescence imaging: simulation of a combined optical-PET (OPET) system." *Phys Med Biol*. 51(8), 2045-53 (2006).

12. H. Dehghani, S. C. Davis, S. Jiang, B. W. Pogue, K. D. Paulsen, and M. S. Patterson. "Spectrally resolved bioluminescence optical tomography." *Opt Lett*. 31(3), 365-7 (2006).

13. A. J. Chaudhari, F. Darvas, J. R. Bading, R. A. Moats, P. S. Conti, D. J. Smith, S. R. Cherry, and R. M. Leahy. "Hyperspectral and multispectral bioluminescence optical tomography for small animal imaging." *Phys Med Biol*. 50(23), 5421-41 (2005).

14. X. J. Gu, Q. H. Zhang, L. Larcom, and H. B. Jiang. "Three-dimensional bioluminescence tomography with model-based reconstruction." *Optics Express*. 12(17), 3996-4000 (2004).

15. Y. Dor, J. Brown, O. I. Martinez, and D. A. Melton. "Adult pancreatic beta-cells are formed by self-duplication rather than stem-cell differentiation." *Nature*. 429(6987), 41-6 (2004).

16. A. H. Hielscher. "Optical tomographic imaging of small animals." *Curr Opin Biotechnol*. 16(1), 79-88 (2005).

17. G. Alexandrakis, F. R. Rannou, and A. F. Chatziioannou. "Tomographic bioluminescence imaging by use of a combined optical-PET (OPET) system: a computer simulation feasibility study." *Phys Med Biol*. 50(17), 4225-41 (2005).

18. V. Ntziachristos, C. Bremer, E. E. Graves, J. Ripoll, and R. Weissleder. "In vivo tomographic imaging of near-infrared fluorescent probes." *Mol Imaging*. 1(2), 82-8 (2002).

19. H. Li, J. Tian, F. Zhu, W. Cong, L. V. Wang, E. A. Hoffman, and G. Wang. "A mouse optical simulation environment (MOSE) to investigate bioluminescent phenomena in the living mouse with the monte carlo method." *Acad Radiol*. 11(9), 1029-38 (2004).

20. G. Zacharakis, H. Kambara, H. Shih, J. Ripoll, J. Grimm, Y. Saeki, R. Weissleder, and V. Ntziachristos. "Volumetric tomography of fluorescent proteins through small animals in vivo." *Proc Natl Acad Sci U S A*. 102(51), 18252-7 (2005).

21. B. W. Rice, M. D. Cable, and M. B. Nelson. "In vivo imaging of light-emitting probes." *J Biomed Opt*. 6(4), 432-40 (2001).

22. C. Kuo, H. Ahsan, J. Hunter, T. L. Troy, H. Xu, N. Zhang, and B. W. Rice. "In vivo bioluminescent tomography using multi-spectral and multi-perspective image data." (2006).

23. O. Coquoz, T. L. Troy, D. Jekic-McMullen, and B. W. Rice. "Determination of depth of in vivo bioluminescent signals using spectral imaging technique." SPIE. 37-45 (2003).

24. C. Kuo, O. Coquoz, T. L. Troy, H. Xu, and B. W. Rice. "Three-Dimensional Reconstruction of In Vivo Bioluminescent Sources Based on Multi-Spectral Imaging." *Journal of Biomedical Optics*. (Submitted.).

25. D. C. Comsa, T. J. Farrell, and M. S. Patterson. "Quantification of bioluminescence images of point source objects using diffusion theory models." *Phys Med Biol*. 51(15), 3733-46 (2006).

26. T. F. Massoud, and S. S. Gambhir. "Molecular imaging in living subjects: seeing fundamental biological processes in a new light." *Genes Dev*. 17(5), 545-80 (2003).

27. W. F. Cheong, S. A. Prahl, and A. J. Welch. "A Review of the Optical-Properties of Biological Tissues." *Ieee Journal of Quantum Electronics*. 26(12), 2166-2185 (1990).

28. H. Dehghani, B. W. Pogue, J. Shudong, B. Brooksby, and K. D. Paulsen. "Three-dimensional optical tomography: resolution in small-object imaging." *Appl Opt*. 42(16), 3117-28 (2003).

29. W. X. Cong, G. Wang, D. Kumar, Y. Liu, M. Jiang, L. V. Wang, E. A. Hoffman, G. McLennan, P. B. McCray, J. Zabner, and A. Cong. "Practical reconstruction method for bioluminescence tomography." *Optics Express*. 13(18), 6756-6771 (2005).

30. V. Ntziachristos, J. Ripoll, L. V. Wang, and R. Weissleder. "Looking and listening to light: the evolution of whole-body photonic imaging." *Nat Biotechnol*. 23(3), 313-20 (2005).

CHAPTER VII

APPROACHES TOWARD CLINICALLY RELEVANT MONITORING OF ISLET MASS

While the data contained within this chapter are not suitable for publication on their own, they present challenges facing clinically relevant imaging of the islet of Langerhans.

7.1. Introduction

Non-invasive measurements of islet mass would greatly facilitate efforts to increase islet mass and to monitor islet mass in both natural development and pathophysiologic states. Currently available approaches are not adequate, relying either on functional measures or sacrificing the animal for post-mortem analysis [1-3]. The primary technical challenge in non-invasive imaging of the pancreatic beta cell stems from its small size and relatively sparse (1-2%) distribution throughout the pancreas. An adequate imaging modality must possess high specificity to distinguish islets from the exocrine pancreas. As islets possess no intrinsic contrast from surrounding tissue, imaging techniques have focused on labeling the pancreatic islet with exogenous contrast agents. The development of novel islet labeling techniques for islet imaging and quantification is an area of active research [4].

Our group and others have used the optical technique of bioluminescence imaging (BLI) to assay the pancreatic islet [5-10]. This technique has proven to be a powerful tool, permitting high throughput imaging of small animals. Light emission was shown to correlate to islet mass [5-7,9,10]. This light emission can then be quantified to estimate islet mass after transplantation. Islet mass can also be tracked in mouse models of diabetes, yielding valuable insight into the progression of diabetes [9,10].

The limitation of bioluminescence imaging is penetration depth: optical attenuation by chromophores – primarily water, hemoglobin, and melanin – limits optical penetration to several centimeters of tissue depth. BLI is thus not adaptable to human studies; its strength lies rather as a pre-clinical tool. A clinically applicable imaging modality would be valuable for tracking islet mass in human diabetics and pre-diabetics. Such a technique could be used for early detection of diabetes prior to metabolic disorders and permit earlier diagnosis and treatment. The impact of early interventions on islet mass could then be monitored using this imaging technique. Clinically relevant

attempts to image the islet of Langerhans have focused on the use of magnetic resonance imaging (MRI) and positron emission tomography (PET).

As the sensitivity of magnetic resonance imaging is inherently low compared to other imaging modalities [11], attempts using MRI have relied primarily on labeling the islet with contrast agents. Islets have been labeled with superparamagnetic iron oxide (SPIO) particles [12,13]. These islets have subsequently been transplanted and are visible as hypo-intensities on MR images. Rejection of transplanted islets has been demonstrated showing the loss of these hypointense spots [14,15]. An alternative labeling technique employs paramagnetic ions to generate hyperintense MR signal. A paramagnetic Gd^{3+} complex was used to label a beta cell line and image the cells after implantation in a hollow fiber [16]. A recent report uses an alternate Gd^{3+} molecule to label and image islets after transplantation to the kidney capsule [17].

Approaches using positron emission tomography benefit from the higher sensitivity of PET [11]. Several PET techniques have focused on ex vivo islet labeling, similarly to MRI attempts. One study internalized an ^{18}F radiotracer into islets to study events immediately post transplantation [18]. An alternate method labeled islets with a PET reporter gene that sequesters an injected radiolabeled probe [19,20]. An alternate PET strategy employs targeted radiolabeled compounds that specifically bind to the islets of Langerhans. The search for suitable radiotracers has encompassed labeled antibodies [21,22], molecules that utilize the unique metabolism of the islet [23-25], and a variety of islet specific ligands [26-29]. However, lack of specificity or high background levels of the radiotracer have rendered most candidates unsuitable for in vivo application [30]. A recent study indicates that a radiotracer targeting the vesicular monoamine transporter 2 may prove useful for PET imaging of the pancreatic islet [31].

7. 2. Materials and Methods

7.2.1. Cell Culture

The immortalized βTC-3 cell line was grown in monolayer culture in 10 cm plates containing Dulbecco's modified Eagle's medium (DMEM) supplemented with 10% fetal bovine serum. Cells were grown to 80% confluence under standard culture conditions (CO_2 incubator: 37°C 5% CO_2) and trypsinized. Cells were washed three times with phosphate buffered saline (PBS) to remove excess trypsin.

7.2.2. Islet Isolation

Murine pancreatic islets were isolated from adult B6D2 and FVB mice. Mouse pancreata were digested with collagenase P (Roche Molecular Biochemicals, Indianapolis, IN) in Hanks buffered saline (0.6 mg/ml) using a wrist action shaker. Islets were then handpicked under microscopic guidance. Islets were cultured in RPMI 1640 (Invitrogen, Carlsbad, CA) with 10% Fetal Bovine Serum (Invitrogen, Carlsbad, CA) and 11 mM glucose.

7.2.3. Islet / Cell labeling

Cultured cells and islets were labeled using similar procedures. Two contrast agents were used. Superparamagnetic iron oxide particles (SPIO) particles consisted of 1.63 μm polymer encapsulated iron oxide particles (Bangs Labs, Fishers, IN). Magnevist (Schering AG, Germany) was used as a paramagnetic labeling agent. Passive labeling consisted of co-culture of islets or cells with the labeling compound for incremental periods of time. Cells/islets were then washed three times with PBS to remove free contrast agent.

Electroporation was performed using the Gene-Pulser system (Bio-Rad, Hercules, CA). Briefly, cells or islets were placed in PBS with the labeling agent (SPIO or Magnevist) in 0.4 cm Gene-Pulser cuvettes. Electroporation parameters were adjusted to 960 μF and 250 mV. Immediately after delivering the electrical pulse cells/islets were re-suspended in media. Cells/islets were washed three times in PBS to remove residual contrast agent.

Fugene 6 (Roche Applied Science, Indianapolis, IN) was used for lipofection of the Magnevist contrast agent into cells/islets. Thirty-six μL of Fugene was incubated in 450 μL of Dulbecco's Modified Eagle Medium (DMEM) at room temperature for 5 minutes. A solution containing 25 μL of 0.5M Magnevist in 100 μL DMEM was then mixed with the Fugene solution and incubated at room temperature for 30 minutes. Cells/islets were incubated with transfection-Magnevist complexes for 4 hours under standard culture conditions (CO_2 incubator: 37°C 5% CO2). Cells/islets were washed 3 times with PBS to remove free contrast particles in the supernatant. Cells were then trypsinized and centrifuged in 15 mL tubes. The supernatant was removed, cells were sonicated to resuspend, and then centrifuged in 1.5 mL tubes to pellet. The supernatant was removed due to the presence of free Magnevist and replaced with water.

7.2.4. Inductively Coupled Plasma - Mass Spectrometry

The iron content of islets incubated with SPIO particles was determined using an inductively coupled plasma mass spectrometer (Perkin Elmer Elan 6100 DRC ICPMS, Wellesley, MA). The purified islet mixture was digested in a 2% HNO_3 matrix. Iron content was quantified by standard calibration and divided by the number of islets in the sample to yield iron content per islet.

7.2.5. Microscopy

Confocal microscopy was performed on islets labeled with fluorescent SPIO particles. Islets were placed between glass cover slips. Imaging was performed using an inverted LSM510 confocal microscope (Zeiss, Germany). A 633 nm filter set was used to image the red fluorescence wavelength of the SPIO.

Pseudo-confocal microscopy was performed on islets labeled with a fluorescent Magnevist analogue. This molecule substituted europium for gadolinium and had a fluorescent antenna to allow visualization of label internalization and localization. A Nikon Eclipse TE2000-U (Tokyo, Japan) microscope was then used to image the fluorescent label.

7.2.6. Cellular MR Imaging

All MR data was acquired at 400 Mhz using a 9.4 Tesla 21-cm horizontal bore MR scanner (Varian, Palo Alto, CA). A 38 mm diameter Litz coil was used for RF transmission and signal reception. For islets labeled with SPIO, islets were suspended in serum albumin in a 6 cm dish positioned in the isocenter of the magnet bore. A T2 weighted gradient echo image was taken for imaging. For cells/islets labeled with Magnevist, cells were pelleted in 1.5 ml micro-centrifuge tubes placed in a water bath to avoid susceptibility effects from surrounding air. A T1 weighted spin echo image was taken with the following parameters: TR = 1000, TE = 12, sampling grid = 128x128.

7.2.7. Targeted Peptide Synthesis

A 20-mer peptide with the sequence LSGTPERSGQAVKVKLKAIP was found to home to the islets of Langerhans using phage display [32]. We modified this 20-mer peptide with biotin on the N-terminal and amidation of the C-terminal and a 6-carbon linker between biotin and the N-terminus (GenScript Corporation, Piscataway, New

Jersey). A near-infrared dye (IRDye800 CW, Licor, Lincoln, Nebraska) was conjugated to avidin, yielding approximately 11.5 dye molecules per avidin. This dye-avidin complex was then conjugated to the peptide-biotin complex.

7.2.8. Targeted Peptide Imaging

In vivo fluorescence imaging was performed on a Xenogen IVIS 200 imaging system (Alameda, CA). FVB mice were anesthetized with constant inhalation of isoflurane. In order to capture the near infrared fluorescence, Cy 5.5 filter sets were used for imaging. The purified dye-peptide complex was injected via retro-orbital injection. Images were taken at incremental periods after injection with a 1 second exposure time. Twenty-four hours after administration animals were sacrificed. Organs were extracted and imaged with the IVIS 200 system to determine label accumulation.

7.3 Results

7.3.1. SPIO labeling

Islets co-incubated for 48 hours with SPIO particles were visible on T2 weighted MRI. These SPIO particles created hypointense signal voids within the homogeneous medium surrounding the islets (Figure 7.1A). After MR imaging, the location of labeled islets was visually verified to coincide with the location of MR hypo intensity.

The location of SPIO accumulation within an islet was determined with confocal microscopy. As SPIO particles were impregnated with a fluorescent dye, the iron particle location could be determined. Figure 7.1B shows the results of a confocal reconstruction of an islet sandwiched between two cover slips. SPIO location is shown in red. The red signal is present predominantly on the edges of the islet, indicated SPIO accumulation peripherally and exclusion from the center of the islet.

As MRI signal is a function of the amount of iron present, ICP mass spectrometry was performed to determine the amount of iron sequestered within islets. Incubation of iron oxide particles with increasing concentrations of SPIOs affected the amount of iron trapped per islet (Figure 7.1C). However, incubation with the same concentration of SPIO did not provide constant iron accumulation per islet; iron content varied by 36%.

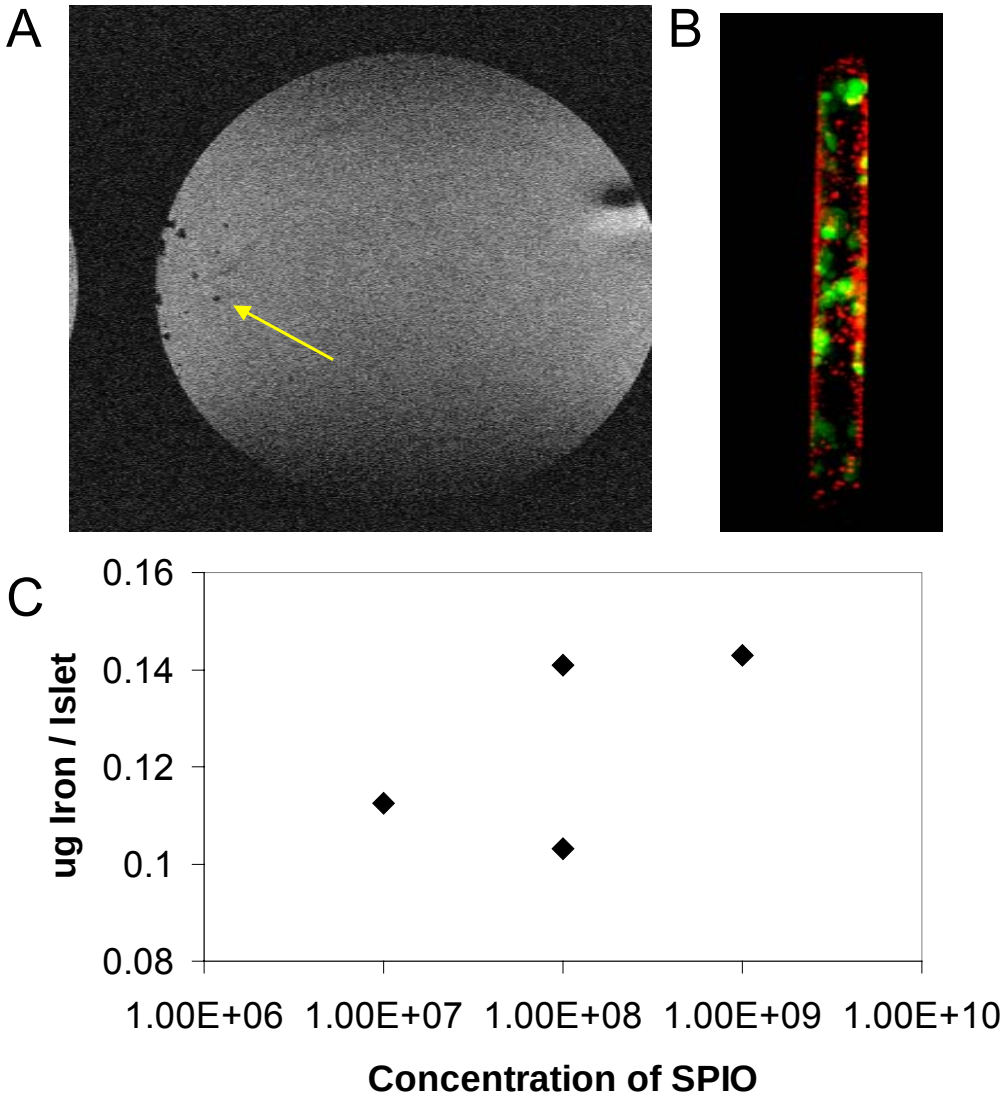

Figure 7.1. (A) T2-weighted MR image of SPIO labeled islets suspended in serum albumin. The labeled islets are visible as hypointense voids. The arrow indicates one such void. (B) Confocal microscopy of an islet labeled with fluorescent SPIOs. The islet is flattened between two cover slips. The red fluorescence comes from a dye within the SPIO; the green fluorescence are islet cells virally transfected with GFP. (C) Iron content of islets as determined by ICP-MS. Islets were co-cultured with various concentrations of SPIOs for 48h.

7.3.2. Magnevist labeling

Several techniques for cellular internalization were used to incorporate the Magnevist contrast agent into islets. The cell line βTC-3 was used as an islet surrogate. Passive co-incubation of Magnevist with cells did not result in any detectable MR signal. Electroporation resulted in some label accumulation, but resulted in high rates of apoptosis. The best results were found using lipofection of βTC-3 cells with Magnevist. Cell pellets lipofected with Magnevist became hyperintense (left tube, Figure 7.2) compared with unlabeled control cells (right tube, Figure 7.2).

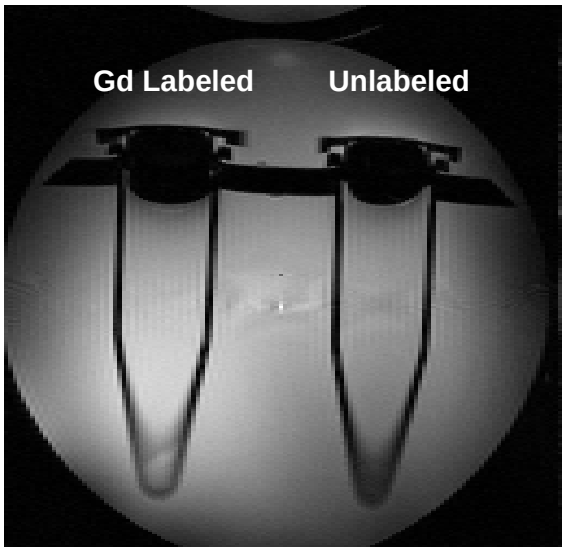

Figure 7.2. βTC-3 cells pelleted in the bottom of micro centrifuge tubes. The left tube was lipofected with Magnevist contrast agent. The right tube contains unlabeled cells as control.

No hyper intensity was present when the same lipofection technique was attempted on pancreatic islets. To visualize Magnevist internalization into islets, a fluorescent Magnevist analogue was synthesized (Figure 7.3A). This compound was then lipofected into islets. Pseudo confocal microscopy was performed to track localization of the compound after lipofection (Figures 7.3B & 7.3C). The optical Magnevist tracer was present throughout the islet.

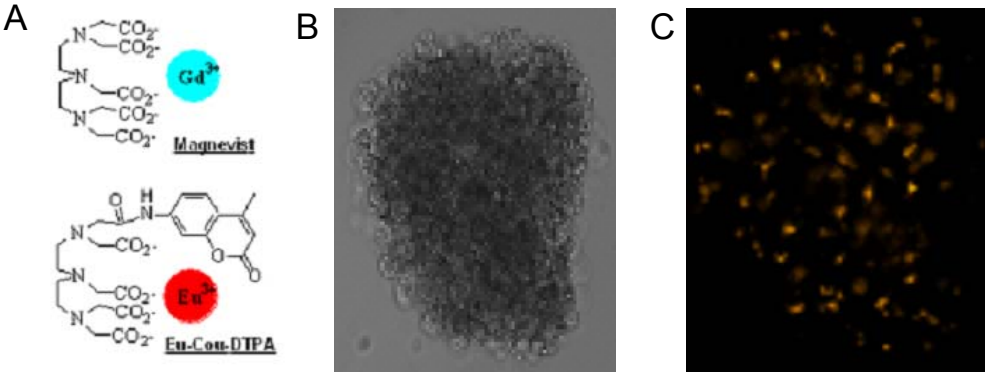

Figure 7.3. (A) Chemical structure of Magnevist and an optical analogue of Magnevist. (B) Phase contrast image of a pancreatic islet. (C) Pseudo confocal fluorescence image of the same islet. The fluorescent Magnevist compound is visible as orange cells distributed throughout the islet.

7.3.3. Targeted Peptide

An islet-targeted peptide was conjugated to a near infrared fluorescent dye for imaging. An avidin-biotin complex was used to attach the components (Figure 7.4). This compound was then injected into FVB mice via retro orbital injection. Thirty minutes after injection free dye was visibly metabolized in a region consist with the location of the liver and excreted in the bladder (Figure 7.4A). The targeted dye appeared sequester in the abdomen, in an area consistent with the anatomical location of the pancreas. However, three hours after injection the targeted dye also appeared to be excreting through the bladed (Figure 7.4B). Twenty-four hours after injection, the liver, pancreas, liver, stomach, and intestines were removed and imaged to determine probe accumulation. Both free (Figure 7.4C) and targeted dye (Figure 7.4D) was found exclusively in the liver, with no detectable levels present in the pancreas. In a subsequent experiment, imaging was performed immediately after injection and the liver and pancreas were exposed for imaging. All probe accumulation was in the liver, with no detectable accumulation in the pancreas (data not shown).

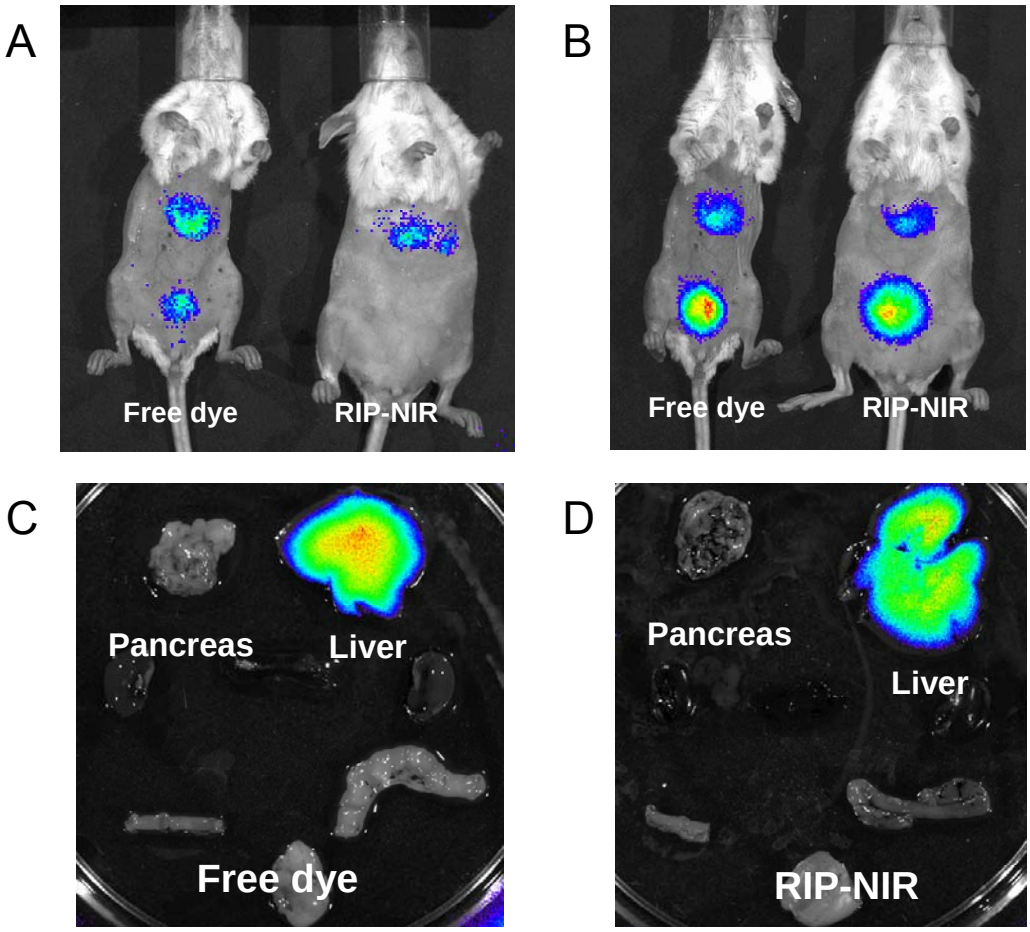

Figure 7.4. (A) In vivo fluorescence image of a mouse injected with free NIR dye (left mouse) and NIR dye attached to a targeting peptide (right) 30 minutes post retro orbital injection. The free dye appears to be cleared through the liver and bladder. (B) In vivo fluorescence image of the same mice injected with free NIR dye (left mouse) and NIR dye attached to a targeting peptide (right) 3 hours post retro orbital injection. Both mice show dye clearance through the liver and bladder. (C) Excised organs from the mouse injected with free NIR dye. (D) Excised organs from the mouse injected with the peptide targeted dye.

7.4. Discussion

Islets labeled with iron oxide particles were detectable as hypo intense spots in MR images. However, confocal microscopy of these particles indicated that these particles were associated solely with the periphery of the islet. As dynamic changes in islet structure accompany islet transplantation [33], an optimal labeling agent must be distributed throughout the islet to accurately reflect islet mass. Furthermore, the amount

of iron associated with each islet was not constant after labeling. Variability in iron internalization was echoed by other studies [14], and has implication for quantifying the number of islets surviving transplantation. As the size of the disturbance in the local magnetic field caused by SPIOs exceeds the size of the islets themselves, it is unclear if a hypo intense spot represents a single islet or a cluster of many islets [12]. Studies seeking to quantify SPIO labeled islets transplanted into the liver have relied on manually counting signal voids on MR images [14,15], a technique prone to islet clustering and user bias.

Islets labeled with a paramagnetic contrast agent are easier to quantify, as the area of signal hyper intensity correlates with the number of labeled cells. Cultured cell lines labeled with Magnevist, a paramagnetic contrast agent, were apparent on T1-weighted MR images. Furthermore, use of an optical Magnevist analogue demonstrated that this label penetrated throughout the islet, likely due to its smaller size than SPIOs. However, attempts to achieve the same contrast with islets failed, owing either to a smaller cell volume or difference in internalization rate.

Techniques using MR contrast agents relied on ex vivo labeling of islets. This caveat limits this technique exclusively to studies of transplanted islets. Native pancreatic islets cannot be labeled in this manner. The practice of transplanting islets to reverse diabetes captivated the diabetes community half a decade ago with the publication of the Edmonton protocol [34]. However, over the course of this project, this early promise has waned. A recently published multi-center evaluation of the Edmonton protocol found that the majority of transplanted islet grafts failed to reverse hyperglycemia two years after transplantation [35]. Thus, the ability to label only transplanted islets is a major weakness of ex vivo labeling with MR contrast agents.

The use of agents that specifically target the pancreatic islet would permit imaging of not only transplanted islets, but also islets in the pancreas. However, the

search for candidate targeting agents has proven largely unsuccessful [21-25,30]. We tested the hypothesis that a peptide found to specifically bind the islet [32] could provide the islet targeting for in vivo labeling. Although our approach utilized near infrared fluorescence, the technique could be easily adapted to clinically applicable modalities such as PET. However, although initial results were promising, the peptide targeting fluorescent agent was home specifically to the liver, with negligible uptake in the pancreas.

7.4. Works Cited

1. D. K. McCulloch, D. J. Koerker, S. E. Kahn, S. Bonner-Weir, and J. P. Palmer. "Correlations of in vivo beta-cell function tests with beta-cell mass and pancreatic insulin content in streptozocin-administered baboons." *Diabetes*. 40(6), 673-9 (1991).

2. S. Bonner-Weir. "Life and death of the pancreatic beta cells." *Trends Endocrinol Metab*. 11(9), 375-8 (2000).

3. A. M. Davalli, Y. Ogawa, L. Scaglia, Y. J. Wu, J. Hollister, S. Bonner-Weir, and G. C. Weir. "Function, mass, and replication of porcine and rat islets transplanted into diabetic nude mice." *Diabetes*. 44(1), 104-11 (1995).

4. B. W. Paty, S. Bonner-Weir, M. R. Laughlin, A. J. McEwan, and A. M. Shapiro. "Toward development of imaging modalities for islets after transplantation: insights from the National Institutes of Health Workshop on Beta Cell Imaging." *Transplantation*. 77(8), 1133-7 (2004).

5. M. Fowler, J. Virostko, Z. Chen, G. Poffenberger, A. Radhika, M. Brissova, M. Shiota, W. E. Nicholson, Y. Shi, B. Hirshberg, D. M. Harlan, E. D. Jansen, and A. C. Powers. "Assessment of pancreatic islet mass after islet transplantation using in vivo bioluminescence imaging." *Transplantation*. 79(7), 768-76 (2005).

6. Y. Lu, H. Dang, B. Middleton, Z. Zhang, L. Washburn, M. Campbell-Thompson, M. A. Atkinson, S. S. Gambhir, J. Tian, and D. L. Kaufman. "Bioluminescent monitoring of islet graft survival after transplantation." *Mol Ther*. 9(3), 428-35 (2004).

7. S. Y. Park, X. Wang, Z. Chen, A. C. Powers, M. A. Magnuson, W. S. Head, D. W. Piston, and G. I. Bell. "Optical imaging of pancreatic beta cells in living mice expressing a mouse insulin I promoter-firefly luciferase transgene." *Genesis*. 43(2), 80-6 (2005).

8. J. Virostko, Z. Chen, M. Fowler, G. Poffenberger, A. C. Powers, and E. D. Jansen. "Factors influencing quantification of in vivo bioluminescence imaging: application to assessment of pancreatic islet transplants." *Mol Imaging*. 3(4), 333-42 (2004).

9. S. J. Smith, H. Zhang, A. O. Clermont, A. C. Powers, D. B. Kaufman, A. F. Purchio, and D. West. "In Vivo Monitoring of Pancreatic beta-Cells in a Transgenic Mouse Model." *Mol Imaging*. 5(2), (2006).

10. X. Chen, X. Zhang, C. S. Larson, M. S. Baker, and D. B. Kaufman. "In vivo bioluminescence imaging of transplanted islets and early detection of graft rejection." *Transplantation*. 81(10), 1421-7 (2006).

11. P. J. Cassidy, and G. K. Radda. "Molecular imaging perspectives." *Journal of the Royal Society Interface*. 2(3), 133-144 (2005).

12. D. Jirak, J. Kriz, V. Herynek, B. Andersson, P. Girman, M. Burian, F. Saudek, and M. Hajek. "MRI of transplanted pancreatic islets." *Magn Reson Med*. 52(6), 1228-33 (2004).

13. N. V. Evgenov, Z. Medarova, G. Dai, S. Bonner-Weir, and A. Moore. "In vivo imaging of islet transplantation." *Nat Med*. 12(1), 144-8 (2006).

14. N. V. Evgenov, Z. Medarova, J. Pratt, P. Pantazopoulos, S. Leyting, S. Bonner-Weir, and A. Moore. "In vivo imaging of immune rejection in transplanted pancreatic islets." *Diabetes*. 55(9), 2419-28 (2006).

15. J. Kriz, D. Jirak, P. Girman, Z. Berkova, K. Zacharovova, E. Honsova, A. Lodererova, M. Hajek, and F. Saudek. "Magnetic resonance imaging of pancreatic islets in tolerance and rejection." *Transplantation*. 80(11), 1596-603 (2005).

16. Q. Zheng, H. Dai, M. E. Merritt, C. Malloy, C. Y. Pan, and W. H. Li. "A new class of macrocyclic lanthanide complexes for cell labeling and magnetic resonance imaging applications." *J Am Chem Soc*. 127(46), 16178-88 (2005).

17. L. Biancone, S. G. Crich, V. Cantaluppi, G. M. Romanazzi, S. Russo, E. Scalabrino, G. Esposito, F. Figliolini, S. Beltramo, P. C. Perin, G. P. Segoloni, S. Aime, and G. Camussi. "Magnetic resonance imaging of gadolinium-labeled pancreatic islets for experimental transplantation." *NMR Biomed*. (2006).

18. C. Toso, H. Zaidi, P. Morel, M. Armanet, A. Andres, N. Pernin, R. Baertschiger, D. Slosman, L. H. Buhler, D. Bosco, and T. Berney. "Positron-emission tomography imaging of early events after transplantation of islets of Langerhans." *Transplantation*. 79(3), 353-5 (2005).

19. Y. Li, G. Li, W. Dong, J. Chen, D. Lu, and J. Tan. "Transplantation of rat islets transduced with human heme oxygenase-1 gene using adenovirus vector." *Pancreas*. 33(3), 280-6 (2006).

20. Y. Lu, H. Dang, B. Middleton, Z. Zhang, L. Washburn, D. B. Stout, M. Campbell-Thompson, M. A. Atkinson, M. Phelps, S. S. Gambhir, J. Tian, and D. L. Kaufman. "Noninvasive imaging of islet grafts using positron-emission tomography." *Proc Natl Acad Sci U S A*. 103(30), 11294-9 (2006).

21. A. Moore, S. Bonner-Weir, and R. Weissleder. "Noninvasive in vivo measurement of beta-cell mass in mouse model of diabetes." *Diabetes*. 50(10), 2231-6 (2001).

22. L. Ladriere, F. Malaisse-Lagae, R. Alejandro, and W. J. Malaisse. "Pancreatic fate of a (125)I-labelled mouse monoclonal antibody directed against pancreatic B-cell surface ganglioside(s) in control and diabetic rats." *Cell Biochem Funct*. 19(2), 107-15 (2001).

23. L. Ladriere, V. Leclercq-Meyer, and W. J. Malaisse. "Assessment of islet beta-cell mass in isolated rat pancreases perfused with D-[(3)H]mannoheptulose." *Am J Physiol Endocrinol Metab*. 281(2), E298-303 (2001).

24. W. J. Malaisse, and L. Ladriere. "Assessment of B-cell mass in isolated islets exposed to D-[3H]mannoheptulose." *Int J Mol Med*. 7(4), 405-6 (2001).

25. W. J. Malaisse, M. Doherty, L. Ladriere, and F. Malaisse-Lagae. "Pancreatic uptake of [2-(14)C]alloxan." *Int J Mol Med*. 7(3), 311-5 (2001).

26. P. B. Clark, H. D. Gage, C. Brown-Proctor, N. Buchheimer, J. Calles-Escandon, R. H. Mach, and K. A. Morton. "Neurofunctional imaging of the pancreas utilizing the cholinergic PET radioligand [18F]4-fluorobenzyltrozamicol." *Eur J Nucl Med Mol Imaging*. 31(2), 258-60 (2004).

27. S. Schneider, P. J. Feilen, M. Schreckenberger, M. Schwanstecher, C. Schwanstecher, H. G. Buchholz, O. Thews, K. Oberholzer, A. Korobeynikov, A. Bauman, S. Comagic, M. Piel, E. Schirrmacher, C. Y. Shiue, A. A. Alavi, P. Bartenstein, F. Rosch, M. M. Weber, H. H. Klein, and R. Schirrmacher. "In vitro and in vivo evaluation of novel glibenclamide derivatives as imaging agents for the non-invasive assessment of the pancreatic islet cell mass in animals and humans." *Exp Clin Endocrinol Diabetes*. 113(7), 388-95 (2005).

28. T. Otonkoski, K. Nanto-Salonen, M. Seppanen, R. Veijola, H. Huopio, K. Hussain, P. Tapanainen, O. Eskola, R. Parkkola, K. Ekstrom, Y. Guiot, J. Rahier, M. Laakso, R. Rintala, P. Nuutila, and H. Minn. "Noninvasive Diagnosis of Focal Hyperinsulinism of Infancy With [18F]-DOPA Positron Emission Tomography." *Diabetes*. 55(1), 13-8 (2006).

29. I. R. Sweet, D. L. Cook, A. Lernmark, C. J. Greenbaum, A. R. Wallen, E. S. Marcum, S. A. Stekhova, and K. A. Krohn. "Systematic screening of potential beta-cell imaging agents." *Biochem Biophys Res Commun*. 314(4), 976-83 (2004).

30. I. R. Sweet, D. L. Cook, A. Lernmark, C. J. Greenbaum, and K. A. Krohn. "Non-invasive imaging of beta cell mass: a quantitative analysis." *Diabetes Technol Ther*. 6(5), 652-9 (2004).

31. F. Souza, N. Simpson, A. Raffo, C. Saxena, A. Maffei, M. Hardy, M. Kilbourn, R. Goland, R. Leibel, J. J. Mann, R. Van Heertum, and P. E. Harris. "Longitudinal noninvasive PET-based beta cell mass estimates in a spontaneous diabetes rat model." *J Clin Invest*. 116(6), 1506-13 (2006).

32. K. N. Samli, M. J. McGuire, C. B. Newgard, S. A. Johnston, and K. C. Brown. "Peptide-mediated targeting of the islets of Langerhans." *Diabetes*. 54(7), 2103-8 (2005).

33. A. M. Davalli, L. Scaglia, D. H. Zangen, J. Hollister, S. Bonner-Weir, and G. C. Weir. "Vulnerability of islets in the immediate posttransplantation period. Dynamic changes in structure and function." *Diabetes*. 45(9), 1161-7 (1996).

34. A. M. Shapiro, J. R. Lakey, E. A. Ryan, G. S. Korbutt, E. Toth, G. L. Warnock, N. M. Kneteman, and R. V. Rajotte. "Islet transplantation in seven patients with type 1 diabetes mellitus using a glucocorticoid-free immunosuppressive regimen." *N Engl J Med*. 343(4), 230-8 (2000).

35. A. M. Shapiro, C. Ricordi, B. J. Hering, H. Auchincloss, R. Lindblad, R. P. Robertson, A. Secchi, M. D. Brendel, T. Berney, D. C. Brennan, E. Cagliero, R. Alejandro, E. A. Ryan, B. DiMercurio, P. Morel, K. S. Polonsky, J. A. Reems, R. G. Bretzel, F. Bertuzzi, T. Froud, R. Kandaswamy, D. E. Sutherland, G. Eisenbarth, M. Segal, J. Preiksaitis, G. S. Korbutt, F. B. Barton, L. Viviano, V. Seyfert-Margolis, J. Bluestone, and J. R. Lakey. "International trial of the Edmonton protocol for islet transplantation." *N Engl J Med*. 355(13), 1318-30 (2006).

CHAPTER VIII

CONCLUSIONS AND FUTURE WORK

8.1. Summary

The overall objective of this research was to develop techniques to non-invasively image the pancreatic islet. These techniques were subsequently validated and applied to applicable models of disease and transplantation.

The review of islet transplantation in Chapter II established the need for an imaging modality capable of imaging the pancreatic islet. The central role of the islets of Langerhans in the pathogenesis of diabetes was highlighted, establishing the impetus for tracking these cells. The challenges facing successful imaging of the islet were discussed. Approaches by other researchers attempting to image the islet were summarized. These techniques spanned a variety of imaging modalities encompassing magnetic resonance imaging, nuclear imaging, and optical imaging. The strengths and weaknesses of each modality were discussed in the scope of islet imaging.

Chapter III presents work using bioluminescence imaging (BLI) to track transplanted pancreatic islets. Islets labeled with the luciferase reporter gene via adenoviral vector were visible in vitro. The light emitted from these islets was found to be proportional to the number of islets. Islets could also be imaged non-invasively after transplantation, with light intensity again correlating to the number of islets transplanted. Viral transfection was shown to have no adverse affect on islet function or morphology.

Chapter IV discusses generation of a transgenic mouse line expressing luciferase under control of the mouse insulin I promoter. The functionality and morphology of transgenic islets was found to be normal. Light emitted from the beta

cells of these animals could be imaged with a CCD camera. As found with virally transfected islets, the amount of light emission correlated with the number of islets. Light emission was also found to be affected by glucose levels. A mouse model of diabetes using the beta cell toxin streptozotocin was applied to transgenic insulin/luciferase mice. Diabetes induced a drop in bioluminescence intensity, correlating with the loss of beta cells. Transgenic islets could be imaged non-invasively after transplantation. As islet survival after transplantation varied, bioluminescence intensity provided an indicator of the number of surviving islets.

Chapter V recounts a set of experiments using light emitting standards to determine factors that influence quantification of bioluminescence imaging. These standards emit known, constant intensity light that mimic the light produced by the luciferase reaction. Using these standards it was determined that surgical artifacts after islet transplantation affect BLI measurements. The affect of transplantation location was also quantified and standardized. Rotation of the animal was found to induce changes in bioluminescence quantification.

A three-dimensional luminescent source reconstruction algorithm is systematically evaluated in Chapter VI. Light emitted standards were employed to determine the accuracy of bioluminescent source position and intensity reconstruction. The accuracy was found to be a function of source depth. Sources more shallow than the mean free path depth led to increased error in the reconstruction. The ability of the algorithm to distinguish two equal intensity sources decreased with increased source depth. Reconstruction of light sources in optically heterogeneous media (such as a mouse abdomen) was less accurate than optically homogeneous media.

Chapter VII summarizes several projects seeking to establish clinically relevant imaging modalities for islet imaging. The previously discussed work using bioluminescence imaging provides a valuable pre-clinical tool, but is not applicable for

human studies. Work using magnetic resonance imaging used islets labeled with MRI contrast agents. However, these techniques suffered from issues with labeling efficiency, sensitivity, and signal quantification. The main inadequacy of the MRI approach used was that it requires ex vivo islet labeling, limiting the technique to studies of transplanted islets. A targeted compound that specifically targets or accumulates in the islet could be labeled for imaging purposes. One such targeted peptide was evaluated for in vivo imaging using near infrared fluorescence. Unfortunately, no islet accumulation was achieved.

8.2. Future Work

The work presented in this dissertation has established the basis for a wealth of future studies. The development of bioluminescence imaging for non-invasive imaging of pancreatic islets is a valuable pre-clinical tool. This modality can be applied to an array of murine models of disease, yielding valuable insight into the dynamics of beta cell loss and regeneration. Several of these studies are currently underway, including using BLI to examine the effects of a high fat diet on beta cell hypertrophy. Bioluminescence imaging can also be applied to transplant settings to determine factors affecting transplant survival and optimizing the optimal engraftment site.

Bioluminescence imaging is limited by optical attenuation to studies involving small animals. Ultimately, a modality applicable to human imaging is sought to guide clinical intervention. The clinically applicable approaches attempted in these studies proved inadequate for assessing islet mass. However, the development of targeted imaging agents is an area of active research. Evaluating promising candidates requires a correlative measure of beta cell mass; bioluminescence imaging can provide such a metric. Future correlation between BLI measurements and alternate modalities will aid evaluation of such modalities. Furthermore, determining the anatomical location of

targeted agent can be difficult, as demonstrated with the studies using a targeted peptide described in Chapter VII. Three-dimensional reconstruction of the location of bioluminescent islets can be used to guide image analysis in co-registered data sets, providing an atlas of the islet location.

8.3. Research Considerations

The protection of research subjects and the societal impact of this research were considered throughout the course of these studies.

8.3.1. Protection of Research Subjects

No human subjects were used in this research. As this research project was directed towards development of in vivo imaging modalities, animal experimentation was necessary. The proper and ethical use of animals in scientific research was ensured in all experimentation. All lab personnel completed the Animal Research Training Program sponsored by the Institutional Animal Care and Use Committee, as required by Vanderbilt University. All experiments were conducted in accordance with National Institutes of Health regulations for the ethical use of animals in research and were pre-approved by the Vanderbilt Institutional Animal Care and Use Committee.

Appropriate training on general lab safety and standard chemical, biological, and radiation safety was required for personnel involved in this study in compliance with institutional guidelines.

8.3.2. Societal Implications

Diabetes mellitus is a prevalent disease with rising incidence rates. An increased understanding of the dynamics of beta cell growth and death will yield valuable insight

into diabetes. This knowledge can be used to guide future treatment of diabetics, leading to increased quality of life and life expectancy.